

DEVELOPMENT AND VERIFICATION OF AN INTEGRATED FURNACE AND
REACTOR MODEL FOR AN INDUSTRIAL STEAM METHANE REFORMER

by

Emre Can BİLİR

B.S., Chemical Engineering, Anadolu University, 2011

Submitted to the Institute for Graduate Studies in
Science and Engineering in partial fulfillment of
the requirements for the degree of
Master of Science

Graduate Program in Chemical Engineering
Boğaziçi University
2015

Dedicated to my family

ACKNOWLEDGEMENTS

First of all, I would like to thank my supervisor Assoc. Prof. Ahmet Kerim Avcı, especially for his cordial support and enlightening vision. I am very proud to have opportunity to work with such valuable person whom I have always appreciated his patience and motivating optimism. Many thanks to him for being the base of a milestone.

I also would like to thank my committee members Assoc. Prof. Burak Alakent and Prof. Hüsni Atakül for devoting their valuable time to read, listen and comment on my thesis and supporting me to graduate.

My special thanks goes to my family. My mother İncilay, my father Süreyya, my brother Cemre, my uncle Batuhan and my grandparents have always supported me under any circumstance. Their moral energy and prayers have pushed me harder and further every time. I am aware that I owe, where I am right now, to my family. I feel everlasting love for all of them. I can never pay back what they have done to me for my whole life.

My private thanks are for my beloved one, Gizem. Even her emotional presence has always showed me the way. Her cordial and unquestionable support has pushed me further whenever I faced difficulties. I have always felt her love and her moral energy deep in my heart.

I want to thank my brothers and sisters in TÜPRAŞ R&D, for everything we have shared in wonderful years. Hilal Fidan Acar, Sadık Ödemiş, Selin Gündür, Fatih Demir, Işıl Kabacaoğlu and Akin Paksoy will always be remembered and missed. I also want to thank my former team leader Mustafa Karakaya. His technical knowledge and brotherhood has always made me stay focused. Their valuable contributions to my life in all aspects will always be respected.

I appreciate and thank Selçuk Güreşçi, Caner Demiryürek and Murat Erol for their cordial helps during this work. They have patiently answered all my questions and always gave constructive feedbacks. Besides, valuable contributions of Ümmühan Canan and Fırat Uzman are all appreciated. Lastly, I thank to my manager, Sarp Yeletayşi, who has shown great empathy and understanding during preparation of this work.

ABSTRACT

DEVELOPMENT AND VERIFICATION OF AN INTEGRATED FURNACE AND REACTOR MODEL OF AN INDUSTRIAL STEAM METHANE REFORMER

Hydrogen demand in refineries is constantly increasing due to effort on processing heavier crudes and producing higher grade transportation fuels in order to meet increasing demand. In this respect, refineries are investing in hydrotreating and hydroprocessing units, and are continuously investigating ways to maximize profit margins through cheaper but reliable sources of hydrogen. Currently, the most economically feasible hydrogen production route is steam methane reforming (SMR). SMR is conventionally carried out in steam reformers in which natural gas is catalytically reacted with steam in tubular reactors placed into a furnace where heat required for endothermic reaction is supplied by combustion of fuels. Among several types of reformer furnaces, Foster Wheeler's Terrace Wall™ type reformer is currently under operation in TÜPRAŞ İzmit Refinery. Due to metallurgical features of reformer tubes wall temperatures should not exceed design values as it strongly reduces expected life span of the tubes. In this respect, prediction of maximum wall temperatures, along with other process outcomes such as product composition and pressure drop under various operating conditions become important issues. For this purpose, a mathematical model, combining the combustion in the furnace and reforming within the reactor tubes, is developed and tested with field data. Simulation results show that, composition of the reformer effluent, especially those of hydrogen and methane can be well predicted with max. 4.3% and 7.2% deviation from plant data respectively. However, other components may show considerable variations most likely due to industrial kinetic parameters. Pressure drop occurred in packed bed is successfully predicted with max. 0.37% deviation. Outer tube wall temperature occurring in the system can also be closely predicted respective to location along the tube with max. 1% deviation. Due to model assumptions and literature parameters, reactor outlet temperature also shows appreciable deviation in the range of 1.9-3.3% although product composition is well predicted. Simulation results show the importance of proper parameter usage for the accuracy of the model results.

ÖZET

ENDÜSTRİYEL METAN BUHAR REFORMLAYICININ ENTEGRE FIRIN VE REAKTÖR MODELİNİN GELİŞTİRİLMESİ VE DOĞRULANMASI

Rafinerilerin hidrojen ihtiyacı, artan yakıt talebini karşılamak için daha ağır ham petrol işleme ve daha yüksek kaliteli taşıt yakıtı üretme çabaları nedeniyle sürekli artmaktadır. Bu sebeple rafineriler hidrotemizleme ve hidroişleme ünitelerine yatırım yapmakta ve sürekli olarak kar marjlarını ucuz ancak güvenilir hidrojen kaynaklarıyla yükseltmenin yollarını aramaktadırlar. Mevcut durumda, hidrojen üretimi için ekonomik olarak en uygun yöntem buharın metanla reformlanmasıdır (SMR). SMR geleneksel olarak fırın içerisine yerleştirilen tüp tipi reaktörlerde metanın su buharı ile katalitik olarak reaksiyona girdiği ve toplamda endotermik reaksiyonlar için gerekli ısının fırında yakılan yakıt ile sağlandığı buhar reformlayıcılarda gerçekleştirilmektedir. TÜPRAŞ İzmit Rafinerisi'nde, reformlayıcı fırınlarının çeşitli türleri arasında Foster Wheeler'ın Teras-Duvar™ tüp reformlayıcı fırını kullanılmaktadır. Reformlayıcı tüplerinin metalürjik özellikleri nedeniyle beklenen ömürlerini çok azaltacağı için tüp cidar sıcaklıkları tasarım değerlerini aşmamalıdır. Bu bağlamda, en yüksek tüp cidar sıcaklıklarıyla beraber çeşitli operasyon koşullarında ürün kompozisyonu, basınç kaybı gibi süreç çıktılarının tahmin edilmesi önemli konular haline gelmektedir. Bu amaç doğrultusunda, fırındaki yanmayı ve tüplerin içinde gerçekleşen reformlama reaksiyonlarını birleştiren bir matematik model geliştirilmiş ve saha verileriyle test edilmiştir. Simülasyon sonuçlarına göre; reformlayıcı çıkış kompozisyonu, özellikle hidrojen ve metanın çıkış kompozisyonları sırasıyla en çok %4.3 ve %7.2 sapmayla iyi bir şekilde tahmin edilebilmektedir. Buna rağmen diğer bileşenler, büyük ihtimalle endüstriyel kinetik parametrelerden ötürü önemli sapmalar gösterebilmektedir. Sabit yatakta gerçekleşen basınç düşüşü en fazla %0.37 sapma ile başarılı bir şekilde tahmin edilmiştir. Sistemde gerçekleşen tüp dış cidar sıcaklıkları da tüp boyunca lokasyona bağlı olarak en fazla %1 sapma ile tahmin edilebilmiştir. Model varsayımlarından ve literatür parametrelerinden ötürü ürün kompozisyonu düzgün tahmin edilse dahi reaktör çıkış sıcaklığı %1.9-3.3 aralığında önemli sayılabilecek bir sapma göstermiştir. Simülasyon sonuçları, doğru sonuçlara ulaşabilmek için doğru parametre kullanımının önemini ortaya koymaktadır.

TABLE OF CONTENTS

ACKNOWLEDGEMENTS.....	iv
ABSTRACT.....	v
ÖZET	vi
TABLE OF CONTENTS.....	v
LIST OF FIGURES	x
LIST OF TABLES.....	xii
LIST OF SYMBOLS	xiv
LIST OF ACRONYMS/ABBREVIATIONS	xix
1. INTRODUCTION	1
2. LITERATURE SURVEY	4
2.1. Chemistry and Thermodynamics of Steam Methane Reforming.....	4
2.2. Steam Reforming Catalysts.....	5
2.3. Steam Reforming Kinetics	7
2.4. Steam Methane Reformers	8
2.4.1. Bottom Fired Steam Reformers	9
2.4.2. Top fired steam reformers.....	9
2.4.3. Side fired steam reformers	10
2.4.4. Terrace wall TM steam reformers.....	10
2.5. Steam-Methane Reforming Process Overview	13
2.5.1. Feed preparation section of steam reformer.....	14
2.5.2. Reactor section of steam reformer	15
2.5.3. Furnace section of steam reformer.....	15
2.5.4. Product purification section	16

2.6. Fundamental Phenomena in Steam Methane Reforming Processes	16
2.6.1. Furnace side phenomena.....	16
2.6.2. Process side phenomena.....	18
2.7. Available Data.....	19
3. METHODOLOGY	20
3.1. Packed Bed Reactor Models	20
3.1.1. One dimensional pseudo-homogeneous model.....	21
3.1.2. One dimensional heterogeneous model	23
3.1.3. Steam methane reforming kinetics for modeling.....	24
3.1.4. Tube to process gas heat transfer coefficient (h_w)	27
3.1.5. Furnace gas to tube convective heat transfer coefficient (h_c)	28
3.1.6. Pressure drop in packed bed reactors	29
3.2. Furnace Models.....	30
3.2.1. Roesler flux methods	30
3.2.2. Hottel zone method	31
3.2.3. Well stirred furnace model.....	32
3.2.3.1. Net rate of heat transfer to tubes.....	34
3.2.3.2. Total exchange area (g_{rad}).....	34
3.2.3.2. Effective tube emissivity (ϵ_{eff}).....	37
4. MATHEMATICAL MODELING STUDIES	40
4.1. Reformer Feed Modification.....	40
4.2. Packed Bed Steam Reforming Reactor Model	40
4.2.1. Energy balance over reformer tube.....	42
4.2.2.1. Tube wall thermal conductivity (k_w).....	43
4.2.2.2. Tube to process gas heat transfer coefficient (h_w).....	43
4.2.2.3. Heat of reaction (ΔH_{rxn}).....	44

4.2.2. Momentum balance over packed bed.....	45
4.3. Well Stirred Steam Reformer Furnace Model	46
4.3.1. Radiative heat flux calculation.....	46
4.3.2. Convective heat flux calculation.....	47
4.4. Furnace Chamber Combustion Model	48
4.5. Model Solution Strategy	49
5. RESULTS AND DISCUSSION.....	52
5.1. Evaluation of User Defined Solution Parameters	52
5.1.1. Effect of number of segments	52
5.1.2. Effect of temperature increment size	53
5.1.3. Effect of convergence tolerance.....	55
5.2. Evaluation of the Process Parameters	56
5.3. Case Studies	63
5.4. Case Study Results.....	66
5.5. Discussion	74
6. CONCLUSIONS AND RECOMMENDATIONS	76
6.1. Conclusions.....	76
6.2. Recommendations	77
APPENDIX A: RADIATIVE HEAT TRANSFER BACKGROUND.....	79
APPENDIX B: PROPERTIES OF SPECIES AND MIXTURES.....	93
APPENDIX C: CODE FLOW CHARTS	99
REFERENCES	104

LIST OF FIGURES

Figure 2.1. Johnson Matthey's KATALCO™ series catalysts.	7
Figure 2.2. Steam reformer furnace configurations.	9
Figure 2.3. Inside of Terrace Wall™ steam reformer radiant box.	11
Figure 2.4. Combined effects of slightly sloped walls and upward firing burners on flue gas recirculation patterns.	12
Figure 2.5. Computational Fluid Dynamics (CFD) modeling study result supporting the well-stirred furnace effect of flue gas recirculation flow patterns.	12
Figure 2.6. Circumferential heat flux profile for double fired tubes.	13
Figure 2.7. Tüpraş hydrogen unit simplified process flow diagram.	14
Figure 2.8. Representative local temperature distribution profile in the furnace as the result of heat interaction between furnace gas and catalytic reactions.	17
Figure 2.9. Catalytic reaction phenomena in packed bed reactors.	19
Figure 3.1. Classification of fixed bed reactor models.	21
Figure 3.2. Radiant energy balance on differential increment in combustion chamber. ...	30
Figure 3.3. Radiation network showing radiant energy transfer pathways for well stirred furnace.	34
Figure 3.4. Equivalent plane surfaces for the case of equal radiation incident on tube row from both sides.	38
Figure 4.1. The schematic representation of shell balance for plug flow packed bed reactor.	41
Figure 5.1. Process gas temperature profile along the tube length with various number of segments.	53
Figure 5.2. Process gas temperature profile along the tube length with various temperature increment step size.	54

Figure 5.3. Process gas temperature profile along the tube length at various convergence tolerances.	56
Figure 5.4. Temperature profiles of tube outer wall and process gas through tube length at different Leva's constants.	59
Figure 5.5. Temperature profiles of tube outer wall and process gas through tube length at different effective gas temperatures.	60
Figure 5.6. Temperature profiles of tube outer wall and process gas through tube length at different effective gas temperatures and Leva's constants.	61
Figure 5.7. Species molar flow profiles through reformer tube for case 1.	68
Figure 5.8. Conversion profiles of methane and steam for case 1.	68
Figure 5.9. Temperature profiles for case 1.	69
Figure 5.10. Pressure profile through reformer tube for case 1.	69
Figure 5.11. Species molar flow profiles through reformer tube for case 2.	70
Figure 5.12. Conversion profiles of methane and steam for case 2.	70
Figure 5.13. Temperature profiles for case 2.	71
Figure 5.14. Pressure profile through reformer tube for case 2.	71
Figure 5.15. Species molar flow profiles through reformer tube for case 3.	72
Figure 5.16. Conversion profiles of methane and steam for case 3.	72
Figure 5.17. Temperature profiles for case 3.	73
Figure 5.18. Pressure profile through reformer tube for case 3.	73

LIST OF TABLES

Table 2.1. Typical reforming catalyst compositions and physical features.	6
Table 2.2. Commercial steam reformer catalysts.	7
Table 3.1. Reaction rate constant activation energies.	25
Table 3.2. Reaction equilibrium constant enthalpy changes of reactions.	25
Table 3.3. Species adsorption coefficient adsorption enthalpies.	25
Table 3.4. Reaction rate constant pre-exponential factors.	26
Table 3.5. Reaction equilibrium constant pre-exponential factors.	26
Table 3.6. Species adsorption coefficient pre-exponential factors.	26
Table 3.7. Corresponding forms of representative tube strips.	38
Table 4.1. Equivalent particle diameter for heat transfer calculations.	44
Table 4.2. Standard enthalpies of steam reforming reactions.	44
Table 4.3. Equivalent particle diameter and estimated void fractions for pressure drop calculations.	46
Table 5.1. Model end results at different number of segments.	52
Table 5.2. Model end results at different increment step sizes.	54
Table 5.3. Model end results at different convergence tolerances.	55
Table 5.4. Simulation results for $T_{fg} = T_{bw}$ at various heat transfer coefficients.	57
Table 5.5. Simulation results for $T_{fg} = T_{bw} + 100\text{ }^{\circ}\text{C}$ at various heat transfer coefficients.	58
Table 5.6. Simulation results for $T_{fg} = T_{bw} + 150\text{ }^{\circ}\text{C}$ at various heat transfer coefficients.	58
Table 5.7. Simulation results for $T_{fg} = T_{bw} + 200\text{ }^{\circ}\text{C}$ at various heat transfer coefficients.	58
Table 5.8. Tube outer wall temperature readings and model results using different parameters.	62
Table 5.9. Input variables for case studies.	64
Table 5.10. Process field data of simulation outputs.	64

Table 5.11. Solution parameters for case studies.	66
Table 5.12. Case 1 results. Plant data vs. model predictions.	66
Table 5.13. Case 2 results. Plant data vs. model predictions.	67
Table 5.14. Case 3 results. Plant data vs. model predictions.	67

LIST OF SYMBOLS

A	Area, m^2
$A(K)$	Pre-exponential factor for reaction equilibrium constant
$A(k)$	Pre-exponential factor of reaction rate coefficient
$A(K^0)$	Pre-exponential factor of adsorption constant
a	Friction factor parameter
A_{total}	Total surface area in fire box (refractory + tubes), m^2
$A_{refractory}$	Total refractory enclosure area, m^2
A_{tube}	External surface area of one tube, m^2
A_{tubes}	External surface area of all tubes, m^2
a_v	External particle surface area per unit reactor volume, $m^2_{particle} m^{-3}_{reactor}$
$a_{g,l}$	Temperature dependent emissivity weighting factors for the l th gray gas
b	Friction factor parameter
B	Ratio of tube center-to-center distance to diameter
b_{cs}	Catalyst bed cross sectional area, m^2
$b_{l,p}$	Emissivity polynomial coefficient p th order for the l th gray gas, Varying units
C_A	Concentration of reactant A, $kmol m^{-3}$
C_{cs}	Concentration on catalyst surface, $kmol m^{-3}$
C_{pg}	Concentration of process gas, $kmol m^{-3}$
$C_{p_{pg}}$	Heat capacity of process gas, $kJ kmol^{-1} K^{-1}$
C_s^s	Molar concentration at the solid surface, $kmol m^{-3}$
D_i	Tube inside diameter, m
D_o	Tube outside diameter, m
D_p	Equivalent particle diameter, m
z	Axial coordinate in reactor, m
E	Activation energy, $kJ kmol^{-1}$
f	Friction factor
E_b	Black body emissive power, W

F_i	Interception factor
F_{i-j}	View factor
F	Molar flow rate, kmol hr^{-1}
G	Irradiation, W m^{-2}
g_{rad}	Total transfer factor, m^2
H	Fire chamber height (tube height), m
h_c	Convective heat transfer coefficient, $\text{W m}^{-2} \text{K}^{-1}$
h_f	Heat transfer coefficient for film surrounding particle, $\text{W m}^{-2} \text{K}^{-1}$
h_w	Tube to process gas heat transfer coefficient, $\text{W m}^{-2} \text{K}^{-1}$
J	Radiosity, W m^{-2}
k	Number of carbon atoms in a hydrocarbon component
k_1, k_3	Reaction rate coefficients for reactions 1,3, $\text{kmol bar}^{1/2} \text{kgcat}^{-1} \text{h}^{-1}$
k_2	Reaction rate coefficients for reaction 2, $\text{kmol kgcat}^{-1} \text{h}^{-1} \text{bar}^{-1}$
K_1, K_3	Reaction equilibrium constants for reactions 1,3, bar^2
K_2	Reaction equilibrium constants for reaction 2
$K_{\text{CH}_4}, K_{\text{H}_2}, K_{\text{CO}}$	Species adsorption coefficients, bar^{-1}
$K_{\text{H}_2\text{O}}$	Dissociative adsorption constant of H_2O
k_g	Mass transfer coefficient from gas to solid interface, $\text{kmol m}^{-2} \text{bar}^{-1} \text{s}^{-1}$
k_i	Pressure absorption coefficient, $\text{atm}^{-1} \text{m}^{-1}$
k_w	Tube wall conductive heat transfer coefficient, $\text{W m}^{-1} \text{K}^{-1}$
L	Fire chamber length, m
L_m	Mean beam length, m
MW	Molecular weight, kg kmol^{-1}
N	Number of surfaces
n	Number of tubes
P	Pressure, bar
p	Partial pressure, bar
Pr	Prandtl's number
Q	Energy, W
q_{rad}	Radiant energy, W
R	Radiation network resistance, m^{-2}

R_g	Universal gas constant, $\text{m}^3 \text{ bar kmol}^{-1} \text{ K}^{-1}$
r	Rate of reaction per unit catalyst mass, $\text{kmol kgcat}^{-1} \text{ h}^{-1}$
S_{cat}	Catalyst surface area, m^2
T	Temperature, K
T_{cs}	Temperature of catalyst surface, K
T_{pg}	Temperature of process gas, K
T_r	Temperature of surrounding (heating medium), K
T_s^s	Temperature at the solid surface, m^2
U	Overall heat transfer coefficient, $\text{W m}^{-2} \text{ K}^{-1}$
u_{pg}	Superficial velocity of process gas, m s^{-1}
V_{cat}	Catalyst particle volume, m^3
W_d	Fire chamber width, m
W	Catalyst weight, kg
wt%	Weight per cent
y	y-axis of coordinate, m
z	Axial coordinate in reactor, m
ν	Species stoichiometric coefficient
σ	Stephan Boltzmann constant, $\text{W m}^{-2} \text{ K}^{-4}$
φ	Packed bed void fraction
ρ	Reflectivity
τ	Transmissivity
α	Absorptivity
λ	Wavelength, m
ε	Emissivity
$(+/- r)$	Production/consumption rate for each reaction, $\text{kmol kgcat}^{-1} \text{ hr}^{-1}$
$(+/- Rt)$	Overall production/consumption rate, $\text{kmol kgcat}^{-1} \text{ hr}^{-1}$
F_{r-t}	View factor from refractory to sink
$(-\Delta H_{rxn}^o)$	Standart reaction enthalpies, kJ kmol^{-1}
$\overrightarrow{Z_e Z_r}$	Directed flux area, m^2

$\overline{gs_r}$	Direct exchange area between gas to refractory, m ²
$\overline{gs_t}$	Direct exchange area between gas to tube, m ²
$\overline{s_r s_t}$	Direct exchange area between refractory to tube, m ²
$(-\Delta H_{rxn})$	Heat of reaction, kJ kmol ⁻¹
(α_{fg})	Flue gas absorptivity
$\Delta^{\circ}C$	Temperature difference, Celcius
Df_{hyd}	Hydraulic diameter of furnace chamber, m
Re_f	Furnace tube's Reynolds number
Re_p	Particle's Reynold Number
T_{wo}	Tube wall outside temperature, Celcius
ϵ_{eff}	Effective emissivity of furnace tubes
ϵ_{fg}	Flue gas emissivity
ϵ_{tube}	Real emissivity of furnace tubes
λ_{pg}	Thermal conductivity of process gas, W m ⁻¹ K ⁻¹
μ_{pg}	Viscosity, Pa s
ρ_{bed}	Catalyst bulk density, kgcat m ⁻³
ρ_{pg}	Density of process gas, kg m ⁻³
b	Black body
bw	Bridge wall
cat	Catalyst
cs	Catalyst surface
e	Emitter
fg	Flue gas
fg – t, r	Flue gas to tube with help of refractory
fg-r	Flue gas to refractory
fg-t	Flue gas to tube
ht	Heat transfer
i	Species index
i	Inside/Inner
in	Inlet

j	Reaction index
l	Number of gray gas components
o	Outside/Outer
out	Outlet
p	Number of temperature polynomial coefficients
part	Participating gases
pd	Pressure drop
pg	Process gas
r	Receiver
ref	Reference
r-t	Refractory to tube
t	Tube surface
w	Tube wall

LIST OF ACRONYMS/ABBREVIATIONS

CCR	Continious Catalytic Reformer
CFD	Computational Fluid Dynamics
CH ₄	Methane
CO	Carbon Monoxide
CO ₂	Carbon Dioxide
DEN	Denominator
H ₂	Hydrogen
H ₂ O	Water
K	Potassium (Potash)
KAlSiO ₄	Kalsilite
LPG	Liquefied Petroleum Gas
MgO	Magnesium Oxide
Ni	Nickel
NiO	Nickel Oxide
NO _x	Nitrogen Oxides
PSA	Pressure Swing Adsorption
PHD	Process Historian Database
SMR	Steam Methane Reforming
WGS	Water Gas Shift
WSGG	Weighted Sum of Gray Gases

1. INTRODUCTION

Hydrogen (H₂) is a promising energy carrier and an important feedstock in chemical industries especially in refineries. Conventionally, hydrogen is produced from fossil fuels and biomass via conversion technologies such as reforming (of hydrocarbons, oils and alcohols), gasifications (partial oxidation) and pyrolysis (of biomass/coal) while other conversion technologies such as electrolysis and photolysis are used in relatively smaller scales when the source of hydrogen is water (Subramani *et al.*, 2010).

The annual worldwide production of hydrogen is estimated to be more than 50 million metric tons with its consumption increasing by approximately 6% per year (Bicakova and Straka, 2012). Petroleum refineries hold great share in both hydrogen production and consumption. In refinery operations hydrogen is used to process crude oil into refined fuels, such as gasoline and diesel, and for removing contaminants, such as sulphur. Parallel to the common trend, hydrogen demand of refineries worldwide is continuously rising because of the need to process heavier and dirtier feedstocks, and of the objective to produce much cleaner transportation fuels that are almost free from sulfur to meet the strict environmental regulations. Processing of heavier and higher-sulfur crude oils will require greater amounts of hydrogen in the future (Subramani *et al.*, 2010).

Hydrogen required in refinery operations mostly comes from two sources, catalytic reformers and 'on-purpose' hydrogen plants, namely, steam reformers. Steam reforming is the reaction between steam and hydrocarbons, in the presence of steam reforming catalyst, to give a mixture of hydrogen, carbon monoxide, carbon dioxide, methane and unconverted steam. The expression reforming may be misleading since it is used also for the well-known process for improvement of the octane number of gasoline. In the gas industry, reforming has generally been used for steam reforming itself (Nielsen, 1984).

Steam reforming of hydrocarbons is undeniably the dominant route for industrial production of hydrogen. Typical feedstock range for steam reforming may vary from natural gas and LPG to liquid fuels including naphtha. Currently more than 80% of hydrogen is produced by steam reforming of natural gas followed by hydrogen separation, which is the

most economical option depending on the availability of natural gas (Gupta, 2009). Having been industrially practiced for over 80 years, steam reforming is a highly established process for converting natural gas and other hydrocarbons into synthesis gas (Stitt, 2003). Within the scope of this thesis, only steam reforming of natural gas, more specifically methane, will be considered in detail.

Commercially, steam methane reforming (SMR) is carried out by a sequence of net endothermic reactions in catalyst filled tubes placed in a specially designed furnace. Required energy is provided by burning natural gas and process off-gas, which is composed of mostly hydrogen and carbon monoxide, in the furnace. A detailed overview of the steam methane reforming process is given in Section 2.5.

The reformer furnace (i.e the reformer) is the primary unit in a steam reforming plant. The reformer can be considered in two separate sides, namely process and furnace sides, that interact with each other through exchange of energy by various mechanisms. The process side, i.e. inside of reformer tubes, consists of reactants, intermediates, products and packed bed of shaped reforming catalysts. The furnace side, except reactor tubes themselves, is composed of the combustion products contained within refractory wall enclosure. There is no material interchange among each side and only interaction between two sides is heat transfer.

Steam reformer tubes are one of the most expensive components of the plant. These tubes are made of metal alloys that face creep at elevated temperatures. Reformer tubes are designed with an expected operation life of ca. 100,000 hours. Possible tube failures due to long term creep formation can lead to expensive tube replacements, plant shut downs and production losses. The creep life is highly sensitive to changes in operation temperature and pressure in the tubes. As a rule of thumb, an increase in tube wall temperature of 20 °C will decay tube life expectancy by half for a given alloy at its design pressure (Saunders, 2014). Besides being vital for secure reformer service, temperature measurements in reformer plants can be an important tool in troubleshooting, debottlenecking and optimizing the plant's operations. Pushing the limits of an existing plant within operational limits for a higher output rate is highly desired.

Being motivated by these facts, the goal of this thesis is to develop a fundamental model that can calculate the outer tube wall temperature profile at specified process conditions of an industrial steam methane reformer plant in Tüpraş İzmit Refinery. Such a model is aimed to help plant engineers and operators to continuously predict the tube wall temperatures that are likely to occur on reformer tubes in order to avoid exceeding temperatures and predict outcomes of the reformer unit. In addition to wall temperature profiles and outlet stream compositions, the model is also able to predict pressure drop through packed bed, process gas temperature profile and tube wall heat flux profile.

This thesis is organized into five chapters, a conceptual introduction, methodology and literature survey, mathematical modeling studies, simulation results and discussion, recommendations and conclusions. Introduction to SMR concept gives an overview of SMR chemistry, SMR process and related issues. Methodology chapter covers the theoretical background of the models and similar studies in the literature. The chapter on mathematical modeling studies describes the development of the model for process and furnace sides together with the simplifying assumptions. Simulation results chapter provides model parameter evaluations and field results. Furthermore, theoretical behavior of constructed model is also considered. The conclusions chapter summarizes the main findings of this study, and suggests areas for model improvement and for future studies.

2. LITERATURE SURVEY

2.1. Chemistry and Thermodynamics of Steam Methane Reforming

Steam reforming of methane consists of three reversible reactions: the strongly endothermic reforming reactions, Equation 2.1 and Equation 2.3, and the moderately exothermic water-gas shift (WGS) reaction, Equation 2.2:

Steam-Methane Reforming Reaction:



Water Gas Shift Reaction:



Global Reaction:



Generic Reaction for C_nH_m :



The reforming reactions are reversible equilibrium reactions, which are also endothermic. High temperatures favor the conversion of such endothermic reactions and push the equilibrium towards product side of the equation. Additionally, the stoichiometric increase in moles of gas from reactants to products means lower pressure operation also favors higher conversion to the product side of the reaction. The water gas shift reaction is used to maximize conversion of the original feeds to hydrogen. Like reforming reactions, WGS is also an equilibrium reaction. However it is slightly exothermic, so equilibrium to a higher conversion toward the product side of the reaction is favored at lower temperatures. This reaction is unaffected by changes in pressure since the reaction stoichiometry is equimolar feed per product. Considering equilibrium natures and stoichiometries of these reactions, they are conducted in two separate reactors at different operating conditions in

industry. Consequently, due to equilibrium characteristics of SMR reactions, the reaction product composition is determined solely by thermodynamics, in the absence of additional limitations such as heat and mass transfer.

2.2. Steam Reforming Catalysts

In industrial practice, steam reforming of natural gas has been performed at high temperatures over Ni-based catalysts. Nickel has been the most applied active metal since it has sufficient activity for obviously low cost and wide availability. Apart from nickel, cobalt, platinum, palladium, irridium, ruthenium, rhodium have also been cited as other potential catalysts.

Regarding catalyst support materials (carriers), a variety of catalyst carriers are available with characteristics applicable to specific reformer design and operation. Typical catalyst supports, compositions and their physical features are provided in Table 2.1. Both refractory alumina and ceramic magnesium aluminate carriers offer high crush strength and stability, including maintenance of crush strength over long periods on stream. Calcium aluminate, a cement, is very hard and has high initial crush strength, but loses it by time under high pressure operation. Due to this reason calcium aluminate supports are used for relatively lower pressure applications.

Besides the active component and the carrier, promoters in small amounts, of a few per cent, play supporting roles in the activity of the catalysts. They can contribute to activity of catalyst in many ways such as poisoning protection, increasing thermal stability and favoring desired reaction pathways. As an example of promoters in steam reforming catalysts, especially in industrial examples, potash (K) is used for enhanced coke removal by accelerating coke's reaction with steam. Alkali metals also show features of increased selectivity and hindered crystal growth (Hagen, 2006) .

From an industrial point of view, great effort has been spent on steam methane reforming catalysts, since it has a great potential of improving steam reformer operation. Several studies are being conducted to address performance issues employing different

approaches, including catalyst preparation, promoter incorporation and support materials (Subramani *et al.*, 2010).

Table 2.1. Typical reforming catalyst compositions and physical features (Lloyd, 2011).

	Calcium Aluminate	α -Aluminate (Refractory)	Magnesium Aluminate
Composition (wt%)			
NiO	15-20	15-20	15-20
Al ₂ O ₃	65-70	80-85	60-65
CaO	10-15	-	-
MgO	-	-	15-20
Bulk Density (kg/m ³)	~1000	~800-900	~1000
Surface Area (m ² /g)	10-20	2-5	10-20

Commercial catalyst pellet design must satisfy several criteria, including high catalyst activity, good heat transfer characteristics, low pressure drop and high mechanical strength (Twiggs, 1989). In this respect, modern steam reformer catalyst pellet structures changed a lot from simple cylinders and rings to hollow bodies with some additional external features such as domes and flutes. Larger external surface area for favoring the access of reacting gas into the pellets leads to higher catalyst activity. In addition to improved catalytic activity, physical features directly affect heat transfer characteristics as well. Catalyst structure has to assure high heat transfer rates since uneven heat distribution can cause temperature gradients, which decrease the tube life span significantly. Enhanced heat transfer characteristics will play important role in resolving these issues, and will result in lower tube wall temperatures and longer tube life. Moreover, by the help of engineered catalysts, higher production rates can be obtained at the same pressure drop. Regarding transport and reactive characteristics of modern engineered catalyst shapes, more information can be found in literature (Taşkın, 2007), (Dixon *et al.*, 2008), (Dixon *et al.*, 2012). A number of industrial reforming catalysts are commercially available by companies such as Johnson Matthey, Südchemie, Haldor Topsøe, etc. A few examples are listed in Table 2.2.

Table 2.2. Commercial steam reformer catalysts (Nielsen, 2008).

Vendor	Commercial Name	Composition	Feed
Johnson Matthey (KATALCO™ Series)	57.4Q	Ni/ α -Al ₂ O ₃	Natural Gas
	25.4Q	Ni/CaAl ₂ O ₄ + K	Light Hydrocarbons
	46.3Q	Ni/KAlSiO ₄	Naphtha
Südchemie	G56H	Ni/ α -Al ₂ O ₃	Natural Gas
	G91	Ni/ α -Al ₂ O ₃ + K	Light Hydrocarbons
Haldor Topsøe	R67	Ni/MgAl ₂ O ₄ + K	Natural Gas
	RK201	Ni/MgO	Light Hydrocarbons
	RKNR	Ni/MgO	Natural Gas/Naphtha



Figure 2.1. Johnson Matthey's KATALCO™ series catalysts.

2.3. Steam Reforming Kinetics

Steam reforming chemistry is dated back to a century ago. Kinetic mechanisms of steam methane reforming have been extensively examined for variety of catalysts and a vast amount of kinetic equations have been reported in the literature since the 1950s (Hou, 1998). An overview of steam methane reforming kinetics has been provided in the literature (Subramani *et al.*, 2010).

Kinetic studies have been carried out with a variety of catalyst compositions, particle sizes, particle shapes and under wide ranges of temperature and pressure. There is no general

agreement on derived kinetic mechanisms in the literature due to the strong interaction between catalyst features and kinetic mechanisms. The change of catalyst composition, for instance, changes not only the structure of the kinetic model but also the values of the parameters in the kinetic model through changes in the mechanism (Soliman *et al.*, 1992). Therefore in order to obtain the best understanding of the mechanism of steam methane reforming on a specified catalyst, kinetic studies have to be carried out on purpose.

In literature, kinetic study reported by Xu and Froment (1989) is by far the most widely used one. In this study, experimental temperatures were in the range of 773-848 K for methane steam methane reforming. Other experimental conditions were pressures from 5-15 bar, a steam/methane ratio of 3-5 and a hydrogen/methane ratio of 1.25. Catalyst under investigation was nickel based catalyst supported on magnesium spinel with 15.2% Ni content. All three fundamental reactions, including water gas shift, were taken into consideration in this work. A large number of reaction mechanisms were tested, first by thermodynamic considerations and then by model discrimination and parameter estimation procedures. None of the reactions was taken to be at equilibrium. Based on the mechanism of an adsorption/surface reaction/desorption model in 13 steps assuming surface reactions were the rate controlling step, the rate equations in Section 3.1.3 were obtained (Xu and Froment, 1989).

2.4. Steam Methane Reformers

The steam reforming furnace can be handled in two parts, namely, radiant and convection sections. Radiant box of a steam reformer is a refractory enclosure including burners and reformer tubes. The convection section which is located on the top of radiant box on the flow direction of flue gas mixture, functions to recover waste heat of the combustion gases leaving the radiant section. The thermal efficiency of the tubular reformer and waste heat recovery section together approaches to ca. 95%, although only 50-60% of the heat can be transferred to the reactor tubes. Rest of the heat is recovered from the flue gas. The recovered heat is used for preheating of the reformer feed and, sometimes, of the combustion air, and for steam production (Nielsen and Christiansen, 2011).

Today, industrial type steam reformers are of four major types (Figure 2.2). Bottom, top and side fired reformers will be described in short while a detailed description will be provided for Terrace Wall™ type reformer, since it is the type that is under operation in İzmit Refinery.

2.4.1. Bottom Fired Steam Reformers

In this configuration, combustion gases and process gas flow in counter-current arrangement and achieves an almost constant heat flux profile along the length of the tubes. However, constant heat flux along the whole tube length is not optimal, considering high endothermicity at the entrance of the catalyst bed. This configuration results in high wall temperatures at the reactor exit (Wesenberg, 2006).

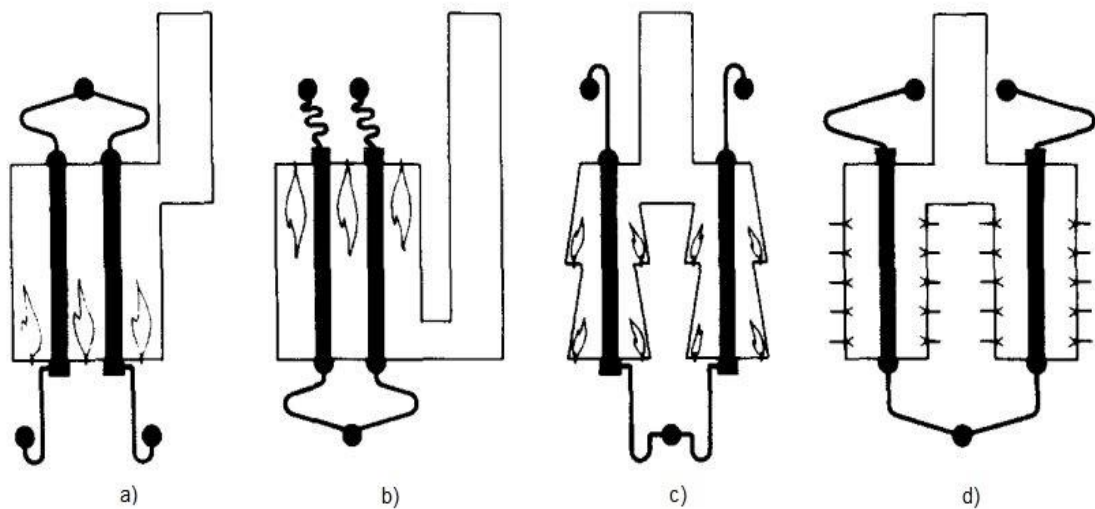


Figure 2.2. Steam reformer furnace configurations. a) Bottom-Fired, b) Top-Fired, c) Terrace-Wall™ d) Side-Fired (Dybkjaer, 1995).

2.4.2. Top fired steam reformers

In this furnace configuration, reactant gas mixture flows in the tubes co-currently with the combustion gases, since burners are located on the top refractory wall and firing downward. Owing to the fact that burners are located near the reactor inlet point, where the heat flux demand is highest, it is a reasonable configuration approach. Besides this, due to

catalyst aging from inlet to outlet by time, the zone where heat flux is highly required migrates downwards by time. The high flux zone can also be moved accordingly by adjusting flame lengths. Flame lengths from such burners can be adjusted from 1 meter to 3 meters to place the high heat flux zone where desired. It must be noted that, both in bottom and top fired furnaces, there is a serious flue gas temperature gradient in the direction of firing through combustion chamber (Quon, 2012).

2.4.3. Side fired steam reformers

In side fired furnace configuration, banks of reformer tubes are located between vertical refractory walls on which numerous burners are present forming a vertical and horizontal grid. Compared with top and bottom fired configurations, such a burner positioning provides higher flexibility of adjusting heat flux profile on reformer tubes. Moreover, grid formation of burners result in significant advantage on NO_x control during the combustion process since it allows shorter flame lengths in comparison to top fired designs. However, such a design results in higher equipment costs due to higher complexity of the grid type burner control system to ensure evenly distributed heat flux (Quon, 2012) .

2.4.4. Terrace wall TM steam reformers

Briefly, Foster Wheeler's proprietary Terrace WallTM design features a vertical radiant section consisting of an enclosure of sloped refractory walls, containing a single verticle row of tubes in the middle with burners on either side of the tubes arranged in two terrace levels. Hot flue gases from burners flow naturally upwards into the convection section providing true counter-current heat transfer for improved radiant efficiency. The convection section has several coil sections, which recover heat from the flue gas leaving the radiant section for various process and utility duties.

The burners fire vertically upward along the refractory-lined walls of the radiant section, essentially parallel to the catalyst tubes, to assure flame stability even with very lean fuels such as PSA tail-gas, and to avoid flame impingement. The burners provide a flat-shaped flame vertically along the brick firing wall and are suitably spaced along the length of the firebox, assuring uniform heat input to the catalyst tubes. Considering all, the sloped

refractory wall essentially becomes a uniform heat re-radiating plane with no discontinuity along the tube length (Bressan and Davis, 2014).



Figure 2.3. Inside of Terrace Wall TM steam reformer radiant box.

With catalyst tubes typically 11 to 14 meters long, control of vertical heat distribution along the tube lengths is typically obtained by providing two levels of burners. Each terrace is capable of being independently fired to provide the particular heat flux desired in a given zone. Besides, sloped walls also contribute to uniform vertical flux profile since the distance from the tube to the radiating wall decreases as the flue gas cools. These provide ability to control heat input as process conditions, such as catalyst activity, vary during operation (Foster Wheeler, 2006).

In addition to the radiation effects, the double firing on sloped firing walls and the multiple level burners firing upward and adjacent to the sloped refractory wall provide highly predictable and desirable flue gas recirculation patterns as shown in Figure 2.4. This effect also matches the desired design feature of a “well stirred box” again assisting in the uniform and predictable heat flux profile as can be seen in Figure 2.5 (Basse, 2014).

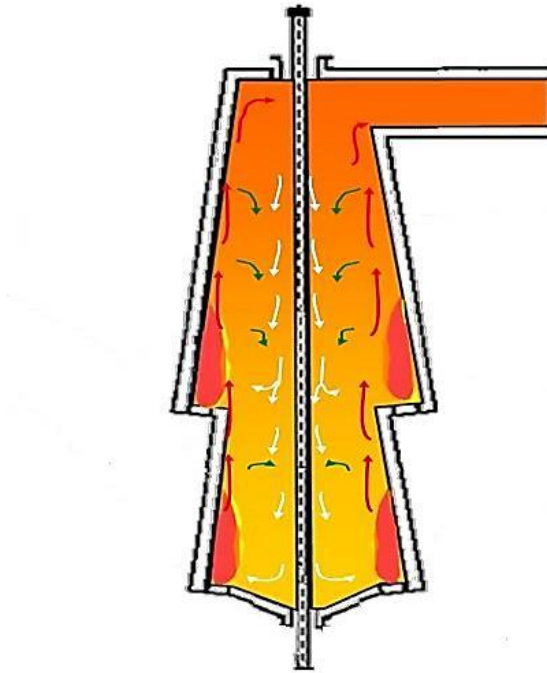


Figure 2.4. Combined effects of slightly sloped walls and upward firing burners on flue gas recirculation patterns (Basse, 2014).

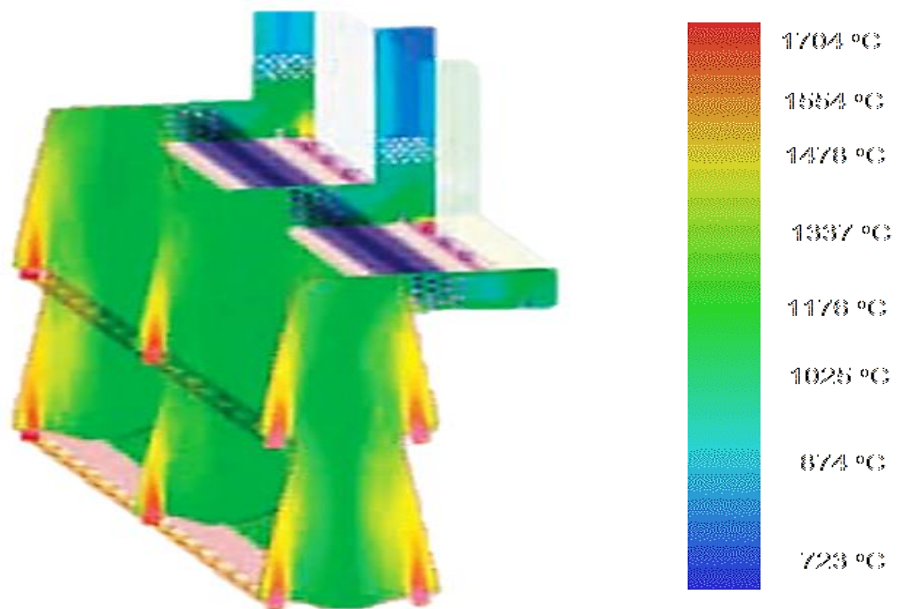


Figure 2.5. Computational Fluid Dynamics (CFD) modeling study result supporting the well-stirred furnace effect of flue gas recirculation flow patterns (Toolsee and Patel, 2006).

Heat flux profile over tube circumference brings additional important consideration into system. It is desired to have uniform circumferential heat flux with minimal angular variation for the sake of tube material durability. Tube and burner arrangement as well as tube spacing, due to shielding effect, have great impact on circumferential heat flux distribution. Firing from both sides and 1.4 to 1.7 tube pitch ratio (ratio of tube center to center distance to tube outside diameter) provides optimal distribution of heat flux (Foster Wheeler, 2006).

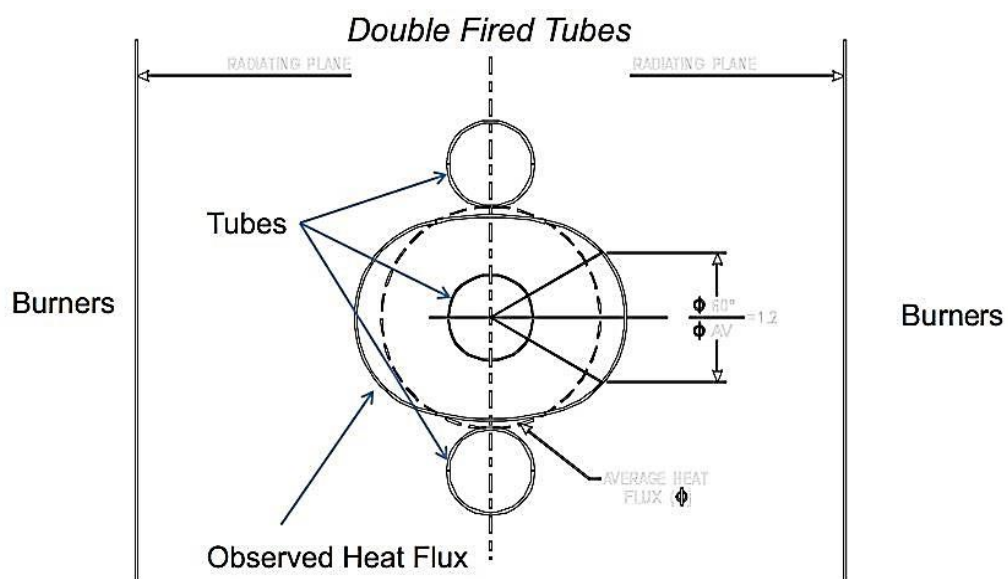


Figure 2.6. Circumferential heat flux profile for double fired tubes (Foster Wheeler Fired Heater Division, 2006).

2.5. Steam-Methane Reforming Process Overview

The steam reforming plants consist of four basic sections:

- (i) Feedstock Treatment: Feedstock is treated to be almost free of sulphur and other contaminants.
- (ii) Steam Methane Reformer: Heart of the plant, catalytic tubular reactors placed in a furnace converting feedstock into syngas at high temperatures and moderate pressures.
- (iii) Shift Reactors: This section works for syngas heat recovery and incorporates water-gas-shift reactors to increase the hydrogen yield.

- (iv) Hydrogen Purification: In order to achieve final product purity, process effluent is purified by employing pressure swing adsorption (PSA) unit.

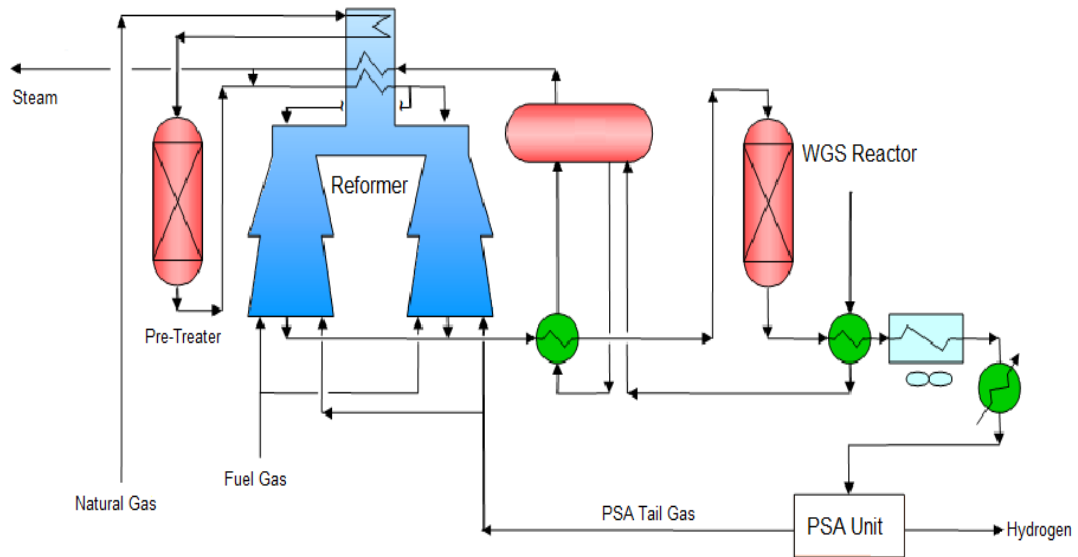


Figure 2.7. Tüpraş hydrogen unit simplified process flow diagram (Caranno & Nava, 2005).

2.5.1. Feed preparation section of steam reformer

On the process side of a steam methane reforming plant, the hydrocarbon feed must be pretreated before it is sent to the reformer. The hydrocarbon feed is first mixed with recycled hydrogen from Continuous Catalytic Reforming (CCR) unit. The mixed feed is first preheated by heat recovered from gases exiting the reformer. The hydrogen enriched feed is then sent to a pre-treater (hydrotreater) where a cobalt-molybdenum or nickel-molybdenum catalyst is used to hydrogenate olefins and to convert organic sulfides into hydrogen sulfide. Olefins are removed from the process side feed to prevent cracking and carbon formation on the catalyst in the catalyst beds, and organic sulfides are removed to prevent reformer catalyst poisoning (Baade *et al.*, 2001). Later, the process side feed is passed through a zinc-oxide bed to remove the hydrogen sulfide. The dry feed is then mixed with steam, resulting in a molar steam to carbon ratio between 1 and 4. The process side feed is heated to around 565 °C using recovered heat before it is sent to the tube side of the reformer (Nielsen, 1984).

2.5.2. Reactor section of steam reformer

The treated feed is preheated in convection section before being joined by preheated steam. Hydrogen, hydrocarbon and steam mixture (process gas) enters the reformer tube from top of the furnace and flows downwards through number of catalyst filled tubes. The outer diameter of the tubes ranges typically from 10 to 15 cm. Inside of tubes, the reactions are catalyzed by a nickel based catalyst and are predominantly endothermic. Typical inlet temperatures are 450-650 °C and the product gas leaves the reformer at 850-950 °C while the operating pressure is over 20 atm. The thermal efficiency of the tubular reformer is quite high, i.e. above ca.90%. Heat leaving the radiant section to convection section is recovered as waste heat, which is used for steam production (Nielsen, 2008). The heat needed to drive the endothermic reactions is provided by the combustion of fuel on furnace side. Reformer internal configuration depends on the type of reformer furnace. Regarding Terrace-Wall™ type reformer, tubes are located vertically between inclined refractory walls adjacent to which two rows of burners are lined up on both sides of the tubes at two different levels. Reformer types, phenomenon occurring inside reformer tubes are discussed in Section 2.6.

2.5.3. Furnace section of steam reformer

Furnace side of the reformer is conceptually simpler than the process side. In addition to being a feedstock, natural gas can also be used as a fuel in the furnace. Furthermore, off-gas from the PSA unit (tail gas) is also fed to the furnace. The tail gas contains combustible species, such as carbon dioxide, hydrogen and methane, which are separated from the process-side effluent after purification section. Furnace fuels are mixed with excess combustion air in the burners (typically 10-15% for natural draft furnaces) at the side walls of the furnace. The furnace gas exists the reformer radiant section at approximately 900 °C, depending on the reformer type, load, etc. Profitable operation of a SMR plant requires the recovery of heat from the flue gas. Excess heat from the furnace gas is used to preheat the process side feed streams and to generate steam to be used in refinery steam ring.

2.5.4. Product purification section

The process gas exits the reformer as a near equilibrium mixture of hydrogen, carbon monoxide, carbon dioxide, steam and methane under normal operation. The process effluent is cooled to approximately 370 °C and the waste heat is recovered (Baade *et al.*, 2001). In the absence of catalyst, no further reaction takes place. The process effluent is then sent to a water gas shift reactor (shift converter (Figure 2.7)). The shift converter increases the hydrogen percent in the effluent by converting carbon monoxide and water into hydrogen and carbon dioxide. After shift converter, the effluent mixture is cooled to less than 120 °C and flashed into a separation drum. Nearly all of the steam in the effluent condenses and is collected for use as boiler feed water. The product stream is now in dry basis. The uncondensed process effluent is cooled to around 40 °C and sent to the pressure swing adsorber (PSA). PSA uses a series of adsorption beds to separate hydrogen from the remaining gas species (methane, carbon monoxide, carbon dioxide, nitrogen and hydrogen), which are collected as tail gas to be used as fuel in the furnace. The purified hydrogen gas is the main product of the SMR plant.

2.6. Fundamental Phenomena in Steam Methane Reforming Processes

In the background of industrial steam methane reformer, there is a highly complex network of simultaneous physical and chemical phenomena. These phenomena are to be identified separately for two sections of a steam reformer.

2.6.1. Furnace side phenomena

Energy required to drive catalytic steam reforming reactions comes from the combustion side of the furnace. The internal energy stored in the chemical bonds of the furnace fuels is released as the fuel combusts to combustion products and increases their temperature. In Terrace-Wall™ furnaces, fuels combust with air in the burners adjacent to sloped walls and flue gas mixture moves upwards through the combustion chamber.

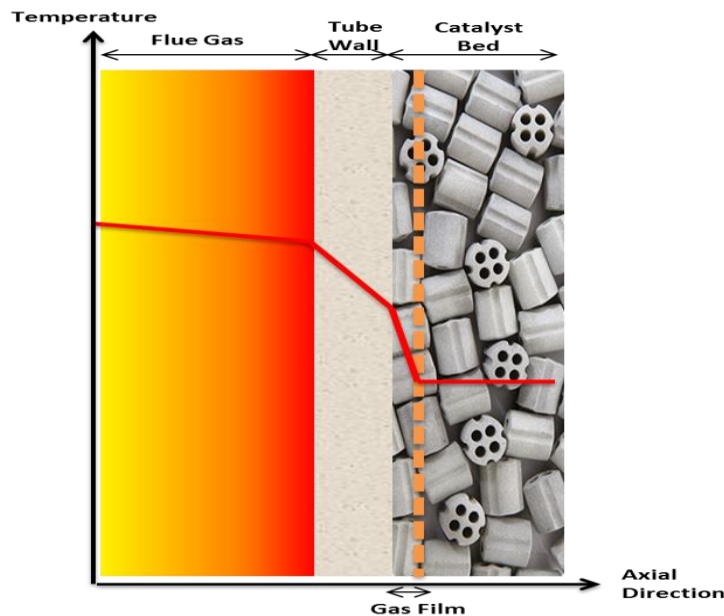


Figure 2.8. Representative local temperature distribution profile in the furnace as the result of heat interaction between furnace gas and catalytic reactions.

Energy released by the combustion of furnace fuels can leave the enclosure in three distinct ways. First, as per purpose, through tube wall to the catalytic side of reactor. Secondly, as loss, through the refractory wall to ambient and third, by bulk motion of flue gas to convection section, which is to be mostly recovered afterwards. At high temperatures, the dominant mode of heat transfer to the tubes and refractory is radiation. Meanwhile convection also contributes to heat transfer. The refractory transfers energy by conduction to the ambient, and receives energy by radiation and convection from combustion gases.

Net energy incident on the outer surface of the tubes travels by conduction through the thickness of tube wall. The inside tube surface is in direct contact with the stationary catalyst particles and process gas mixture in motion. The dominant modes of heat transfer inside of the tubes are conduction from the inner tube walls to the catalyst and through the bed of catalyst particles, convection from the inner tube wall to the process gas, and convection between the process gas and the catalyst particles. Since rigorous evaluation of these effects is clearly sophisticated and infeasible, experimental determination via empirical approach has been followed as described in Section 3.1.4. This is done for heat transfer through the fictitious gas film layer formed on the inner tube surface as demonstrated in Figure 2.8.

2.6.2. Process side phenomena

As described earlier, structured catalyst particles are randomly filled into steam reformer tubes to form the packed bed of catalysts, shown in Figure 2.9. As the feed gas mixture enters reformer tubes, catalytic reactions occur by a series of incidents taking place among the porous catalyst phase and bulk phase. This process taking place on the catalyst may be broadly subdivided into the following separate steps:

- (i) Transport of reactants and energy from the bulk fluid up to the catalyst pellet exterior surface, to say, particle boundary layer, macropores and micropores.
- (ii) Transport of reactants and energy from the external surface into the porous pellet.
- (iii) Adsorption (chemisorption), chemical reactions of species with active sites, and desorption of products from catalyst active sites.
- (iv) Transport of products from the catalyst interior to the external surface of the catalyst pellet and transport of products into the bulk fluid.

The simultaneous occurrence of transport processes along with chemical reaction on active sites in reality lead to concentration and temperature gradients within the pellet, between the catalyst surface or both. This issue gains importance for exothermic reactions, especially when the run-away conditions may occur. For endothermic steam reforming reactions, such gradients may be neglected till some point.

For catalytic reactions in particular, usually one or at most two of the five steps mentioned can be slow relative to other steps, and may have rate determining effect on overall rate of the reaction in the pellet. Briefly, the reaction is intraparticle transport controlled (diffusion limited), if transport of reactants into catalyst surface is slow. The reaction is surface reaction controlled, if the surface reactions are slow. Finally, the process is external transport controlled if the diffusion of the species across the boundary layer is the slowest step. Although catalytic steam reforming reactions are reported to be diffusion limited (Pantoleonos *et al.*, 2012), Xu and Froment's intrinsic kinetics are used in the modeling scheme to be described in Chapter 3.

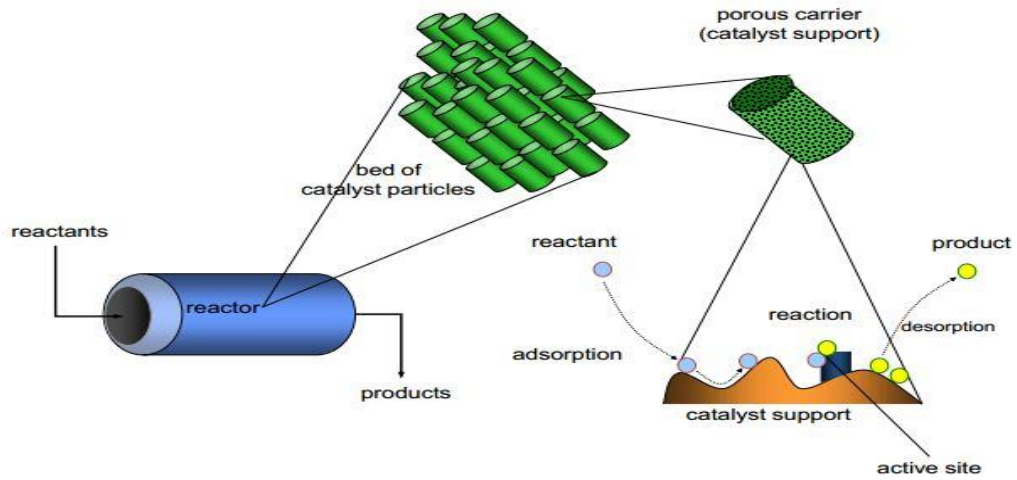


Figure 2.9. Catalytic reaction phenomena in packed bed reactors (Rothenberg, 2008).

2.7. Available Data

Plant instruments constantly measure and collect process parameters. The data collected in real time can be retrieved from historical database. The available variables in real time are the temperatures, pressures, and flow rates of feed and fuel streams flowing into reformer, temperature, pressure and flow rate of reformer outlet stream and reformer fire box bridge-wall temperature. Data regarding inlet and outlet flow compositions are tested all together once in a month. Furthermore, tube wall temperatures are measured by pyrometers from peepholes twice in a day (morning & night). These measurements are manually logged and can be matched with the historical hourly data. In this perspective, a whole data set that the model can be tested with is available.

3. METHODOLOGY

The earliest steam reforming modeling studies commenced in 1960s. Reformer models available in the literature show differences that come from the assumptions used to describe steam methane reformer. Briefly, process side models can be distinguished by their considerations for axial and radial gradients, by the assumption types for mass transfer, reaction kinetics, pressure drop, flow patterns and fixed bed heat transfer characteristics. Meanwhile furnace side models can be classified by their sub-models to describe radiative heat transfer, convective heat transfer correlations, combustion patterns and flue gas flow patterns. Within the scope of this thesis, only related methods/models will be described with some detail, while remaining will either be discussed in short or uncovered.

3.1. Packed Bed Reactor Models

Reactor model should include sufficient representation of essential mechanisms involved in order to successfully describe the system. Meanwhile, it is desired to be as simple as possible, since the mathematical approaches become more complex as number of distinct mechanisms increase. In this respect, reduction of mechanisms that are not essential for the reactor performance may help in reducing the degree of sophistication. The fixed bed reactor models are grouped in two broad categories, namely pseudo homogeneous and heterogeneous models. Pseudo homogeneous models do not account explicitly for the presence of catalyst, unlike heterogeneous models, which lead to separate conservation equations for fluid phase and fluid inside catalyst pores. The distinction is based on an analysis of difference in temperature and concentration from the process gas (pg) to the catalyst surface (cs) (Toledo *et al.*, 2011), (Froment *et al.*, 2011).

For pseudo homogeneous models, $T_{pg} = T_{cs}$ and $C_{pg} = C_{cs}$, both of which mean that catalyst surface is totally exposed to bulk conditions so there is no fluid to particle heat and mass transfer resistances. However, for heterogeneous model, $T_{pg} \neq T_{cs}$ and $C_{pg} \neq C_{cs}$. Subtypes of the packed bed reactor models are shown in Figure 3.1 (Froment *et al.*, 2011).

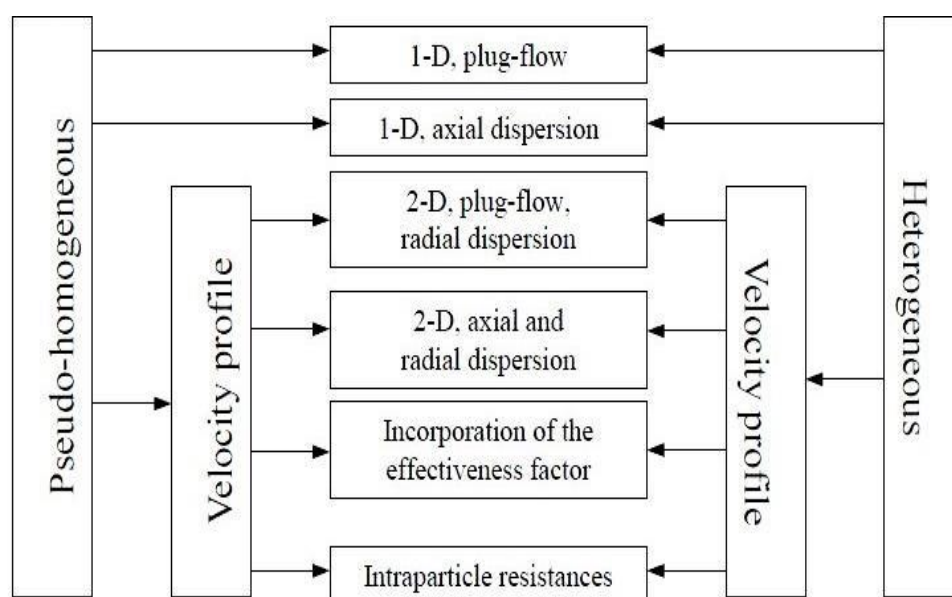


Figure 3.1. Classification of fixed bed reactor models (Iordanidis, 2002).

The design of fixed catalyst bed tubular reactors has generally been based on one dimensional models which consider only axial changes along the reactor. However, in many real cases, radial gradients, such as temperature and concentration can be present. Regarding steam methane reactions, which is a combination of net endothermic reactions, neglecting radial gradients in the bed is a plausible approach as described in Chapter 2. As an example, Wesenberg and Svendsen in their two-dimensional study of a gas heater reformer concluded that the radial heat transport in tubular packed beds of reformer is rapid resulting in flat radial profiles (Wesenberg and Svendsen, 2007). Furthermore, considering small tube diameters with high gas flow rates inside also favors the use of plug flow models. In this perspective, only one dimensional homogeneous and heterogeneous models will be described with some detail.

3.1.1. One dimensional pseudo-homogeneous model

Pseudo-homogeneous one dimensional model only considers transport by plug flow in the axial direction since the only transport mechanism operating in that direction is accepted to be the overall flow itself. According to this model, gas-solid film heat and mass transport rates are much faster than surface reactions. Since gas moves in plug motion, it describes only axial profiles of radially averaged concentrations and temperatures. The physical

properties of the fluid are assumed to be constant in each cross section differential throughout the reactor. In addition, some type of mixing in the axial direction may be superposed on the plug flow in order to approach non ideal flow conditions (Froment *et al.*, 2011).

Pseudo-homogeneous models require global (apparent) rate expressions. Under conditions where no gradients occur between catalyst phase and reactant medium, the global reaction rate becomes intrinsic reaction rate, which is evaluated at the bulk fluid composition and temperature. When such differences become important, global reaction rate is likely to be higher or lower than the intrinsic rate. For steady state and a single reaction ($A \rightarrow \text{Products}$) carried out in a cylindrical tube, the conservation equations of one dimensional plug flow can be expressed as the set of the following ordinary differential equations (Froment *et al.*, 2011):

Mass Balance:

$$-\frac{d(u_{pg}C_A)}{dz} = r_A\rho_{bed} \quad (3.1)$$

Energy Balance:

$$u_{pg}\rho_{pg}c_{p_{pg}}\frac{dT}{dz} = (-\Delta H_{rxn})r_A\rho_{bed} - 4\frac{U}{D_i}(T_{pg} - T_r) \quad (3.2)$$

Momentum Balance:

$$-\frac{dP}{dz} = f\frac{\rho_{pg}u_{pg}^2}{D_p} \quad (3.3)$$

with the following initial conditions: At $z=0$, $C_A = C_{A_{in}}$, $T_{pg} = T_{pg_{in}}$, $P_{total} = P_{in}$.

In literature, one dimensional pseudo-homogeneous models have been extensively used by authors (Singh and Saraf, 1979), (Murty and Murthy, 1988). Within the scope of this thesis, one dimensional homogeneous model is used and derivation of the model equations used are given in Chapter 4.

3.1.2. One dimensional heterogeneous model

For the use of highly active catalysts results in very rapid reactions which eventually cause an important heat effect, it may be necessary to implement more detailed models (Toledo *et al.*, 2011). The heterogeneous model considers only transport by plug flow again, but distinguishes between conditions in the fluid and on the solid by accounting gas-solid film transfer effects. For a single reaction ($A \rightarrow \text{Products}$) carried out in a cylindrical tube, conservation equations become the set of ordinary differential and algebraic equations as shown below:

For the fluid phase:

$$-u_{pg} \frac{dC_A}{dz} = k_g a_v (C_A - C_s^s) \quad (3.4)$$

$$u_{pg} \rho_{pg} c_{p_{pg}} \frac{dT}{dz} = h_f a_v (T_s^s - T_{pg}) - 4 \frac{U}{D_i} (T_{pg} - T_r) \quad (3.5)$$

For a cross section of the bed including solid and fluid:

$$\rho_{bed} r_A = k_g a_v (C_A - C_s^s) \quad (3.6)$$

$$(-\Delta H) \rho_{bed} r_A = h_f a_v (T_s^s - T_{pg}) \quad (3.7)$$

With boundary conditions at $C_A = C_{A_{in}}, T_{pg} = T_{pg_{in}}$.

One dimensional heterogeneous models have been used in steam reformer modeling literature and used by some authors (Plehiens and Froment, 1989), (Zamaniyan *et al.*, 2008). Heterogeneous models also consider the gradients inside the catalyst bed, in other words intraparticle gradients, in addition to interfacial gradients expressed above (Froment *et al.*, 2011).

3.1.3. Steam methane reforming kinetics for modeling

As discussed in Section 2.3, steam reforming show different characteristics over different catalysts. Since such kinetic model is not available for an industrial type catalyst in hydrogen unit of TÜPRAŞ İzmit Refinery, the most widely accepted Xu and Froment's Langmuir-Hinshelwood (Houghen-Watson) type kinetic model of has been chosen as reference (Xu and Froment, 1989). In literature, Xu and Froment's kinetics have been used by majority of authors (Soliman *et al.*, 1988), (Plehiens and Froment, 1989), (Pedernera *et al.*, 2003), (Wesenberg and Svendsen, 2007).

Steam-Methane Reforming Reaction Rate:

$$r_1 = \frac{k_1 (p_{CH_4} p_{H_2O} - p_{H_2}^3 \frac{p_{CO}}{K_1})}{p_{H_2}^{2.5} (DEN^2)} \quad (3.8)$$

Water Gas Shift Reaction Rate:

$$r_2 = \frac{k_2 (p_{CO} p_{H_2O} - p_{CO_2} \frac{p_{H_2}}{K_2})}{p_{H_2} (DEN^2)} \quad (3.9)$$

Global Reaction Rate:

$$r_3 = \frac{k_3 (p_{CH_4} p_{H_2O}^2 - p_{CO_2} \frac{p_{H_2}^4}{K_2})}{p_{H_2}^{3.5} (DEN^2)} \quad (3.10)$$

$$DEN = 1 + K_{CO} p_{CO} + K_{H_2} p_{H_2} + K_{CH_4} p_{CH_4} + K_{H_2O} p_{H_2O} / p_{H_2} \quad (3.11)$$

Reaction Rate Coefficient:

$$k_i = A(k_i) \cdot \exp\left(\frac{E_i}{R \cdot T}\right) \quad (3.12)$$

Reaction Equilibrium Coefficient:

$$K_i = A(K_i) \cdot \exp\left(\frac{\Delta H_i}{R \cdot T}\right) \quad (3.13)$$

Species Adsorption Coefficient:

$$K_j = A(K_j^0) \cdot \exp\left(\frac{\Delta H_j}{R \cdot T}\right) \quad (3.14)$$

In Equations (3.8)-(3.14) i is reaction index (SMR, WGS, Global) and j stands for species index (CH₄, H₂O, CO, H₂). Kinetic parameters of the steam methane reforming reaction rates are given in Tables (3.1)-(3.6) below:

Table 3.1. Reaction rate constant activation energies (Xu and Froment, 1989).

Activation Energy		Unit
E ₁	240100	kJ/kmol
E ₂	67130	kJ/kmol
E ₃	243900	kJ/kmol

Table 3.2. Reaction equilibrium constant enthalpy changes of reactions (Xu and Froment, 1989).

Standart Reaction Enthalpies		Unit
ΔH ₁	206100	kJ/kmol
ΔH ₂	-41150	kJ/kmol
ΔH ₃	164900	kJ/kmol

Table 3.3. Species adsorption coefficient adsorption enthalpies (Xu and Froment, 1989).

Species Adsorption Enthalpies		Unit
ΔH _{CH₄}	-38200	kJ/kmol
ΔH _{H₂O}	88680	kJ/kmol

Table 3.3. Species adsorption coefficient adsorption enthalpies (cont.).

Species Adsorption Enthalpies		Unit
ΔH_{H_2}	-82900	kJ/kmol
ΔH_{CO}	-70650	kJ/kmol

Table 3.4. Reaction rate constant pre-exponential factors (Xu and Froment, 1989).

Pre-Exponentials		Unit
A(k ₁)	4.225 E+15	kmol bar ^{1/2} kg ⁻¹ h ⁻¹
A(k ₂)	1.99 E+06	kmol bar ⁻¹ kg ⁻¹
A(k ₃)	1.020 E+15	kmol bar ^{1/2} kg ⁻¹ h ⁻¹

Table 3.5. Reaction equilibrium constant pre-exponential factors (Xu and Froment, 1989).

Pre-Exponentials		Unit
A(K ₁)	4.707 E+12	bar ²
A(K ₂)	1.142 E-02	-
A(K ₃)	5.375 E+10	bar ²

Table 3.6. Species adsorption coefficient pre-exponential factors (Xu and Froment, 1989).

Pre-Exponentials		Units
A(K ^o _{CH₄})	6.65 E-04	bar ⁻¹
A(K ^o _{H₂O})	1.77 E+05	bar ⁻¹
A(K ^o _{H₂})	6.12 E-09	-
A(K ^o _{CO})	8.23 E-05	bar ⁻¹

Apart from Xu and Froment's kinetics, reaction kinetics proposed by Avetnisov and Kou can also be used in a similar manner (Hou, 1998), (Zyskin *et al.*, 2007).

3.1.4. Tube to process gas heat transfer coefficient (h_w)

Tube to process side heat transfer coefficient, h_w , is implemented to determine the heat transfer rate between tube inner wall temperature and the combined catalyst and process gas medium. It is designated experimentally by observing heat transfer rates in tubular systems filled with different packing materials and shapes at various flow conditions. The main characteristic of most wall heat transfer coefficients is that they are observed under non-reacting conditions where various packing shapes are in contact with hot air, in other words, where system works as a heat exchanger rather than a reactor. This situation leads to a fitting procedure unless correlation is structured for a specified system. The other characteristic is, wall Nusselt's number, Nu_w , is smoothly correlated with particle Reynold's number, Re_p (Beek, 1962). Very comprehensive information can be found in literature (Wakao and Kagueli, 1982), (Kulkarni and Doraiswamy, 1980). In one dimensional homogeneous packed bed reactor models, Beek's correlation and Leva and Grummer's correlation are commonly used, considering convection as the dominant heat transfer mechanism.

Particle Reynold's number:

$$Re_p = \frac{D_p \cdot u_{pg} \cdot \rho_{pg}}{\mu_{pg}} \quad (3.15)$$

Prandtl's number:

$$Pr = \frac{\mu_{pg} \cdot Cp_{pg}}{\lambda_{pg}} \quad (3.16)$$

Leva and Grummer's correlation (Leva and Grummer, 1948):

$$h_w = constant \cdot 0.813 \cdot \frac{\lambda_{pg}}{D_i} \cdot \exp\left(-6 \frac{D_p}{D_i}\right) \cdot (Re_p)^{0.9} \quad (3.17)$$

Beek's correlation (Beek, 1962):

$$h_w = constant \cdot \frac{\lambda_{pg}}{D_p} (2.58 \cdot Re_p^{0.33} \cdot Pr^{0.33} + 0.094 \cdot Re_p^{0.8} \cdot Pr^{0.4}) \quad (3.18)$$

Constant parameter in both equations can be used as fitting parameter to field values by covering the effects of catalyst bed thermal conductivity, catalyst particle shape and

packing structure. As an example, Hyman calculated the convective heat transfer coefficient for an industrial reformer with Rasching rings was 40% of the value calculated by Beek's correlation. Beek's correlation is implemented by (Hyman, 1968), (Singh and Saraf, 1979), (Murty and Murthy, 1988), (Sankararao and Lee, 2012), (Ghouse and Adams II, 2013). Leva and Grummer's correlation is used by (Soliman *et al.*, 1988), (Yu *et al.*, 2006). Besides, there are other correlations developed for heterogeneous and two dimensional systems which are not covered here and used by (Zamaniyan *et al.*, 2008), (Pedrnera *et al.*, 2003).

3.1.5. Furnace gas to tube convective heat transfer coefficient (h_c)

In industrial steam reformers, due to elevated combustion chamber temperatures, radiation is the dominant mechanism of heat transfer from flue gas to reformer tube. In modeling studies, convective contribution may be included but neglected by many authors. In steam reformer literature, two correlations proposed by Dittus Boelter (McCabe *et al.*, 2001) and Geankoplis (Geankoplis, 1983) come into prominence:

Furnace tube Reynold's number :

$$Re_f = \frac{Df_{hyd} \cdot u_{fg} \cdot \rho_{fg}}{\mu_{fg}} \quad (3.19)$$

Prandtl's number:

$$Pr_f = \frac{Cp_{fg} \cdot \mu_{fg}}{\lambda_{fg}} \quad (3.20)$$

Dittus Boelter Correlation:

$$h_c = \frac{\lambda_{fg}}{Df_{hyd}} \cdot (0.023 \cdot Re_f^{0.8} \cdot Pr_f^{0.33}) \quad (3.21)$$

Geankoplis correlation :

$$h_c = 0.163 \cdot (Re_f^{0.632} \cdot Pr_f^{0.33}) \quad (3.22)$$

Among examples who included convection, Dittus Boelter correlation was used by (Murty and Murthy, 1988), (Yu *et al.*, 2006) while Geankoplis correlation was chosen by (Zamaniyan *et al.*, 2008), (Sanaye and Baheri, 2007).

3.1.6. Pressure drop in packed bed reactors

The pressure drop in steam reformer tubes may be neglected due to stoichiometric volume expansion but a complete reformer model should include this issue. Pressure drop in fixed bed tubular reactors can be calculated by using the momentum balance (Froment *et al.*, 2011). The form of the momentum balance can be regarded as fixed, the adjustability of the equation comes from the friction factor, f . Friction factor, just like heat transfer coefficients, is an experimentally measured and empirically correlated function of system parameters. Besides being related to flow characteristics, the main features of friction factor are its strong dependence on particle shape (e.g. hollow cylinder, sphere) and also on the bed properties, i.e. void fraction. The most commonly used friction factor in literature by far is that of Ergün (Ghouse and Adams II, 2013), (Plehiens and Froment, 1989), (Latham, 2008):

$$f = \frac{(1 - \varphi)}{\varphi} \cdot \left(a + \frac{b \cdot (1 - \varphi)}{Re_p} \right) \quad (3.23)$$

In Ergün equation, $a=1.75$ and $b=150$. Hicks found that the Ergün equation does not predict pressure drop for industrial steam reformers well since flow regime is highly turbulent (Froment *et al.*, 2011). Friction factor can also be calculated by the Hick's correlation (Froment *et al.*, 2011).

$$f = 6.8 \cdot \frac{(1 - \varphi)^{1.2}}{\varphi^3} \cdot Re_p^{-0.2} \quad (3.24)$$

Wesenberg and Svendsen made comparison for pressure drop prediction from Ergün and Hicks friction factors. They have found that Hicks factor gives smaller pressure drop which is more suitable for industrial steam reformers (Wesenberg and Svendsen, 2007).

3.2. Furnace Models

Model accuracy of thermal radiation in furnaces is highly important for prediction of product quality, production rates and overall thermal efficiency. Due to the multi-dimensional nature of radiation, prediction of radiative transfer of heat is a complex task. Particularly, in a furnace for instance, it depends on many factors including component positions, geometries, local temperature and compositions. All techniques available involve different approaches as described in the introduction of this chapter. Combustion and flow pattern issues will be out of interest due to the model structure according to purpose. Only radiative heat transfer models, namely Roesler Flux, Hottel Zone and Well Stirred models, and convective contribution will be discussed to some extent. Information and comparison regarding modeling techniques for radiative heat transfer, including other techniques such as Monte Carlo and Hybrid methods, can be found in the literature (Viskanta and Mengüç, 1987).

3.2.1. Roesler flux methods

Conceptually, Roesler divides the furnace chamber into increments and makes balance on the radiant energy in each section which is in interaction with process gas, furnace refractory and tubes as shown in Figure 3.2 and in Equation 3.25:

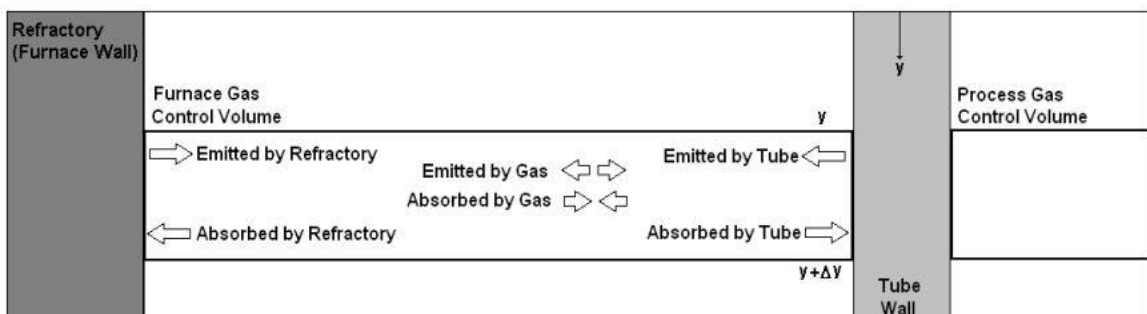


Figure 3.2. Radiant energy balance on differential increment in combustion chamber (Latham, 2008).

$$\begin{aligned}
& \left[\begin{array}{c} \text{Radiation} \\ \text{Entering} \\ \text{from} \\ y \end{array} \right] - \left[\begin{array}{c} \text{Radiation} \\ \text{Exiting} \\ \text{from} \\ y + \Delta y \end{array} \right] + \left[\begin{array}{c} \text{Radiation} \\ \text{Emitted} \\ \text{by} \\ \text{Refractory} \end{array} \right] - \left[\begin{array}{c} \text{Radiation} \\ \text{Absorbed} \\ \text{by} \\ \text{Refractory} \end{array} \right] \\
& + \left[\begin{array}{c} \text{Radiation} \\ \text{Emitted} \\ \text{by} \\ \text{Flue Gas} \end{array} \right] - \left[\begin{array}{c} \text{Radiation} \\ \text{Absorbed} \\ \text{by} \\ \text{Flue Gas} \end{array} \right] + \left[\begin{array}{c} \text{Radiation} \\ \text{Emitted} \\ \text{by} \\ \text{Tubes} \end{array} \right] - \left[\begin{array}{c} \text{Radiation} \\ \text{Absorbed} \\ \text{by} \\ \text{Tubes} \end{array} \right] = 0
\end{aligned} \tag{3.25}$$

The resulting differential equation yields the change in radiant energy per differential increment in the furnace, i.e., (dq_{rad}/dy) . Unlike chemical species transport, radiation can travel in both directions at the same time, i.e. along $(-y)$ and $(+y)$ directions. In this respect, the most basic version of Roesler's equation covers two differential equations, (dq_{rad}^+/dy) and (dq_{rad}^-/dy) , describing the change in both directions. These differential equations are then coupled with the furnace gas energy and material balance. In case appropriate boundary conditions are provided, these sets can be solved numerically. Depending on the number of spatial dimensions and fictitious gray gases being considered, number of differential equations changes so does their complexity (Latham, 2008). For steam reformer modeling purpose, flux method has been used by (Murty and Murthy, 1988), (Soliman *et al.*, 1988).

3.2.2. Hottel zone method

In Hottel zone method, furnace is divided into volume and surface zones, each of which is assumed to have a uniform distribution of temperature and radiative properties and energy balance is performed on each zone.

The system geometry is taken into account by defining three areas in the system. They are, *directed flux areas*, calculated from *total exchange areas*, which are respectively calculated from *direct exchange areas*. These issues will be covered with some detail in the next section and in Appendix A. The most difficult part of the Hottel Zone method is the calculation of these areas which is needed to be done once for a given system. Direct exchange areas can be determined by evaluating multiple integrals. Due to complexity of these integrals, charts for commonly found geometries have been developed (Tucker, 1986). For more complex geometries, direct exchange areas can be calculated by Monte Carlo ray

tracing methods. More detailed information regarding calculation of mentioned areas can be found elsewhere (Modest, 2003).

An iterative algebraic equation solver is used with seed values of temperatures for each element in the furnace. Since radiation do not require any media to be transferred, any zone in the furnace can exchange energy with any other zone in the furnace enclosure. The rates of radiative heat emission and absorption by a zone are proportional to the black emissive power (σT^4) of the emitting zone. That proportionality constant is named as directed flux area, and is presented by the symbol $\overline{Z_e Z_r}$ where zone e is the emitter and r is the receiver as shown in equations below (Rhine and Tucker, 1991).

$$\left[\begin{array}{c} \text{Radiation} \\ \text{In} \end{array} \right] = \left[\begin{array}{c} \text{Radiation Emitted by other Zones} \\ \text{and Absorbed by Zone } r \end{array} \right] = \sum_{\text{all } e} \overline{Z_e Z_r} \sigma T_e^4 \quad (3.26)$$

$$\left[\begin{array}{c} \text{Radiation} \\ \text{Out} \end{array} \right] = \left[\begin{array}{c} \text{Radiation Emitted by Zone } r \\ \text{and Absorbed by other Zones} \end{array} \right] = \sum_{\text{all } e} \overline{Z_r Z_e} \sigma T_r^4 \quad (3.27)$$

Hottel zone can be grouped into three types, namely, Long Furnace Type 1-2 and Well Stirred Furnace model, which is considered in this study. Hottel Zone Method is the most common method for advanced steam reformer modeling, (Plehiens and Froment, 1989), (Yu *et al.*, 2006), (Zamaniyan *et al.*, 2008).

3.2.3. Well stirred furnace model

Well Stirred Furnace model is actually a sub-type of Hottel Zone Method and is well known for making substantially correct predictions of the overall heat transfer performance for a wide range of furnace types. Model is somewhat general and can therefore be applied to any fire chamber geometry by modifications. The simple but efficient idea standing behind the model is the presumption that many industrial furnaces operate with sufficient combustion gas momentum in the fire box that result in fairly well stirred furnace chamber. Such assumption reduces the highly complex problems due to radiative nature and leads to simpler solution compared to other methods.

Unlike Hottel Zone method, which considers numerous individual zones, this model regards the furnace chamber by using three broad zones. A single gas zone to represent the flame and combustion products within the chamber, and two surfaces zones to represent the heat sink and refractory, respectively. Within the context of original model the following assumptions are made (Mullinger and Jenkins, 2014):

- (i) Combustion gas mass and flame are assigned a single temperature T_{fg} due to high gas momentum in the fire chamber.
- (ii) Combustion gas will be taken as a gray gas with an average emissivity ε_{fg} .
- (iii) Surface of heat sink, area A_{tubes} , is gray, with a true emissivity ε_{tube} and effective emissivity of ε_{eff} , and is usually assigned to a single temperature T_{wo} but can also be treated by vertical uniform temperature segments (Farhadi *et al.*, 2005).
- (iv) Refractory surface is radiatively adiabatic. This assumption is applicable especially for furnaces under operation for a long time. It expresses the radiative equilibrium condition which means net radiative heat flux to refractory is zero. All radiation incident on refractory will be diffusely reflected.
- (v) For well-stirred furnaces, the temperature of the gas leaving the fire box may be regarded as the effective temperature of the furnace, T_{fg} . However, in some configurations, the combustion gases can be considered to leave the radiant section of the furnace (bridge-wall) at a temperature Δ °C below T_{fg} which allows for imperfect mixing effect in the chamber. This assumption will be stressed for Terrace-Wall™ type reformer since temperature uniformity is favored.
- (vi) Heat loss through refractory walls to environment by means of convection. As a plausible approximation, it may be conveniently taken as 2-3% of total heat input.
- (vii) Radiation loss through openings in the furnace walls are neglected. Considering the total refractory surface area, openings occupy negligible percentage of the total.

Within the scope of this work, not all but some fundamental features of Well Stirred Furnace model are adopted. The adopted issues will be covered and discussed in detail.

3.2.3.1. Net rate of heat transfer to tubes. With these assumptions net rate of heat transfer from flue gas mixture to the heat sink (reformer tubes) by radiation and convection can be written as:

$$\dot{Q}_s = g_{rad}\sigma(T_{fg}^4 - T_{wo}^4) + h_c A_{tubes}(T_{fg} - T_{wo}) \quad (3.28)$$

Since the temperature in combustion chamber is very high, radiation is the dominant mechanism, but both radiation and convection work together. Thus, total heat transfer to a reformer tube becomes the sum of two individual heat transfer rates. The first term on the right hand side of Equation (3.28) is radiative and the second term on the right hand side is convective in Equation 3.28.

3.2.3.2. Total exchange area (g_{rad}). The term, g_{rad} or more explicitly $g_{fg-t,r}$, is called Total Exchange Area or Total Transfer Factor, meaning the total exchange area from furnace gas to A_{tubes} , with assistance from the refractory surface. It accounts for geometric complexities of the furnace chamber, including multiple reflections at all surfaces.

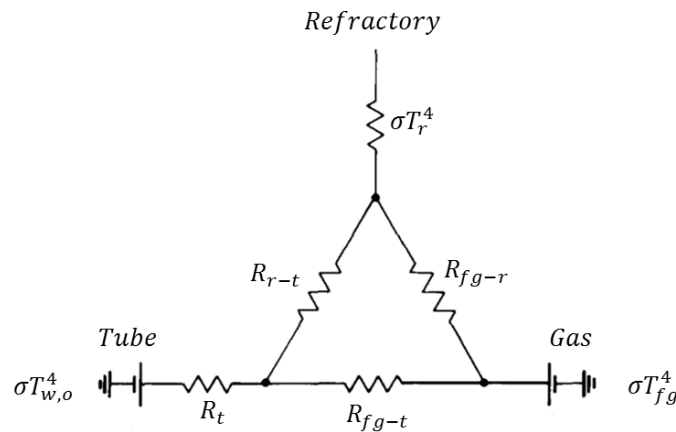


Figure 3.3. Radiation network showing radiant energy transfer pathways for well stirred furnace (Truelove, 1983).

Total exchange area takes different forms and values depending on how combustion gases are modeled (gray, gray + clear, etc.) and how three surfaces are defined (i.e, black, gray, no-flux). In the original form of the Well Stirred Furnace model (as well as in this

study), combustion gases are considered to be single gray gas, meaning that the, total gas emissivity (ϵ_{fg}) and total gas absorptivity (α_{fg}) are the same and equal to an average value. In the Well Stirred Furnace model, total exchange area for a system composed of gray sink enclosed in a adiabatic surface filled with single gray gas can be conveniently determined from radiation network (electric circuit analogy), whose details are described in Section A.5.3.

Physical interpretation of network analogy in Figure 3.3 can be done in the following way. In present case, source of radiation is combustion gas mixture that will be modeled as a single gray gas. Radiation from gray gas, whose potential is σT_{fg}^4 can be transferred to reformer tubes in two ways. First, directly by passing through R_{fg-t} resistance, and indirectly by reflecting from refractory by passing through R_{fg-r} and then through R_{r-t} resistances. Irradiation (total radiation incident) over reformer tubes must pass another resistance due to surface reflection shown by the resistance R_t . The refractory is assumed to be a diffuse reflector, in other words, it is radiatively adiabatic and its potential is represented by a floating node without any radiative contribution (Truelove, 1983).

Other factors that effect radiative heat transfer (i.e, geometric properties etc.) are embedded in resistances between bodies. Resistances between the nodal points in Figure 3.3 express how bodies interact radiatively with each other. Briefly, they are separated into two groups that are called *space* and *surface resistances*. Space resistances include geometric and participating medium properties of the system while surface resistances cover radiative surface properties and arrangements of solid bodies present in the system.

Resistances between the bodies, i.e *space resistances*, are:

$$R_{fg-t} = \frac{1}{A_{tubes}\epsilon_{fg}} = \frac{1}{g_s t} \quad (3.29)$$

$$R_{fg-r} = \frac{1}{A_r\epsilon_{fg}} = \frac{1}{g_s r} \quad (3.30)$$

$$R_{r-t} = \frac{1}{A_r F_{r-t}(1 - \epsilon_{fg})} = \frac{1}{s_r s_t} \quad (3.31)$$

Radiative exchange factors between two zones comprising the relative orientation of any zone pairs and allowance for participating medium between the pairs are called direct exchange areas (Batu and Selçuk, 2002). They are calculated for each pair of zones, which are gas to tube ($\overline{gS_t}$), gas to refractory ($\overline{gS_r}$) and refractory to tube ($\overline{S_rS_t}$). Total exchange area is calculated from direct exchange areas but differ from them. Total exchange area account for all of the radiation that leaves the emitting zone and is absorbed by the receiving zone, regardless of the path taken. Total exchange area includes radiation that travels directly between the zones and radiation reflected off from the multiple intermediate zones, and that arrives at and is eventually absorbed by the receiving zone.

F_{r-t} is the configuration factor between refractory and sink. F_{r-t} depends on the arrangement of refractory and sink surfaces within the furnace chamber. Rigorous evaluation of F_{r-t} is usually not possible for highly complex systems however, several cases can be identified that yield relatively simple expressions for total transfer factor g_{rad} , which is also adopted in this work (Truelove, 1983).

Since the only absorbing/emitting solid surface is the reformer tube surface, it has the only resistance on the black body potential of surface, i.e. *surface resistance*, given in Equation (3.32). Refractory wall is excluded in terms of surface resistance, since it is considered radiatively adiabatic (i.e. no resistance). Effective tube emissivity, different than true tube emissivity is to be described in further sections.

$$R_t = \frac{1 - \epsilon_{eff}}{A_{tubes}\epsilon_{eff}} \quad (3.32)$$

Similar to direct exchange areas, g_{rad} can also be formed with respect to overall resistance between sink (reformer tubes) and source (radiating gas):

$$g_{rad} = g_{fg-t,r} = \frac{1}{R_{Total}} \quad (3.33)$$

A general expression of total exchange area for an enclosure consisting single gray gas, gray sink with diffuse adiabatic refractory may be formulated by using electric circuit

fundamentals (i.e. circuits in series and parallel according to Kirchhoff's Circuits Law) can be given as follows:

$$g_{rad} = \frac{1}{(R_t + 1/[(1/R_{fg-t}) + 1/(R_{fg-r} + R_{r-t})])} \quad (3.34)$$

It is clear that g_{rad} carries high importance for making the model agree with reality. Total transfer factor will be re-shaped after defining effective tube emissivity.

3.2.3.2. Effective tube emissivity (ϵ_{eff}). In furnaces, tubes placed with some space in between each pair and some of the radiation from combustion gas does not strike directly to the tubes, but hits the refractory wall behind where it is re-radiated and contributed to heat consumption of the sink. Due to mutual shielding effects of adjacent tubes, indirect interaction of gas radiation and tubes result in sophisticated situation causing circumferential radiative heat flux variation. The ratio of peak to mean heat flux is a function of tube pitch to diameter ratio, B . This factor is important in determining allowable heat transfer rating of a furnace, since it is the peak heat flux, as visualized in Section 2.4.4, which is a common limiting factor in furnace operations

A very convenient simplification was provided by Hottel in which the heat sink is defined as a verticle equivalent plain strip having an area equal to that covered by the tubes with an effective emissivity, ϵ_{eff} , which gives the same radiative heat transfer as the previous tube plane (Hottel, 1974).

Effective emissivity depends on center-to-center distance of tubes, tube diameter and tube's true emissivity. It also consideres geometric orientation and formation of tubes and refractory walls (single & double row, refractory backed or centered formation, etc.) hence form of the equation should be placed accordingly (Truelove, 1983). Treatment of effective emissivity of tubes requires replacing each tube by plane vertical strips (surfaces) that intercepts the same radiation as would the tubes, as illustrated in Figure 3.4.

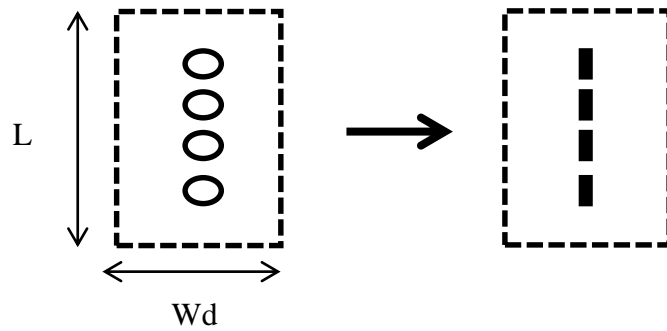


Figure 3.4. Equivalent plane surfaces for the case of equal radiation incident on tube row from both sides.

Since most of the radiation is from the gas, the height (L in Figure 3.4) of a replacing strip should be the tube pitch, in other words center-to-center tube spacing P , multiplied by the interception factor F_i given below (Hottel, 1974):

$$F_i = 1 - \frac{1}{B} \left[(B^2 - 1)^{1/2} - \cos^{-1} \left(\frac{1}{B} \right) \right] \quad (3.35)$$

F_i is defined as the fraction of radiation incident on the tube plane that is intercepted by the tubes while B is the ratio of tube center-to-center distance to tube outside diameter as shown below:

$$B = \frac{\text{Pitch}}{D_o} \quad (3.36)$$

In the new form of tube screen, relevant surface areas *per unit dimension* normal to the plane of Figure 3.4 (which is height of the reformer tubes in three dimensions) where “ n ” is the number of the real tubes in the tube row, are given in Table 3.7.

Table 3.7. Corresponding forms of representative tube strips.

Real Form	Equivalent Form
A_{tubes}	$2nPF_i (\approx 2LF_i)$

Table 3.7 Corresponding forms of representative tube strips (cont.).

Real Form	Equivalent Form
A_r	$2(L+Wd)$
A_{total}	$2(L+Wd + nPF_i)$
L_m (Mean Beam Length)	$Wd/2$

An emissivity expression should now be expressed, called effective emissivity, for the representative strips which will replace the tubes (Truelove, 1983):

$$\varepsilon_{eff} = \frac{1}{1 + \left(\frac{2BF_t}{\pi}\right) \left[\left(\frac{1}{\varepsilon_t}\right) - 1\right]} \quad (3.37)$$

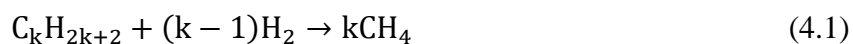
In Equation 3.37 ε_t is the true emissivity of tubes (usually 0.8 – 0.9). The equation of F_i is valid for all single row tube formations (for both refractory backed and irradiated from both sides) but the form of effective emissivity has to be changed depending on the configuration of the system. As an example, effective emissivity equation presented here is valid only for single row of tubes being exposed to radiation from both sides (Truelove, 1983). This statement is acceptable for the operating conditions of a Terrace-Wall™ type steam reformer tubes, since the refractory wall structure, as well as burner allocations are in the favor of uniform circumferential radiation flux. Furthermore, effective emissivity has greater value than true emissivity of the tubes because former takes internal reflections in the tube banks into account. The effective temperature of the equivalent surface is equal to the true temperature of the tubes (Hottel, 1974).

Complete structure and solution algorithm of Well Stirred Furnace model will not be provided here since only related parts are adopted. Comprehensive knowledge can be found in literature (Truelove, 1983), (Hottel, 1974), (Hottel and Sarofim, 1967). What has been provided so far will form the backbone of the model.

4. MATHEMATICAL MODELING STUDIES

4.1. Reformer Feed Modification

As described in Section 2, steam reformer feed is the combination of gas streams containing mainly hydrogen and natural gas from various resources. According to both laboratory analysis of TÜPRAŞ and literature, higher hydrocarbons (C_2H_6 to C_6H_{14}) are likely to be present in the feed in small/trace amounts. Steam reforming of such higher alkanes depicts different reaction characteristics than methane. Since dealing with kinetics for each different hydrocarbon species present in the feed is unnecessarily complex, the hydrocarbon components that are not methane are assumed to be hydrocracked to methane in the presence of hydrogen according to Equation 4.1. As a consequence, steam methane reforming reaction can be described by methane reforming kinetics irrespective to unit feed composition. Such treatment of higher alkanes was used by (Singh and Saraf, 1979), (Murty and Murthy, 1988), (Latham, 2008).



4.2. Packed Bed Steam Reforming Reactor Model

Reactor model equation set of an industrial steam reformer must be constructed for a non-adiabatic, non-isothermal reactor system covering multiple simultaneous reactions. System boundaries must be determined to be able to write mass balance or mole balance on any system. When the boundaries are determined, mole (mass), energy and momentum balances can be written.

The system is assumed to be at steady state, thus the accumulation term vanishes for each balance. Shell balance can be formed for a ΔW catalyst weight in control volume and mole balance is accomplished. The schematic representation of shell balance is shown in Figure 4.1.

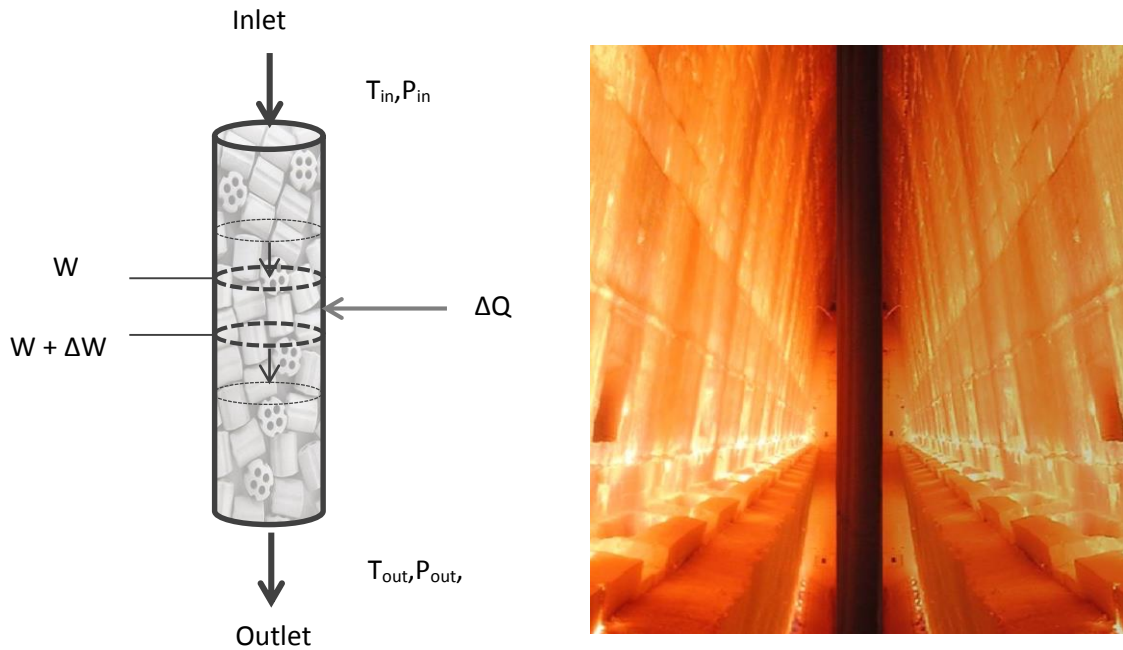


Figure 4.1. The schematic representation of shell balance for plug flow packed bed reactor.

Mass balance for the components can be given as follows:

Methane Balance:

$$\frac{dF_{\text{CH}_4}}{dW} = -(-Rt_{\text{CH}_4}) \quad (4.2)$$

Water Balance:

$$\frac{dF_{\text{H}_2\text{O}}}{dW} = -(-Rt_{\text{H}_2\text{O}}) \quad (4.3)$$

Hydrogen Balance:

$$\frac{dF_{\text{H}_2}}{dW} = +(Rt_{\text{H}_2}) \quad (4.4)$$

Carbon Monoxide Balance:

$$\frac{dF_{\text{CO}}}{dW} = +(Rt_{\text{CO}}) \quad (4.5)$$

Carbon Dioxide Balance:

$$\frac{dF_{CO_2}}{dW} = +(Rt_{CO_2}) \quad (4.6)$$

Nitrogen Balance:

$$\frac{dF_{N_2}}{dW} = 0 \quad (4.7)$$

Solution of each differential equation yields change in the molar flow rate of corresponding species. Nitrogen is also likely to be present in the feed in small amounts, it is considered to be inert thus its change stands for zero. It's presence in the model is included since it acts indirect role in heat transfer and reaction phenomena. Where Rt terms correspond to overall production/consumption rate for each species present in the system marked with + and – respectively. By using stoichiometry, they can be treated in terms of individual reaction rates, described in Section 3.1.3, as follows:

$$(-Rt_{CH_4}) = -(r_1 + r_3) \quad (4.8)$$

$$(-Rt_{H_2O}) = -r_1 - r_2 - 2r_3 \quad (4.9)$$

$$(-Rt_{H_2}) = +3r_1 + r_2 + 4r_3 \quad (4.10)$$

$$(+Rt_{CO}) = +r_1 - r_2 \quad (4.11)$$

$$(+Rt_{CO_2}) = r_2 + r_3 \quad (4.12)$$

4.2.1. Energy balance over reformer tube

$$\frac{dT}{dW} = \frac{\frac{4 \cdot h_w}{\rho_{bed} \cdot D_i} \cdot (T_{w,i} - T_{pg}) - [\sum_{i=1}^3 (-r_{ij} \cdot \Delta H_{rxn_j})]}{\sum_{j=1}^6 F_j C_{p_j}} \quad (4.13)$$

The equation above yields temperature variation of reactant mixture also that of the catalyst bed for pseudo-homogeneous models, through each catalyst bed cross section

treated. Nominator stands for the difference of energy input from furnace flue gas to process gas and energy required to drive steam reforming reactions (Fogler, 2005). Where h_w is the tube to process gas heat transfer coefficient as explained in Section 3.1.4.

The form of the wall heat transfer coefficient can be replaced with overall heat transfer coefficient hence extended to where we define the energy balance region between furnace and reacting medium. The reason why the balance covers tube inner wall temperature but not the furnace gas will be given in model solution strategy in Section 4.5.

4.2.2.1. Tube wall thermal conductivity (k_w). The tube wall conductive heat transfer coefficient, k_w , is used to calculate the rate of heat transfer between the tube outer and inner walls. Its determination is straightforward since it is experimentally obtained for each type of tube material at different operating temperatures. Such representative data can be found in open sources (Engemasa Engenharia e Materias LTDA., 2011).

For a 25Cr35NiNb alloy reformer tube, thermal conductivity in the units of ($W m^{-1} K^{-1}$), can be fitted to a linear function for reformer operating temperature range in Kelvin:

$$k_w = 0.016T_{w0} + 6.9098 \quad (4.14)$$

4.2.2.2. Tube to process gas heat transfer coefficient (h_w). In the model structure, as tube to process gas heat transfer coefficient, Leva and Grummer's correlation is used (Leva and Grummer, 1948):

$$h_w = \text{constant} \cdot 0.813 \cdot \frac{\lambda_{pg}}{D_i} \cdot \exp\left(-6 \frac{D_{pht}}{D_i}\right) \cdot (Re_p)^{0.9} \quad (4.15)$$

Equivalent particle diameter used for heat transfer purposes has the following form:

$$D_{pht} = \sqrt[3]{\frac{6V_{cat}}{\pi}} \quad (4.16)$$

This type of equivalent diameter is defined as the diameter of a sphere having the same volume as the catalyst particle (Yang, 2003). Since steam reformer is composed of two catalyst beds packed with different size catalysts, equivalent spherical diameter for each catalyst particle is given below:

Table 4.1. Equivalent particle diameter for heat transfer calculations.

	D_{pht} (m)
Catalyst Bed 1	0.014
Catalyst Bed 2	0.01683

All thermodynamic and transport properties of process gas species are calculated at process gas conditions according to procedures given in Appendix B.

4.2.2.3. Heat of reaction (ΔH_{rxn}). Heat of reaction is a very important, temperature dependent parameter for a proper model since high endothermicity is involved:

$$\Delta H_{Rxn}(T) = \Delta H_{Rxn}^0(T_{Ref}) + \int_{T_{Ref}}^T C_P dT \quad (4.17)$$

$$\int_{T_{Ref}}^T C_P dT = \int_{T_{Ref}}^T \left(\sum_{i=products} v_i C_{p_i} - \sum_{j=reactants} v_j C_{p_j} \right) dT \quad (4.18)$$

Table 4.2. Standard enthalpies of steam reforming reactions.

	Standard Enthalpy of Reaction (kJ/kmol)
Steam Reforming Reaction	+ 206000
Water Gas Shift Reaction	- 41200
Global Reaction	+ 164800

In Equation 4.18 stoichiometric coefficient of each reaction component is designated with v . Heat capacities are calculated as stated in Appendix B. Standard enthalpies of

reactions at reference condition (298.15 K, 1 atm), are calculated from standard heats of formations provided in Table 4.2.

4.2.2. Momentum balance over packed bed

Pressure drop in fixed bed tubular reactors can be calculated by using the following momentum balance (Froment *et al.*, 2011):

$$\frac{dP}{dW} = -f \cdot \left(\frac{\rho_{pg} \cdot u_{pg}^2}{D_{ppd}} \right) \cdot \left(\frac{1}{(1-\varphi)} \cdot \frac{1}{bcs} \cdot \frac{1}{\rho_{cat}} \right) \quad (4.19)$$

As explained in Section 3.1.6, friction factor have flexibility to be adapted on packed bed type. In this study, Ergün friction factor has been chosen as below:

$$f = \frac{(1-\varphi)}{\varphi} \cdot \left(1.75 + \frac{150 \cdot (1-\varphi)}{Re_p} \right) \quad (4.20)$$

In literature, it has been observed that equivalent particle diameter may be treated in different ways for heat transfer and pressure drop calculations (Shayegan *et al.*, 2008). The equivalent particle diameter type used for pressure drop calculations is given in Equation 4.21. This type of equivalent diameter, also known as surface-volume or Sauter diameter, is defined as the diameter of a sphere having the same external-surface-area-to-volume ratio as the particle (Yang, 2003).

$$D_{ppd} = \frac{6V_{cat}}{S_{cat}} \quad (4.21)$$

$$\varphi = 0.38 + 0.073 \cdot \left[1 + \frac{\left(\frac{D_i}{D_{ppd}} - 2 \right)^2}{\left(\frac{D_i}{D_{ppd}} \right)^2} \right] \quad (4.22)$$

Mean packed bed voidage for equivalent shape of catalyst particles is also estimated by correlation (Carberry and Arvind, 1987) given in Equation 4.22. Equivalent particle diameter and estimated void fractions for each catalyst bed is given in Table 4.3.

Table 4.3. Equivalent particle diameter and estimated void fractions for pressure drop calculations.

	D_{ppd} (m)	Estimated Void Fractions
Catalyst Bed 1	0.005	0.50
Catalyst Bed 2	0.006	0.52

4.3. Well Stirred Steam Reformer Furnace Model

4.3.1. Radiative heat flux calculation

Coming from the fundamental Equation 3.34 and replacing steam reformer tubes by representative gray strips as given in Table 3.8, total transfer factor, g_{rad} , can now be re-defined for a system in which gray heat sink and adiabatic refractory surfaces are segregated with a graygas participating medium as the sink laying in a single plane (Hottel, 1974):

$$g_{rad} = \frac{1}{\frac{1}{A_{tubes}} \left[\frac{1}{\epsilon_{eff}} + \frac{1 - \epsilon_{fg}}{\epsilon_{fg}} \cdot \frac{nPF}{H + W} \right]} \quad (4.23)$$

Concerning total heat flux to reformer tube, or to a section of reformer tube, it is the sum of individual radiative and convective fluxes. Taking into account well stirred medium, whose effective temperature is constant at T_{fg} , radiative heat flux can be calculated by Equation 4.24. Where σ is Stephan Boltzman constant; $5.6703E-08$ ($Wm^{-2}K^{-4}$), A_{tube} is outside surface area of a reformer tube and n ; number of reformer tubes.

$$Q_{rad} = \frac{g_{rad} \cdot \sigma \cdot (T_{fg}^4 - T_{wo}^4)}{n \cdot A_{tube}} \quad (4.24)$$

4.3.2. Convective heat flux calculation

Even though convective heat transfer to reformer tubes is considered negligible in comparison to radiation by many authors, convection effect is included with some simplifications. As the correlation, widely accepted Dittius Boelter correlation (McCabe *et al.*, 2001) is chosen:

$$h_c = \frac{\lambda_{fg}}{Df_{hyd}} \cdot (0.023 \cdot Re_f^{0.8} \cdot Pr_f^{0.33}) \quad (4.25)$$

Since hydraulic diameter of furnace chamber in the flow direction of flue gas is required for calculation of Reynold's number, fire box is approximated to a rectangular duct. Hydraulic diameter of a rectangular duct having the dimensions of furnace chamber is calculated as below:

$$Df_{hyd} = \frac{2 \cdot Length \cdot Width}{(Length + Width)} \quad (4.26)$$

Linear velocity of flue gas flowing counter currently to process gas is also calculated in similar manner. Combustion calculations for fuel being fed have been done separately with complete combustion assumption and volumetric flow rate of combustion products is calculated. Assuming the flow area available is roughly equal to that of horizontal section of rectangle furnace chamber minus the total cross sectional area of reformer tubes, an approximate linear velocity could be achieved.

All thermodynamic and transport properties of combustion species are calculated at average film temperature over outer surface of steam reformer tube according to procedures given in Appendix B. Considering well stirred medium, whose effective temperature is constant at T_{fg} , convective heat flux can be calculated by:

$$Q_{convective} = h_c \cdot (T_{fg} - T_{w,o}) \quad (4.27)$$

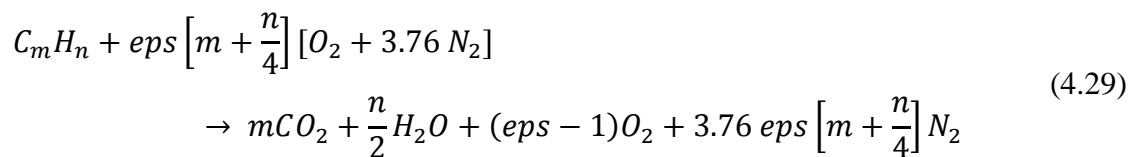
Finally, total heat flux from furnace to tube wall is simply the summation of radiative and convective heat fluxes.

$$Q_{fg-t} = Q_{radiative} + Q_{convective} \quad (4.28)$$

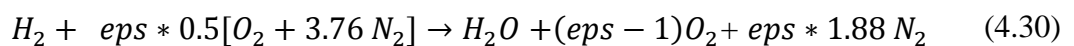
4.4. Furnace Chamber Combustion Model

Radiation model described in Section 3.2 describes how energy of combustion gas is transferred to reformer tubes, but still requires features of flue gas mixture such as composition, in turn, gas emissivity. Since furnace is a natural draft type, it operates at atmospheric pressure with excess air entrance, typically 15-20% for lean fuels. Online analyzer in TÜPRAŞ İzmit Refinery analyzes the joint stack gas composition of both fire boxes. In this regard, the flue gas composition in each furnace chamber is essentially presumable but can be regarded as unknown. In this respect, fuel feed to furnace is known with all properties (flow, composition etc.) hence combustion gas composition can be straightforwardly calculated with complete combustion assumption plus excess air (taken as 15%). Laboratory analysis for composition of the fuel streams (Fuel gas and Tail gas) covers eleven compounds ranging from CH₄ to C₆H₁₄, in addition to H₂, CO, CO₂, O₂ and N₂. Assuming O₂, CO₂ and N₂ as inerts, hence neglecting any NO_x formation, complete combustion equations are defined for all other combustible species.

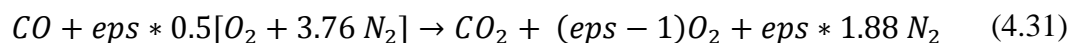
Hydrocarbon Combustion:



Hydrogen Combustion:



Carbon Monoxide:



Excess air percentage is denoted with eps . Since H_2O and CO_2 are radiating species, calculation of their percentage in the whole mixture gains more importance. In this respect, including CO_2 contribution coming from PSA Tail-gas is essential, taking large feed rates of tail gas into account.

Gas emissivity is calculated from combustion gas and furnace enclosure properties. Gas emissivity calculations are highly complex, in this aspect, an engineering treatment of radiating gas is essential. Detailed information regarding engineering approach to problem is discussed in Section A.6.1. Weighted sum of gray gases method (WSGGM), demonstrated by Hottel and Sarofim (Hottel and Sarofim, 1967) is used to model combustion gas emissivity, where required coefficients are obtained from Dorigon's work (Dorigon *et al.*, 2013). Combustion gas is considered to be represented by three gray plus one clear gas in Dorigon's work. Since radiative model is actually constructed for a single gray gas, emissivity value calculated by WSGGM at the mean beam length for an isothermal system is assigned to value of the single gray gas at specified conditions. In the reformer enclosure, radiating gas temperature is again, T_{fg} and mean beam length is specified as width of the combustion chamber as stated in Table 3.7. More comprehensive information regarding WSGGM and coefficients used can be found in Appendix A.

4.5. Model Solution Strategy

Furnace and steam reformer tubes are in interaction through tube outer wall via heat transfer. In this perspective, two individual models built for furnace side and process side should be integrated to each other through tube outer wall. Radiative heat flux from furnace to tube outerwall and process side heat gain are both dependent on each other and neither of them can be rigorously calculated unless tube outer wall temperature value is known. This uncertainty requires an iterative solution methodology.

In literature, well stirred furnace model is usually defined with the assumption of single and constant temperature for tube outer surface. For realistic treatment of a reformer tube temperature profile, tube surface must have different temperatures at different locations. This over-simplification is eliminated by segmentation. In order to connect furnace model to reactor model, with variable heat flux and temperature profile through the length of the tube,

packed bed is divided into desired number of longitudinal segments. This structure of the reformer tube can be treated similar to sequentially connected packed bed reactors in series each having heat transfer with environment. Configuration factors of each segment relative to refractory walls are assumed to be same. In this respect, there is no distinction between any segments of reformer tube due to their location in the furnace chamber.

Segmentation begins from the entrance of steam reformer tube. Solution procedure starts with assigning a seed value to outer tube wall temperature of the first segment. By using this seed value, furnace model calculates the total heat flux from furnace to subject tube segment as explained in Section 4.3. Afterwards, furnace model forward the heat flux value and tube outer wall temperature value to reactor model where tube inner wall temperature of the subject segment is calculated by energy balance according to the formula below:

$$T_{wi} = T_{wo} - \frac{Q_{total} D_o \ln\left(\frac{D_o}{D_i}\right)}{2 k_w} \quad (4.32)$$

It is assumed that conductive heat transfer through tube wall is driven in radial direction only. Since system is operating at steady state with no accumulation, and loss free, heat received by outer surface of reformer tube is equal to conducted heat through it, consequently both of them are equal to the amount of heat gained by process gas.

Continuing from the first segment of reformer tube, tube inner wall temperature and initial conditions for reformer inlet both are now known, hence integration can now be initiated to calculate composition, temperature and pressure change through catalyst bed belonging to segment under consideration. For the solution of ODE set, given in Section 4.2 for molar flow, temperature and pressure, MATLAB™ standard ODE solver, ode15s is used. “ode15s” type is a solver integrating with automatic step size. Middle values coming from ODE solver are neglected but the last values calculated by solver at the defined segment limit (i.e. 0.5 kgcatalyst/segment) are taken as the results of integration.

Heat flux from inner tube wall to process gas is in turn calculated according to formula below:

$$Q_{t-pg} = h_w(T_{w,i} - T_{pg}) \quad (4.33)$$

Seed value assumed for outer wall temperature of the segment, after all calculations, must satisfy the criterion given in Equation 4.34 within the limits of user defined accuracy, i.e, 5%. If this criterion is satisfied within the tolerance, model moves forward to next segment by taking process side results of the previous segment as the initial values for the next step integration. If criterion fails, algorithm searches for the new tube outer wall temperature value.

$$\frac{Q_{fg-t}}{Q_{t-pg}} = \frac{D_i}{D_o} \quad (4.34)$$

Choosing proper seed value is important for convergence. The solution searching algorithm, coded in MATLAB™, in this work is straightforward and searches solution by constantly increasing the seed temperature by a fixed step size defined by user. Therefore, higher initial values than actual model value will not converge. One should make an educated guess, considering lowest temperature in the model inputs, which is the reformer hydrocarbon mixture feed temperature (above 500 °C). Meanwhile considering the model solution speed, model searching for wall temperature values beginning from 500 °Cs with very small step sizes in every segment will be time consuming. In order to avoid this situation, tube outer wall temperature of segments which correspond to initial 10% of the reformer tube, where highest endothermicity is, are constantly investigated from a relatively lower and constant temperature seed value to ensure determination of possible local wall temperature decrease. After 10% of tube length, in case of successful convergence, model begins searching tube wall temperature of succeeding segment from the outer tube wall temperature of the preceding segment. Since number of reactor segments, step size and convergence criteria accuracy limits are all user defined, model accuracy, precision and solution speed are dependent on choices. In an ideal case, high number of segments with small step size and high accuracy is the best approach.

5. RESULTS AND DISCUSSION

5.1. Evaluation of User Defined Solution Parameters

As stated in Section 4.5, solution algorithm requires four parameters to be defined by user, which are, number of segments that reformer tube to be divided, step size of temperature increment for iteration, convergence tolerance percentage of iteration and seed temperature value for the initial part of the reformer tube. After model structure has been set up, the effects of user-defined values had to be identified, even regardless of the approach to real values, in order to have a more precise sight of view to model solution mechanism. Within this perspective, numbers of simulations are performed using same input data by varying values of user defined parameters within plausible limits.

5.1.1. Effect of number of segments

Number of individual segments that reformer tube divided into is actually the measure of how precise the reactor is evaluated. The effect of number of segments to the model performance, in terms of methane slip, which is the volume % of methane on dry basis in the reactor effluent, is shown below (increment size, convergence tolerance and seed value are kept constant at 1 °C, 3% and 620 °C, respectively):

Table 5.1. Model end results at different number of segments.

	T _{out} (°C)	CH ₄ Slip (%)
100 Segments	802.62	5.63
150 Segments	800.58	5.76
200 Segments	799.70	5.82
Plant Data	827	5.97

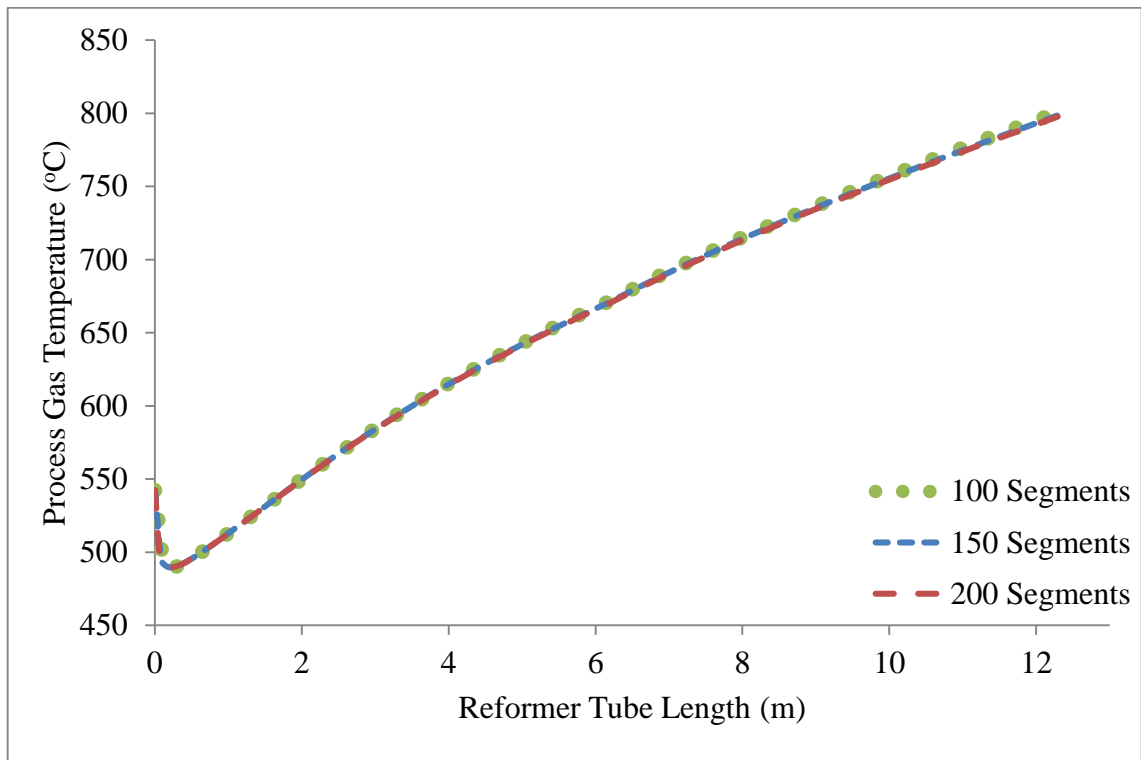


Figure 5.1. Process gas temperature profile along the tube length with various number of segments.

One should keep in mind that Table 5.1 does not represent the reality of the model yet since all parameters are kept constant and system can be adjusted by means of wall heat transfer coefficient. Process gas temperature profile show almost no difference in all three numbers of segments at specified conditions. However, due to small natural variation, outlet conditions show minor differences. Although number of segments is expected to show significant variation in terms of solution due to stepwise integration, the result why it does not affect so much can be the usage of automatic step MATLAB ODE solver (ode15s) as well as small increment size of wall temperature (1 °C).

5.1.2. Effect of temperature increment size

Temperature increment, as explained in Section 4.5, constantly increases the tube wall temperature in order to satisfy convergence criterion. Increment size is important since the smaller step size results in the earlier conversion if conditions are feasible. The effect of

increment size to the model performance is shown below (number of segments, convergence tolerance and seed value are kept constant at 100, 3% and 620 °C, respectively):

Table 5.2. Model end results at different increment step sizes.

	T _{out} (°C)	CH ₄ Slip (%)
Increment Step = 1.0	802.62	5.63
Increment Step = 0.5	800.85	5.74
Increment Step = 0.1	799.84	5.81
Plant Data	827	5.97

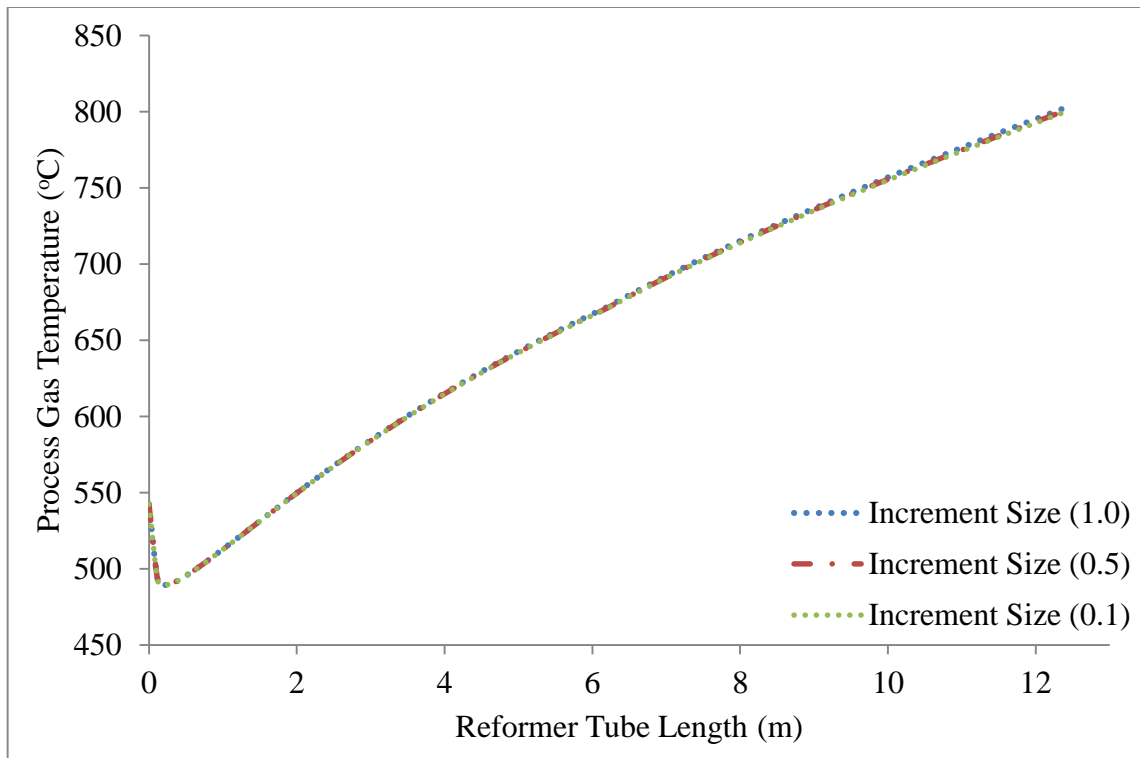


Figure 5.2. Process gas temperature profile along the tube length with various temperature increment step size.

As seen in Figure 5.2, different increment sizes show almost identical profiles with different end-results with very narrow variation. Smaller step size allows better prediction of the plant data by the mathematical model. For a highly accurate model, step size is desired to be as small as possible, provided that computational effort is not an issue.

5.1.3. Effect of convergence tolerance

The ratio of heat fluxes from furnace to tube outer wall and from tube inner wall to process gas must satisfy a convergence criterion within tolerance limits. Convergence tolerance is normally expected to have significant effects on model accuracy. Effect of convergence tolerance to the model performance is shown below (number of segments, increment size and seed value are kept constant at 100, 1 °C and 620 °C, respectively):

Table 5.3. Model end results at different convergence tolerances.

	T _{out} (°C)	CH ₄ Slip (%)
Convergence Tolerance = 10%	790.22	6.46
Convergence Tolerance = 5%	799.11	5.86
Convergence Tolerance = 3%	802.62	5.63
Convergence Tolerance = 1%	Not Converged	Not Converged
Plant Data	827	5.97

Increase in convergence tolerance brings relaxation to model capability to achieve a final result while sacrificing from model accuracy. As tolerance increases, model becomes able to converge even with high increment sizes, while strict tolerances require proportionally small increment steps sizes in order not to miss out convergence criterion.

Parameters discussed above have both individual and combined effects on model performance and accuracy. It has been observed that tube wall temperature seed value alone has small impact on simulation results due to solution searching method. However, its selection is highly important as mentioned in Section 4.5.

Tube wall temperature increment step size affects the simulation run time significantly, but do not have notable effects on results when provided in a reasonable range. Higher step sizes are very likely not to converge with strict convergence tolerances. MATLAB's automatic step size ODE solver seems to minimize individual effects of parameters that are normally expected to have significant impacts on self constructed solvers.

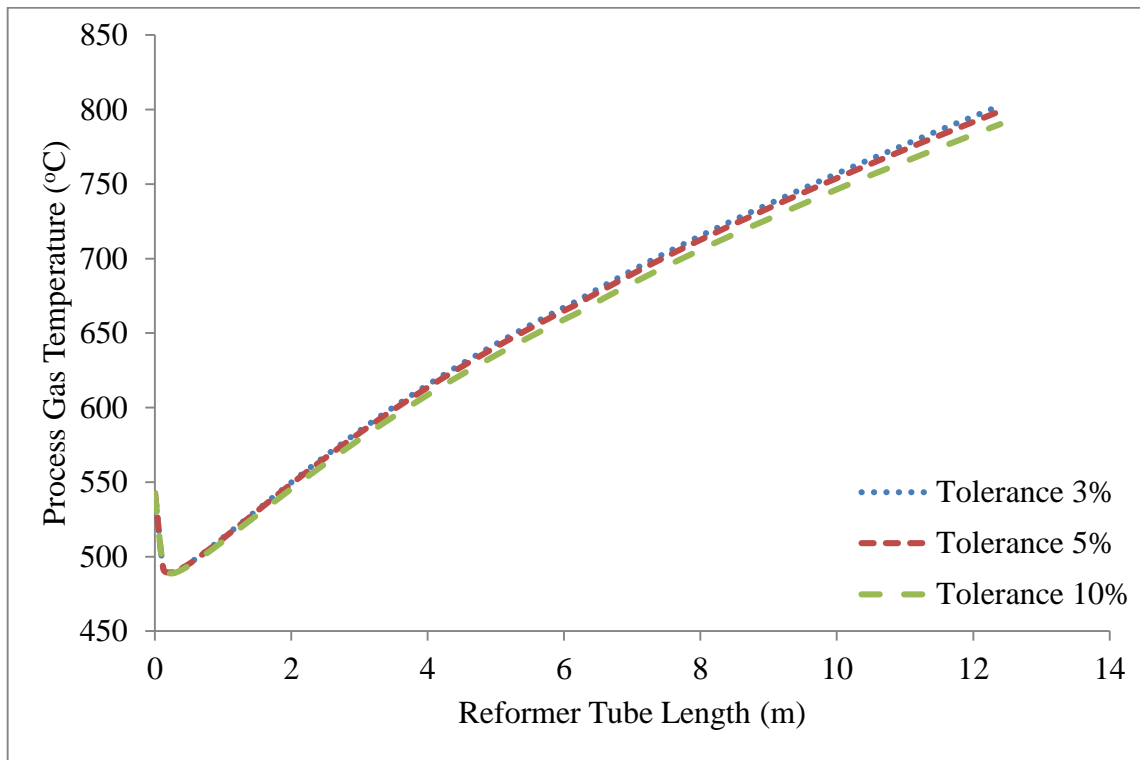


Figure 5.3. Process gas temperature profile along the tube length at various convergence tolerances.

When all parameters are taken into account, it can be concluded that model will result in different ways with each parameter defined. Under ideal circumstances, a model should deliver the best results with maximum number of segments, minimum step size and convergence tolerance. In this respect, 100 reactor segments, 3% convergence tolerance, 1 °C temperature increment with an initial seed value 620 °C has been chosen as basis for all simulation studies.

5.2. Evaluation of the Process Parameters

Industrial steam reforming furnace models have three kinds of parameters, namely the kinetic parameters, tube to process gas heat transfer coefficients and effective gas temperature, all of which are known to affect the simulation results. The effective gas temperature is the temperature controlling radiant transfer in the heater radiant section. It represents the overall temperature of the fire box in Well Stirred Furnace model. Kinetic parameters are omitted in this section, since relevant parameters of a similar type of catalyst

available in literature are used. In this section, the effects of, heat transfer coefficient and effective gas temperature will be evaluated.

Effective gas temperature is assumed to be equal to bridge-wall temperature readings by using features of a Terrace-Wall™ type reformer as described in detail in Section 2. Heat transfer coefficient constant is varied within range of 0.3- 1.2 and simulations are performed and the model outcomes, methane slip and exit temperature, are compared.

Table 5.4. Simulation results for $T_{fg} = T_{bw}$ at various heat transfer coefficients.

Leva's Constant	Simulation Results		Plant Data	
	CH ₄ % (v/v)	T _{out} (°C)	CH ₄ % (v/v)	T _{out} (°C)
0.3	17.67	674	5.97	827
0.813 (Original)	15.08	696		
1.1	Not Converged			
1.2	Not Converged			

Simulation results in this case showed great discrepancy with the field data even heat transfer coefficient is manipulated in a significant range. With these results, it can be concluded that for a combined model that uses well-stirred approach, bridge-wall temperatures cannot be assumed as the effective gas temperature of the Terrace-Wall™ type furnace chamber.

After this conclusion, simulations are repeated with effective gas temperatures that are 100, 150 and 200 °C higher than the bridge-wall temperature. This a rule of thumb gathered from literature stating that, for high temperature heaters with tall narrow fireboxes and wall firing, effective gas temperature may be 95 to 150 °C higher than the bridge-wall temperature (Ibrahim, 2010). Results of these simulations are tabulated below:

Table 5.5. Simulation results for $T_{fg} = T_{bw} + 100\text{ }^{\circ}\text{C}$ at various heat transfer coefficients.

Leva's Constant	Simulation Results		Plant Data	
	CH ₄ % (v/v)	T _{out} (°C)	CH ₄ % (v/v)	T _{out} (°C)
0.3	11.28	732	5.97	827
0.813 (Original)	8.6	762		
1.1	8.06	769		
1.2	Not Converged			

Table 5.6. Simulation results for $T_{fg} = T_{bw} + 150\text{ }^{\circ}\text{C}$ at various heat transfer coefficients.

Leva's Constant	Simulation Results		Plant Data	
	CH ₄ % (v/v)	T _{out} (°C)	CH ₄ % (v/v)	T _{out} (°C)
0.3	8.42	764.60	5.97	827
0.813 (Original)	5.83	799.44		
0.9	5.63	802.62		
1.1	5.3	808.86		
1.2	5.19	809.62		

Table 5.7. Simulation results for $T_{fg} = T_{bw} + 200\text{ }^{\circ}\text{C}$ at various heat transfer coefficients.

Leva's Constant	Simulation Results		Plant Data	
	CH ₄ % (v/v)	T _{out} (°C)	CH ₄ % (v/v)	T _{out} (°C)
0.3	5.85	799.25	5.97	827
0.813 (Original)	3.41	843		
0.9	3.25	847		
1.1	2.93	854		
1.2	2.82	857.76		

As can be seen from the end results of simulations, effective temperature of the Terrace-Wall™ type furnace is likely to be more than 150 °C above the bridge-wall temperature. In order to visualize the effect of heat transfer coefficient constant over

simulation results, $T_{bw} + 150$ °C case with Leva's constants 0.813 and 1.2 can be plotted as follows:

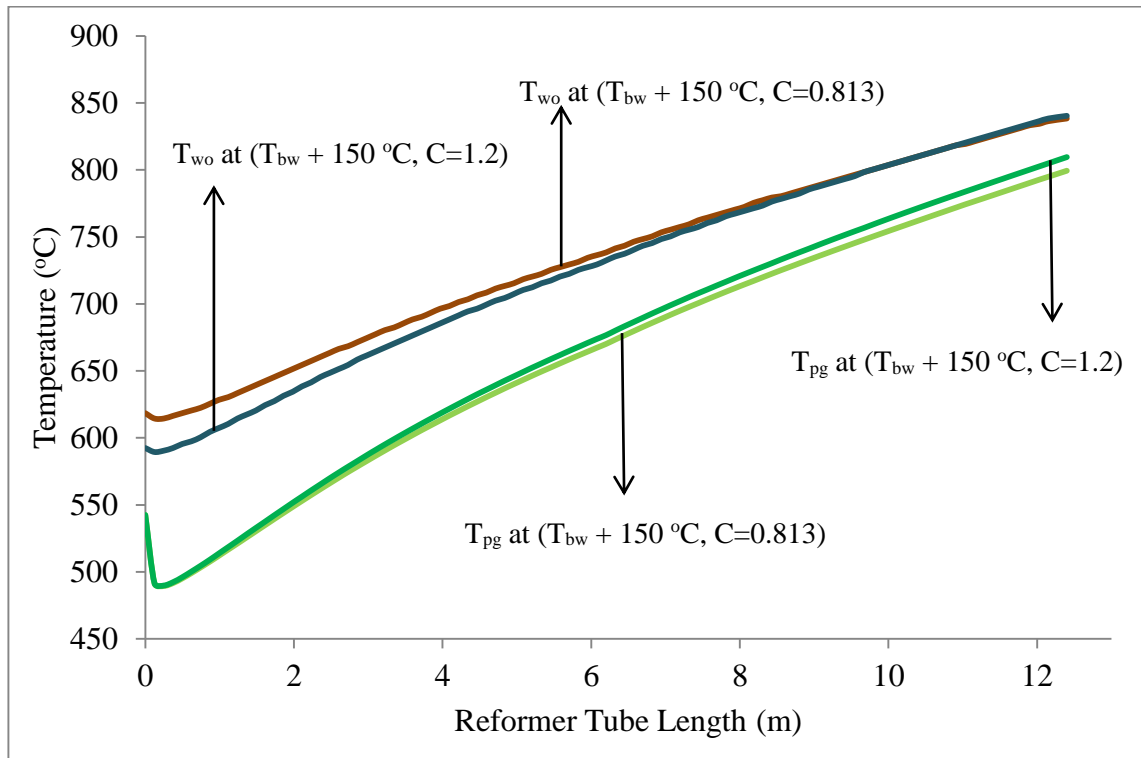


Figure 5.4. Temperature profiles of tube outer wall and process gas through tube length at different Leva's constants.

Heat transfer coefficient constant plays significant role in the temperature profiles of process gas and outer tube wall. Therefore, proper determination of heat transfer coefficient is essential, as low and high values may lead to fail in convergence. The trends shown in Figure 5.4 are meaningful since the highest heat transfer coefficient, i.e., the lowest heat transfer resistance, results in the highest capability of heat absorption by the reactant mixture, hence cause proximation between outer tube wall and process gas temperature profiles.

When the effect of different effective flue gas temperature with the same heat transfer coefficient constant is evaluated, profiles for $T_{bw} + 200$ °C and $T_{bw} + 150$ °C at Leva's constant of 0.3 can be shown in Figure 5.5 below:

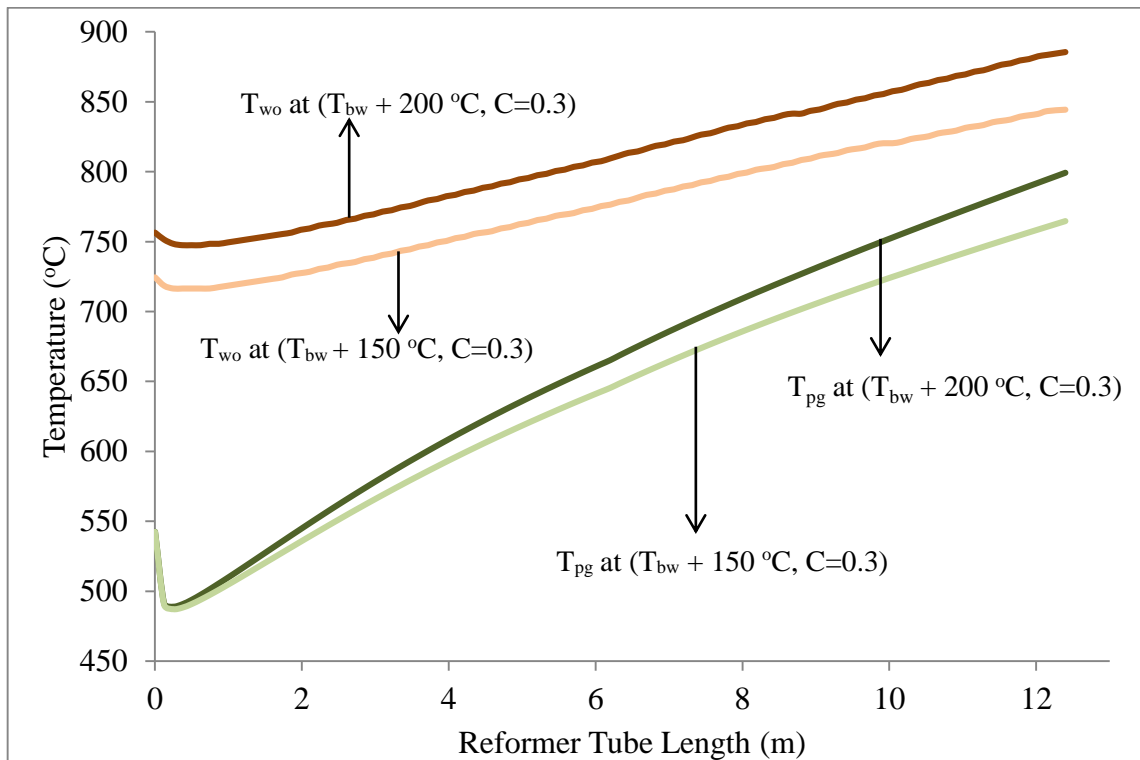


Figure 5.5. Temperature profiles of tube outer wall and process gas through tube length at different effective gas temperatures.

Change in effective flue gas temperatures with same heat transfer coefficient constants simply make profiles shift in the direction of temperature change. Process gas temperature does not show significant variation in the tube section where endothermicity is at its peak value. However, process gas temperature profile shifts through the rest of the tube. Regarding tube outer wall temperature, the affection from heating ambient is more obvious than process gas temperature.

Again from tabulated results, it can be noted that $T_{bw} + 150\text{ °C}$ and $T_{bw} + 200\text{ °C}$ cases with Leva's coefficients 0.813 and 0.3, respectively, yield very similar end results. When the whole process is evaluated not only in terms of end results but also the temperature profiles they possess, the following results can be obtained (Figure 5.6):

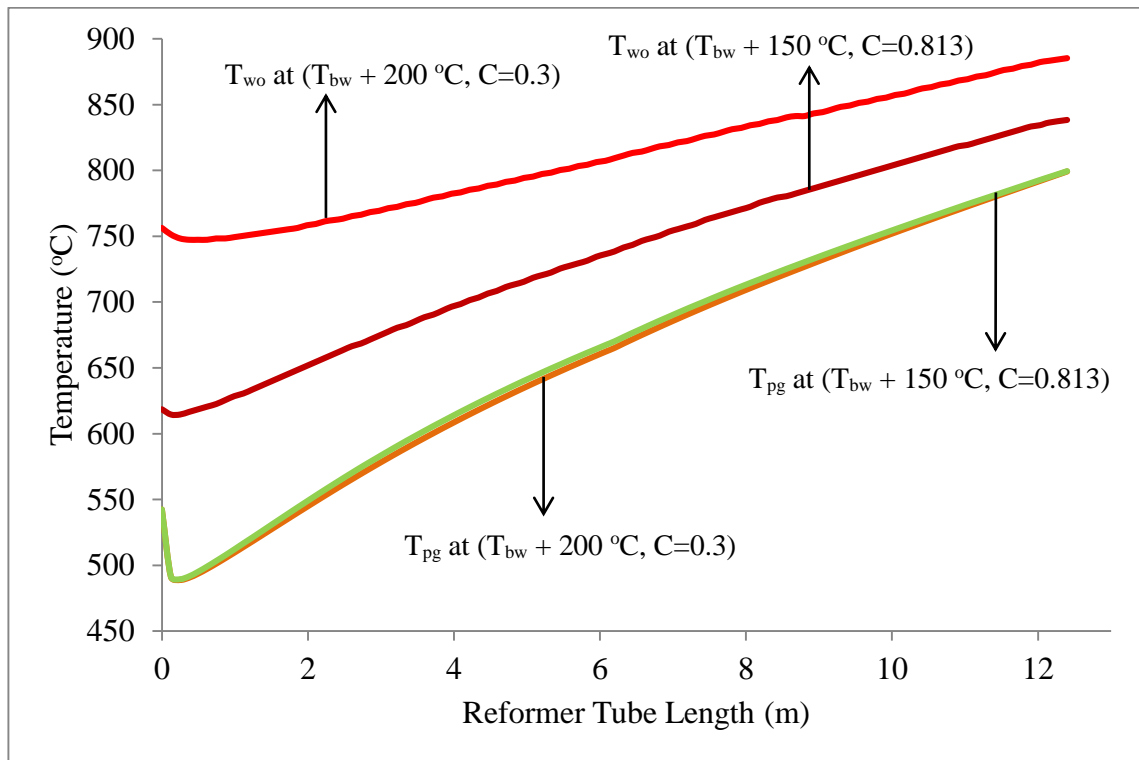


Figure 5.6. Temperature profiles of tube outer wall and process gas through tube length at different effective gas temperatures and Leva's constants.

Although all input data are the same except effective flue gas temperatures and Leva's constant, these simulations differ from each other significantly in terms of outer tube wall temperature profiles while resulting in identical process side results. This case particularly implies the importance of proper determination of model parameters as they highly influence the outcomes. Furthermore, regarding all cases, there are temperature decreases in the first part of the tubes for both process gas and tube outer wall due to endothermicity. After strong endothermicity is overcome, temperatures of process gas and tube begin increasing continuously due to strong heat transfer to reformer tubes.

The proper determination, that is to say realistic representation of the parameters, must now be carried out considering additional cross check values. The new parameters should be temperature readings on the reformer tubes. These readings will be covered in detail in Section 5.3. For the time being, outer tube wall temperature readings regarding the case considered so far are provided in Table 5.8:

Table 5.8. Tube outer wall temperature readings and model results using different parameters.

	T_w (6m from top)	T_w (11m from top)
$T_{fg} = T_{bw} + 150\text{ }^\circ\text{C}$ Leva's constants = 0.9	734.5 $^\circ\text{C}$	820.5 $^\circ\text{C}$
$T_{fg} = T_{bw} + 200\text{ }^\circ\text{C}$ Leva's constants = 0.3	806.5 $^\circ\text{C}$	869.43 $^\circ\text{C}$
Plant Result	785 $^\circ\text{C}$	853 $^\circ\text{C}$

These results show that tube wall temperatures of a Terrace-Wall™ type steam reformer can be closely predicted even with literature kinetics and roughly predicted parameters. It is demonstrated that successful prediction can be achieved if an extensive parameter investigation procedure can be applied for unknown process parameters which are essential for model accuracy, such as heat transfer coefficient. It should also be noted that, values provided in this section for effective gas temperature and Leva and Grummer's equation constants are applicable for Xu and Froment's intrinsic kinetics. Parameter estimation should include, effective flue gas temperature, tube to process gas heat transfer coefficient and parameters of the steam reforming rate equations. The strong relation between process gas outlet temperature and product composition is due to the parameters of steam reforming kinetics used. Considering three most important outcomes of a steam reformer monitoring model which are, tube wall temperature profile, process gas outlet temperature and composition, only tube wall temperature profile and either process gas outlet temperature or outlet composition can be predicted provided that proper model parameters are assigned. Simultaneous prediction of these variables absolutely requires knowledge of commercial catalyst kinetic parameters.

By using the knowledge gained from discussions in this section, simulations will be continued by using effective flue gas temperature as ($T_{bw} + 190\text{ }^\circ\text{C}$), and tube to process gas heat transfer coefficient as 0.35.

5.3. Case Studies

Within the scope of this thesis, case studies are performed by the constructed models and estimated parameters with inputs gathered from Process Historian Database (PHD). Afterwards, results are compared with laboratory analysis outcomes and manual observations, i.e. pyrometer readings. As discussed in Section 2.7, full process information that the model can be tested with is quite limited. In this respect, meaningful datasets are identified and tested by model.

Steam reformer's outlet stream composition is tested once in a month in order to observe catalytic activity. Furthermore, reformer tube temperatures are observed by pyrometers, remote sensing devices that intercept and measure thermal radiation. They represent a background radiation problem for which temperature reading should be corrected. There are more accurate methods, i.e. gold cup, to measure tube skin temperature but their daily usage is very limited. Pyrometers measure temperatures of the tube which are directly facing to peep-holes at two terrace levels in the side section of furnace box. Besides general eye observation on reformer tubes, measurements done by pyrometers, on twice in a day, and are regarded to give a general representation of the furnace chamber status. In terms of laboratory analysis, composition analysis for each feed, fuel and reformer effluent (once in a month) stream are done on dry basis (i.e. without water content).

Flow rates, temperatures and pressures of each feed and fuel streams are taken from PHD at the time when samples are collected for compositional analysis (06:00 a.m). Those flows are not used as raw values in the model. First, an in house flow compensation procedure is applied since measuring devices are calibrated for values different than operating conditions. Then, individual feed streams are mixed together and component based feed stream is created by using compositional analysis. Based on field knowledge, it is assumed that composition of the reformer feed does not change significantly in the hydrodesulphurization (HDS) reactors. Pyrometer measurements are also taken at the same time for laboratory sampling to check tube wall temperature predictions of the model. In this regard, constructed model inputs taken from fields are given in Table 5.9 as follows:

Table 5.9. Input variables for case studies.

	Case 1	Case 2	Case 3
$F_{eq.}$ (kmol/hr)	14.73	15.918	15.928
T_{in} (°C)	542.5	546	549
P_{in} (bar(a))	25.527	25.527	25.527
CH ₄ % (v/v)	22.65	20.1	20.51
H ₂ O % (v/v)	68.8	63.14	63.14
H ₂ % (v/v)	7.93	16.45	15.86
CO % (v/v)	0	0	0
CO ₂ % (v/v)	0.02	0.016	0.02
N ₂ % (v/v)	0.6	0.294	0.29
T_{bw}	876	876	884

All three cases differ from each other from several aspects. Under normal operation, equivalent molar flow rates and inlet pressures are substantially stable. Moreover, feed inlet temperature does not vary appreciably. Most significant differences are feed compositions and, as a result, bridge-wall temperatures. Furthermore, bridge-wall temperature is directly related to fuel consumption, which depends on desired hydrogen production rate. Field data for model outputs of corresponding cases are given below:

Table 5.10. Process field data of simulation outputs.

	Case 1	Case 2	Case 3
T_{out} (°C)	827	829	828
P_{out} (bar(a))	24.34	24.25	24.24
CH ₄ % (v/v)	5.97	5.82	5.39
H ₂ % (v/v)	77.71	75.63	77.73
CO % (v/v)	10.17	10.43	10.10
CO ₂ % (v/v)	5.05	5.70	5.55
N ₂ % (v/v)	1.11	2.43	1.23
T_{bw}	876	876	884

Table 5.10. Process field data of simulation outputs (cont.).

	Case 1	Case 2	Case 3
$T_{w,o}(6m)$ –Avg.	785	790	793
$T_{w,o}(11m)$ –Avg.	853	862	866

A brief interpretation of process parameters and their interactions is vital by evaluating the process output field data given in Table 5.10. When cases 2 and 3 are compared, effect of increased bridge-wall temperature can be clearly seen on hydrogen yield and methane slip. Due to elevated temperatures, endothermic reactions are favored. Besides, tube skin temperature is also relatively higher. When cases 1 and 2 are considered, whose bridge wall temperatures are same but differ significantly in terms of hydrogen content in the feed, analysis of feed composition effect can be done. Since hydrogen is in the product side of the SMR equilibrium reactions, its presence favors reactions in the reverse direction. In case 1, hydrogen amount is smaller hence SMR reactions push forward to product side and result in higher hydrogen yield, even with relatively smaller input temperature contribution. Furthermore, endothermicity effect can also be seen in wall temperatures. Although bridge-wall temperatures are same, tube wall temperatures at different locations of the tube are different in each case. Since lack of hydrogen favors endothermicity in first case, tube skin temperatures are relatively lower than in case 2.

When cases are taken into account all at once, the variation in pressure drop reported in Table 5.10 is expected due to stoichiometric volume expansion along reformer tube. Moreover, compared to the other parameters, the change in the outlet temperature is found to be small. When considering outlet temperature readings, it should be noted that temperature readings are done from a distance away from reactor outlet so the seasonal ambient variations do have effect on temperature reading. As one may clearly expect, outlet temperature readings to be a little bit higher than actually measured.

5.4. Case Study Results

All simulations for field cases were performed on the same basis as stated below:

Table 5.11. Solution parameters for case studies.

	Value
Number of Segments	100
$T_{w,o}$ temperature increments	1 °C
Tolerance	3%
Leva's Correlation Constant	0.35
Effective Gas Temperature	$T_{bw} + 190$ °C
Excess air	15%

Conversions are given for methane and steam indicating that how much of reactant reacted in fractional basis.

Table 5.12. Case 1 results. Plant data vs. model predictions.

Case 1 (18.09.2014)			
	Plant Data	Model Result	Deviation (%)
T_{out} (°C)	827	800	-3.26
P_{out} (bar(a))	24.34	24.41	-0.29
CH ₄ %(v/v)	5.97	5.81	-2.68
H ₂ %(v/v)	77.71	74.35	-4.32
CO %(v/v)	10.17	10.95	7.67
CO ₂ %(v/v)	5.05	8.21	62.57
N ₂ %(v/v)	1.11	0.66	-40.54
$T_{w,o}$ (6m)	785 (Avg.)	790	0.64
$T_{w,o}$ (11m)	853 (Avg.)	857.45	0.52

Table 5.13. Case 2 results. Plant data vs. model predictions.

Case 2 (15.01.2015)			
	Plant Data	Model Result	Deviation (%)
T _{out} (°C)	829	807.65	-2.58
P _{out} (bar(a))	24.25	24.34	-0.37
CH ₄ %(v/v)	5.82	5.40	-7.22
H ₂ %(v/v)	75.63	77	1.81
CO %(v/v)	10.43	10.27	-1.53
CO ₂ %(v/v)	5.70	6.94	21.75
N ₂ %(v/v)	2.43	0.33	-86.42
T _{w,o} (6m)	790 (Avg.)	796.15	0.78
T _{w,o} (11m)	862 (Avg.)	861.15	-0.10

Table 5.14. Case 3 results. Plant data vs. model predictions.

Case 3 (19.02.2015)			
	Plant Data	Model Result	Deviation (%)
T _{out} (°C)	828	812.20	-1.91
P _{out} (bar(a))	24.24	24.32	-0.33
CH ₄ %(v/v)	5.39	5.22	-3.15
H ₂ %(v/v)	77.73	76.93	-1.03
CO %(v/v)	10.10	10.62	5.15
CO ₂ %(v/v)	5.55	6.90	24.32
N ₂ %(v/v)	1.23	0.318	-74.15
T _{w,o} (6m)	793 (Avg.)	800.25	0.91
T _{w,o} (11m)	866 (Avg.)	866.25	0.03

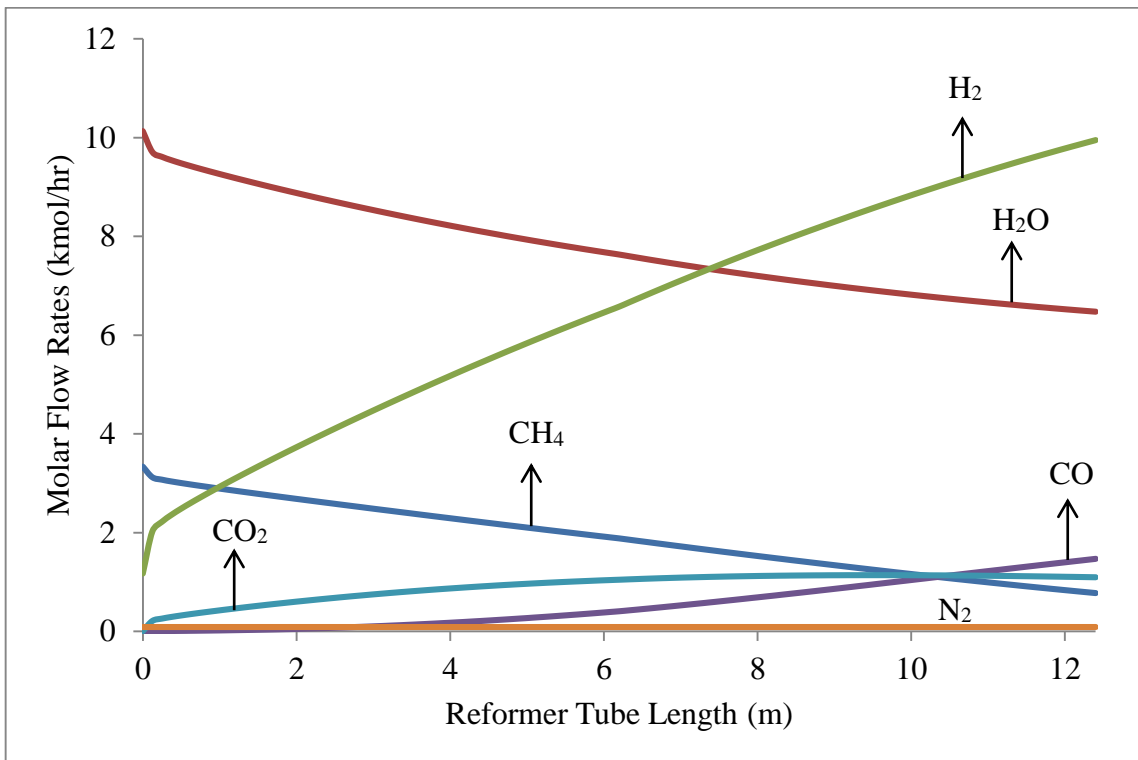


Figure 5.7. Species molar flow profiles through reformer tube for case 1.

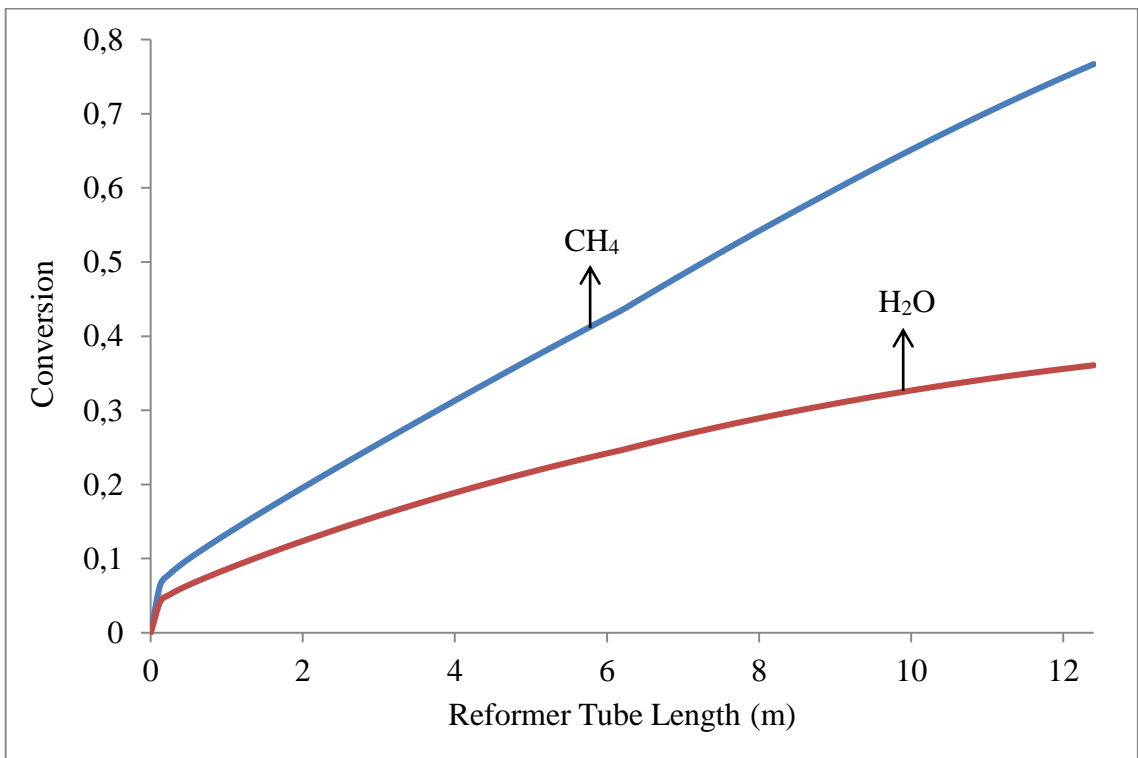


Figure 5.8. Conversion profiles of methane and steam for case 1.

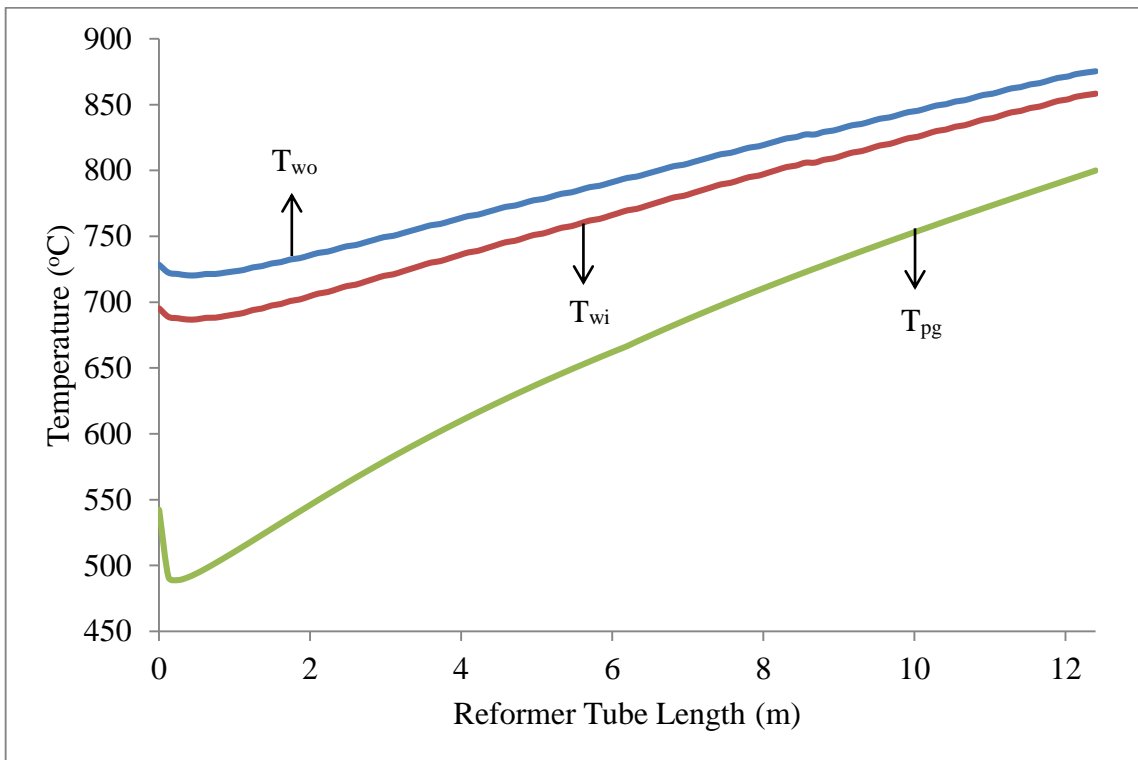


Figure 5.9. Temperature profiles for case 1.

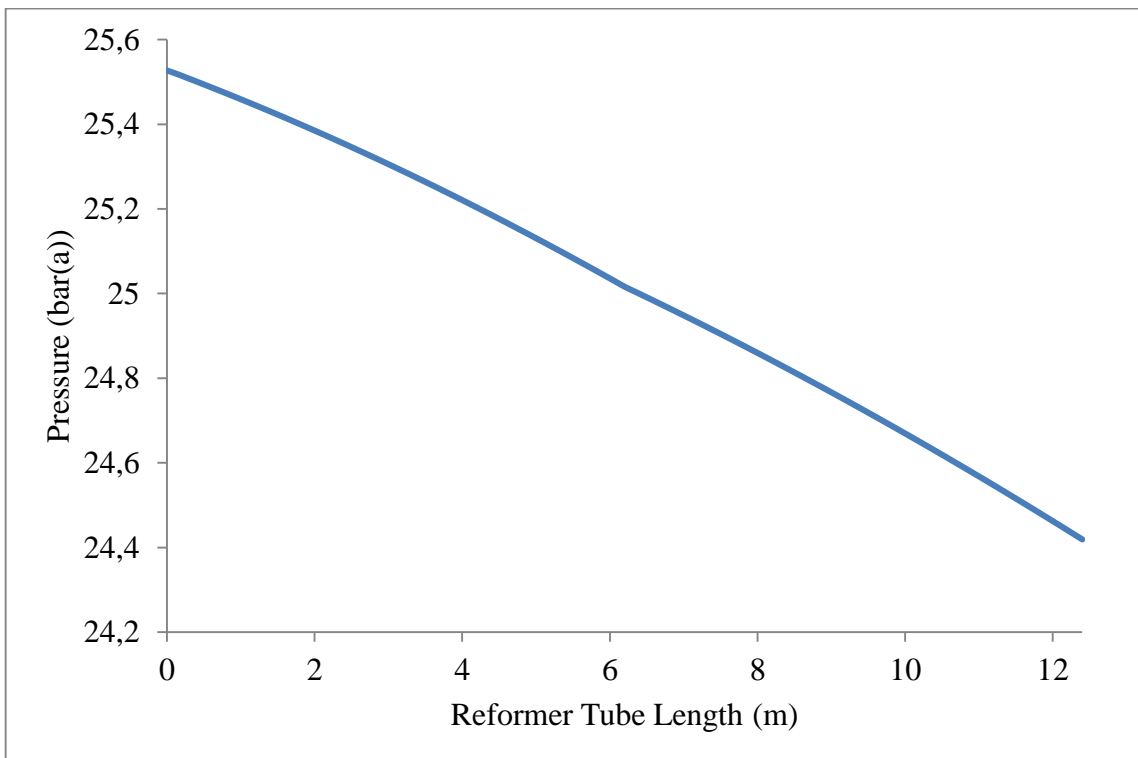


Figure 5.10. Pressure profile through reformer tube for case 1.

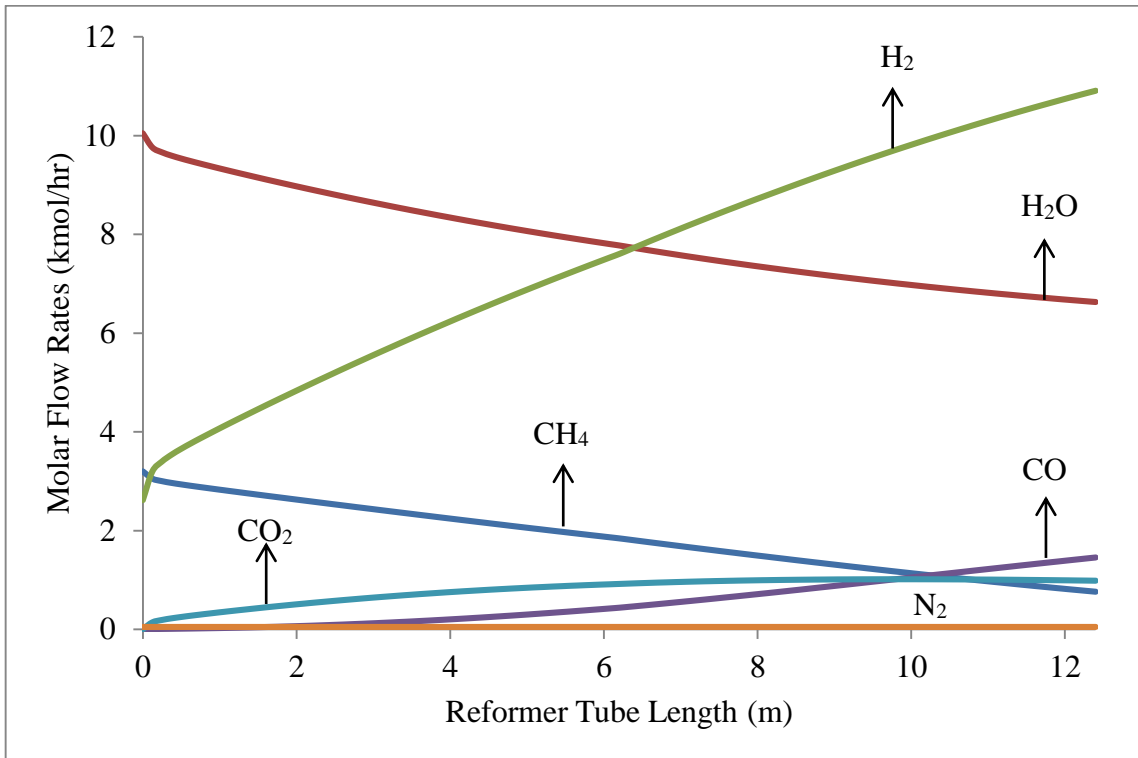


Figure 5.11. Species molar flow profiles through reformer tube for case 2.

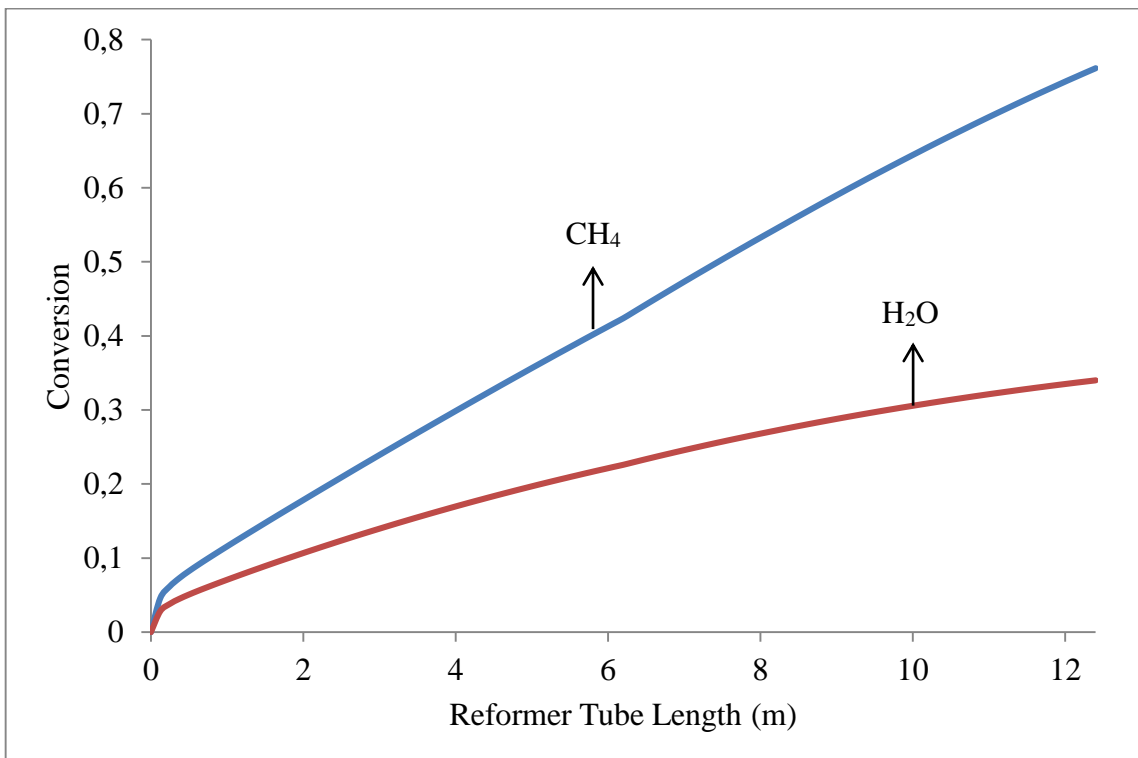


Figure 5.12. Conversion profiles of methane and steam for case 2.

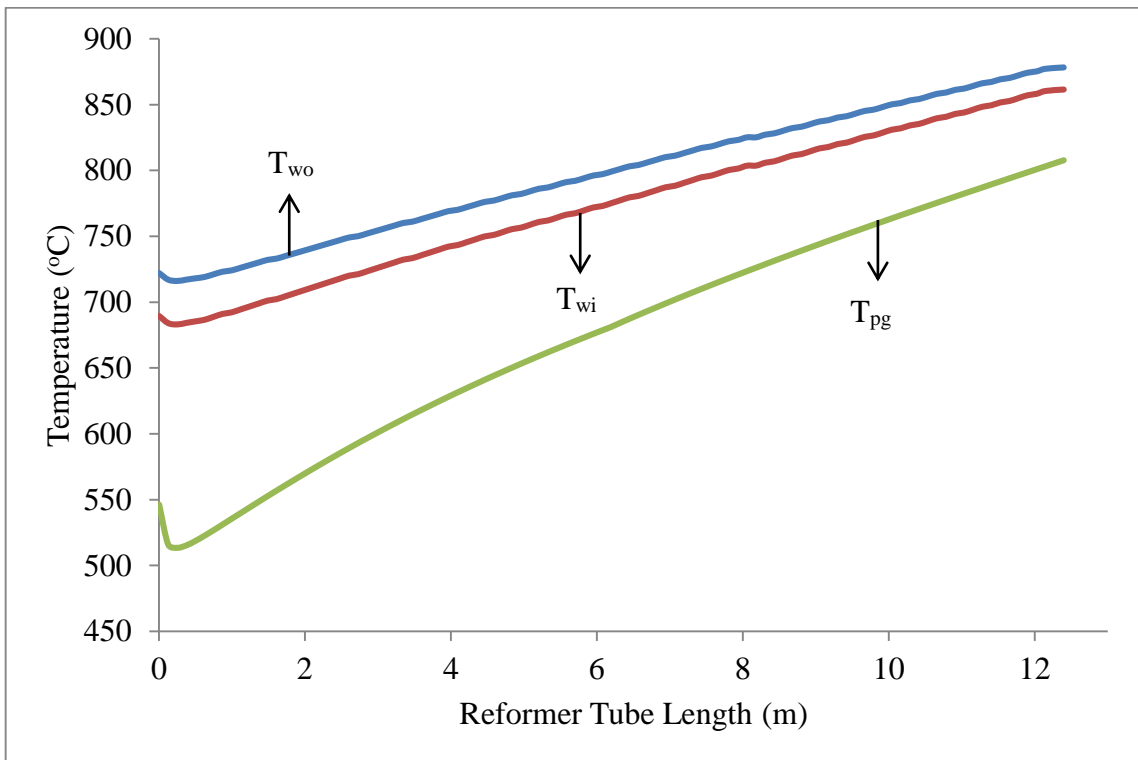


Figure 5.13. Temperature profiles for case 2.

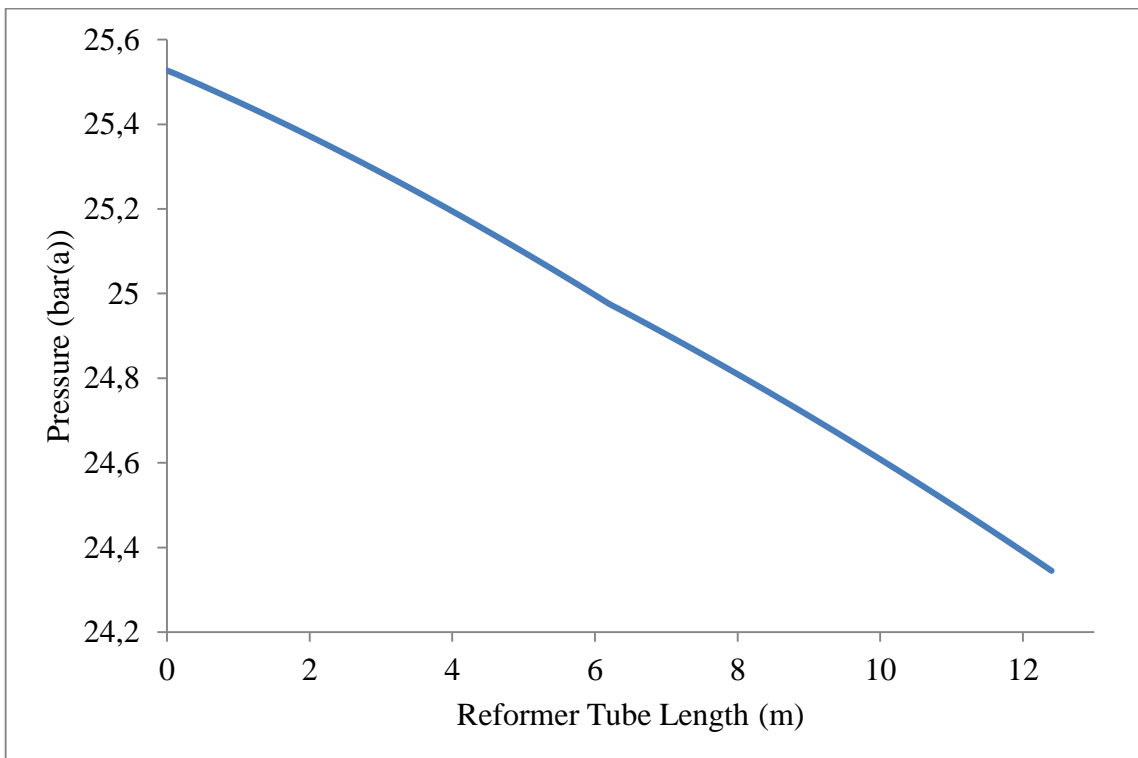


Figure 5.14. Pressure profile through reformer tube for case 2.

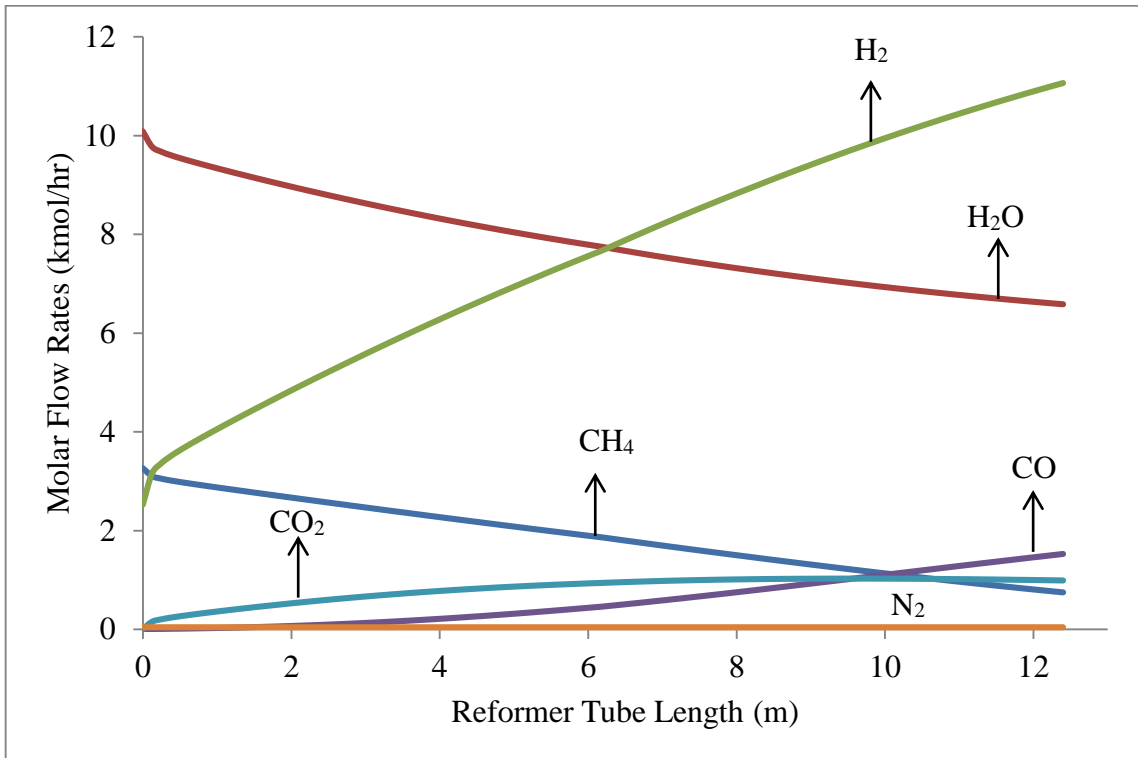


Figure 5.15. Species molar flow profiles through reformer tube for case 3.

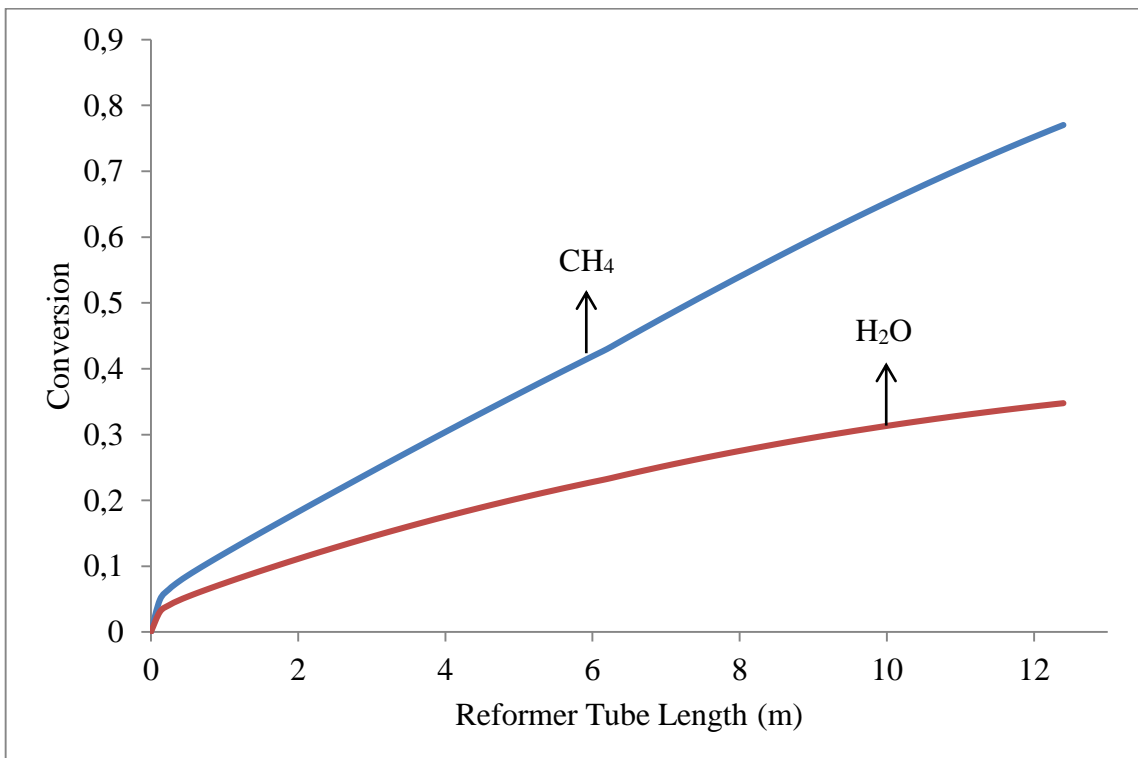


Figure 5.16. Conversion profiles of methane and steam for case 3.

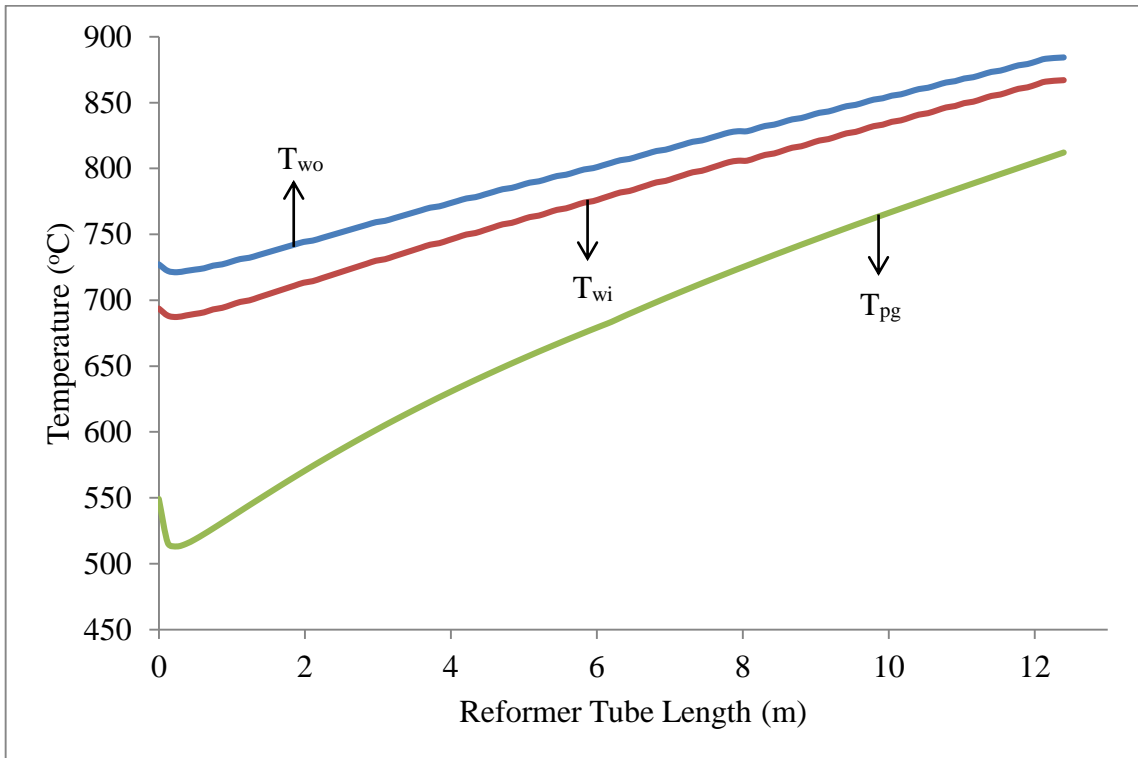


Figure 5.17. Temperature profiles for case 3.

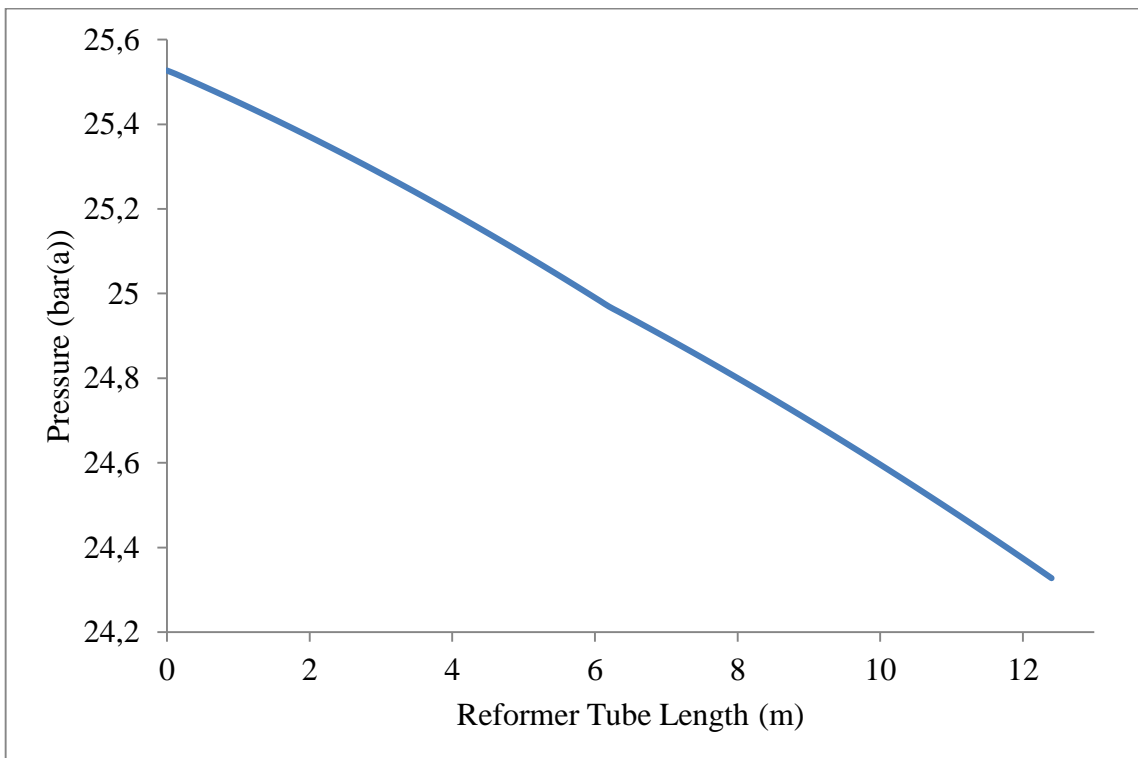


Figure 5.18. Pressure profile through reformer tube for case 3.

5.5. Discussion

Model results show that one dimensional pseudohomogeneous packed bed reactor model using literature kinetics integrated with a well stirred furnace model, which is using effective gas temperature 140 – 190 °C above bridge-wall temperature of a Terrace-Wall™ type reformer, give satisfactory results in terms of product yields. This is an expected result according to the literature, since it has been stated that at elevated temperatures close to reformer outlet temperature, equilibrium composition of process gas mixture is close to that of kinetic calculations (Rostrup-Nielsen, 1984). However, at process conditions through the length of the reactor, equilibrium composition diverges considerably from catalyst activity. As a result, for reformer simulation purposes, kinetics must be taken into account.

Although key features of product distribution are well-estimated, percentage of CO₂ predicted in the product is remarkably higher than what is measured in the laboratory analysis. The main reasons behind are the catalytic features of the industrial catalyst. Since kinetics and parameters of a catalyst commonly regarded in literature is used, it is likely to represent different characteristics. In this instance, industrial catalyst is likely to promote main steam reforming reaction while others reactions, producing CO₂, are not favored.

Process gas outlet temperatures are always predicted lower than field data due to combination of different effects. In the pseudohomogeneous model employed in this study, solid catalyst phase and its properties (solid heat capacity, thermal conductivity) are neglected. Hence, process gas temperature is normally expected to be higher than the field value. Kinetic parameters affect product distribution and temperature of process gas. Also, tube to process gas heat transfer coefficient has great impact on the results, since it affects the amount of energy that the reacting fluid can gain. Regarding the process side, results show that either product distribution or process gas temperature can be predicted by current kinetic parameters.

When tube wall temperature is considered, it can be stated that reactor model integrated to well-stirred furnace model can predict tube outer wall temperatures relatively close to corrected pyrometer measurements provided that the parameters are well estimated

for corresponding coefficients. Combustion chamber is considered to be a uniform medium due to structural features of Terrace-Wall™ furnace, however it does not fully represent the reality. Since rows of burners located on each terrace level fire parallel to sloped refractory walls, their physical presence closely affects the heat transfer to tubes facing them. The present furnace model, physical presence of burners and their combustion patterns are not taken into account. In the Terrace-Wall™ modeling work of Zamaniyan (2008), physical presence of burners at each terrace level shows their effect as two local temperature maxima in the middle and bottom section of the tubes where directly facing the burners which current model is unable to provide them (Zamaniyan *et al.*, 2008).

6. CONCLUSIONS AND RECOMMENDATIONS

6.1. Conclusions

The objective of the thesis is to develop a model that can calculate the outer tube wall temperature profile at specified process conditions of an industrial steam methane reformer plant in Tüpraş İzmit Refinery. The intention of the mathematical model developed is to help plant engineers and operators to continuously predict the tube wall temperatures that are likely to occur on reformer tubes in order to avoid exceeding temperatures and predict various outcomes (temperature, molar flow and conversion profiles along with pressure drop) of the reformer unit.

Complete model is based on the integration of two sub-models developed for furnace side and process side. Furnace side is regarded as a well-stirred combustion chamber, referring to structural features of Terrace-Wall™ type reformers. Radiative interactions between furnace components are built by accounting for tube and refractory arrangements with various simplifications and assumptions. Process side is considered to behave like a pseudo-homogeneous phase and modeled as a plug flow packed bed reactor. These two models are integrated to each other on tube outer wall temperature and an iterative solution procedure is applied to each segment through the end of reformer tube.

First of all, effects of user-defined solution parameters on the results are evaluated with sample data. After determining possible individual effects of these parameters on the results, suitable parameters are chosen to yield accurate results at short computational times. By using these solution parameters, individual effects of unknown model parameters, e.g. effective gas temperature and heat transfer constant, are evaluated afterwards and results are cross checked with the available plant data. After evaluation and selection of proper solution and model parameters, three case studies are performed by using field data as inputs and control values. Simulation results show close approach to field data only if proper model parameters are chosen. Although reformer kinetics are different, kinetics found in literature showed to be sufficiently applicable for an industrial application in terms of product composition. However, such kinetics uses specific parameters that further result in failure of

process gas outlet temperature prediction although its trend is likely to be successfully predicted. In this instance, either product composition or process outlet temperature can be determined due to the kinetic parameters.

Model can relatively predict tube wall temperatures at specified locations but is unable match whole profile through the reformer tube as in literature due to simplifications. Results show that tube wall temperature prediction is more successful in warmer sections of the reformer tube, whereas it diverges significantly through colder sections.

Consequently, the present model can be regarded as fast, efficient and straightforward way to monitor status of steam reformer tubes and outcomes of the reformer unit if proper model parameters are used.

6.2. Recommendations

Recommendations regarding the present work can be classified in two distinct groups namely, model modifications and parameter estimations. Results show that well-stirred furnace approach can be a simple and straightforward method to model radiative heat transfer in the combustion chamber of a Terrace-Wall™ reformer. However, considering the importance of the radiative heat transfer in the steam reforming furnace operation 20 °C difference in tube operating temperature has drastic effects on tube life, radiative heat transfer can better be modeled with a more specific and non-generalized method, such as the Hottle Zone method. Furthermore, the physical identification of energy release patterns and burners can make substantial development in the model accuracy.

Packed bed reactor models can be modeled, not necessarily as two dimensional but heterogeneous, including heat transfer properties of solid catalyst phase into account. Although this implementation can bring more realistic properties to the packed bed model, only this modification itself will not be enough since kinetics must also be changed accordingly. In this respect, even with the present model, an extensive parameter estimation procedure can be followed to find out suitable parameters for kinetics as well as heat transfer coefficients. In this respect, well-stirred furnace approach can be more applicable, since all of its current sub-model parameters are solely gathered from literature. Parameter estimation

procedure should cover the following steps: Temperature readings of reformer tube walls, and relevant process information including, temperatures, pressures and compositions of all feeds, products and fuels should be gathered all at once for several times. Afterwards, effective flue gas temperature, tube to process gas heat transfer coefficient and kinetic parameters should be fitted accordingly. Fitted values should then be tested with a different data set and their accuracy should be validated.

As a future work, Computational Fluid Dynamics (CFD) analysis can be considered since it is getting more attention day by day. Highest accuracy for such analysis of tube wall temperature and three dimensional analysis of temperature gradients as well as flow patterns can be obtained by a comprehensive CFD study.

APPENDIX A: RADIATIVE HEAT TRANSFER BACKGROUND

A.1. Radiative Heat Transfer Background

Radiative heat transfer is a highly complex subject and modeling of systems that involve radiation is always a challenging task. In this perspective, the definitions, equations and concepts regarding radiative heat transfer are limited to provide sufficient background for the subject “Well Stirred Furnace Model”. More information can be found in literature (Modest, 2003).

A.2. Radiation

Radiation is an energy transmission process in which energy is transmitted through a vacuum or through matter containing media. Energy transmitted by radiative transport is named as radiant energy, however, the term *radiation* is also commonly used to describe the radiant energy itself. Radiation is considered as an electromagnetic wave which carries energy in its oscillating electric and magnetic fields moving with speed of light. These waves are characterized by their wavelengths which differ significantly in their behavior (Viskanta and Mengüç, 1987). Electromagnetic radiation, in wavelength range of 0.1-100 μm , unlike microwaves etc., is produced solely by the temperature of a body and called thermal radiation (Karan and Baukal, 2013).

A.3. Interaction of Radiation with Surfaces

The electrons, atoms and molecules of all solids, liquids and gases above zero Kelvin are constantly in motion hence in practice all materials continuously emit and absorb thermal radiation by lowering or raising their molecular energy levels (Çengel, 2012). That means, unlike convection and conduction, radiative heat transfer does not require any driving force to occur. When thermal radiation, to be called radiation in this thesis from now on, emanate from the surface travel through medium (gas or vacuum) this progress is called emission. When a matter is exposed to radiation, some of it is absorbed by the receiving body and reconverted into internal energy as heating up the material, while the remaining energy is

reflected from or transmitted through the body. The fractions of radiation reflected, transmitted and absorbed by a surface are known, respectively, as reflectivity (ρ), transmissivity (τ), and absorptivity (α). The sum of these fractions equals one (Kalogirou, 2014).

$$\rho + \tau + \alpha = 1 \quad (\text{A.1})$$

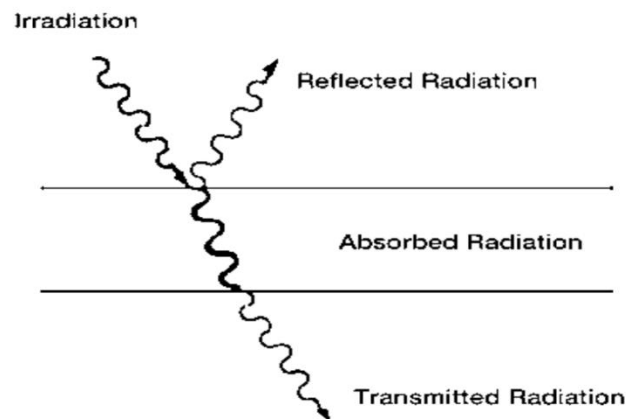


Figure A.1. Radiant energy absorbed, reflected and transmitted through material (Baukal, 2000).

For most solid materials, the transmissivity is low. The reflectivity of most solids is also low, unless they are highly polished and smooth (e.g. new stainless steel) that causes mirror-like effect. Most industrially important materials possess rough surfaces, that is, their surface irregularities are large compared to the wavelength of radiation. Reflection of radiation from this kind of surface occurs indiscriminately in all directions and is called *diffuse*. Diffuse reflection has wide acceptance, including industrial applications. For most gases, the transmissivity is generally very high with negligible absorptance and reflectance. These radiative properties are extremely important in determining how much radiation will be transferred to and from a medium (Gray and Müller, 1974) (Baukal, 2000).

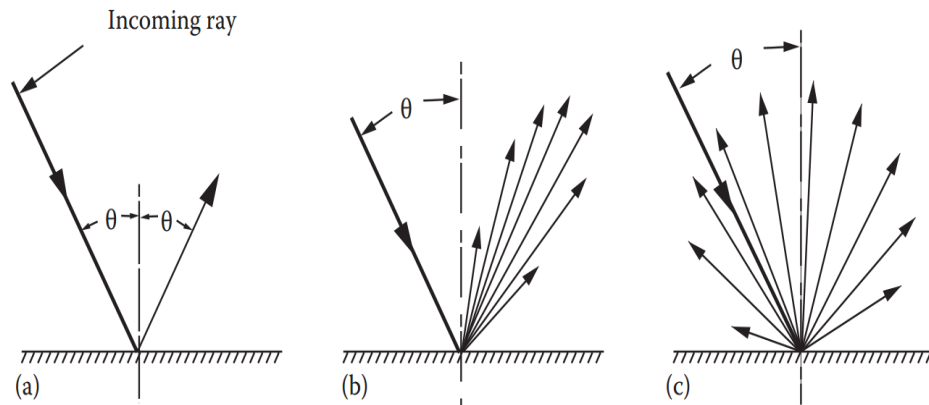


Figure A.2. Surface reflections (a) Mirror-like reflection of incoming ray, (b) reflection which is between specular and diffuse (a real surface) (c) Diffuse radiation in which directions of departure are uninfluenced by incoming ray angle (Minea, 2013).

Emissivity, reflectivity, absorptivity and transmissivity are functions of wavelength, temperature, incoming direction (except emissivity), and outgoing direction (except absorptivity). For heat transfer applications, the dependence on incoming direction for absorptivity (as well as reflectivity and transmissivity) and outgoing direction for emissivity is generally weak and is commonly neglected; i.e, it is assumed that the surface absorbs and emits diffusely (Modest, 2000). Bodies, in which emittance from surface is independent of direction, that is to say same for all directions, are diffuse emitters or *Lambert surfaces*. Industrial surfaces are generally rough and they approach diffuse characteristics. Thus Lambert concept provides the basis for most calculations in high temperature engineering.

A.4. Surface Radiation

The blackbody is an ideal surface that absorbs all incident radiation regardless of wavelength, direction and surface properties. Furthermore, a blackbody is a diffuse emitter, that is emitted intensity is the same in all directions. At any prescribed wavelength and temperature, no surface can emit more energy than a blackbody (Zhang and DeWitt, 2009). The maximum radiant energy emitted from a surface per wavelength, per unit time and per area is defined as the monochromatic (single or very narrow wavelength (λ)) blackbody emissive power by Planck's equation:

$$E_{\lambda,b} = f(\lambda, T) \quad (\text{A.2})$$

Where $f(\lambda, T)$ is provided in many textbooks (Kalogirou, 2014). The total blackbody emissive power (E_b) is the maximum amount of energy that can be emitted from a surface at a given temperature over all wavelengths. It is defined by Stefan-Boltzman Law, which in terms found by integration of Planck's distribution over entire wavelength spectrum.

$$\int_0^{+\infty} E_{\lambda,b}(\lambda, T) d\lambda = E_b = \sigma T^4 \quad (\text{A.3})$$

Real surfaces emit less energy than corresponding blackbodies. The ratio of the total emissive power, E , of a real surface to the total emissive power, E_b , of a blackbody, both at the same temperature, is called the emissivity (ε) of a real surface.

$$\varepsilon = \frac{E}{E_b} \quad (\text{A.4})$$

The emissivity of a surface generally varies strongly and in complex ways with wavelength, emission direction, temperature, as well as depending on the material, surface layer composition and surface structure (roughness). The radiant heat transfer absorbed/emitted by real surfaces is a function of the absorptivity/emissivity of the surface. Total radiant energy emitted by a blackbody can be calculated from:

$$E = \varepsilon \sigma A T^4 \quad (\text{A.5})$$

A.4.1. Kirchoff's law and graybody concept

A matter in thermal equilibrium with surroundings will continue to emit and absorb radiation. Since equilibrium conditions are established, matter's surface must emit same amount of energy that of absorbed in order to attain temperature of the surroundings. Kirchoff's Thermal Radiation Law states that at any given temperature and wavelength, monochromatic emissivity and absorptivity are equal. Hence, if emissivity is known absorptivity is also determined.

$$\varepsilon(\lambda, T) = \alpha(\lambda, T) \quad (\text{A.6})$$

If the incident and emitted radiation have the same spectral distribution, in addition to the temperature equilibrium at the surfaces, total emissivity and absorptivity can be related over the entire wavelength.

$$\varepsilon(T) = \alpha(T) \quad (\text{A.7})$$

Such conditions are rarely met in real life; to simplify the analysis of radiation problems, however, the assumption that monochromatic properties are constant over all wavelengths is often made. This assumption leads to a characteristic surface type called *gray body* (Kalogirou, 2014). Gray body absorbs, and hence emits, the same fraction of energy at each wavelength, which means its properties are independent of wavelength. Spectral emissive power of a graybody can be written as (Modest, 2000):

$$E_{\lambda} = \varepsilon_{\lambda} \sigma A T^4 \quad (\text{A.8})$$

Eventhough real surfaces do not meet this specification exactly, it is often possible to choose suitable average values for the emissivity and absorptivity to make the graybody assumption acceptable for engineering analysis. By nature, graybody approach is a more realistic approximation than blackbody idealization and also simplifies the analysis.

At a given operating temperature a gray surface ought to emit the same radiation as the real surface it represents. Therefore, selection of gray body emissivity to equalize the areas under the emission curves of the real and gray surfaces is the key for successful approximation.

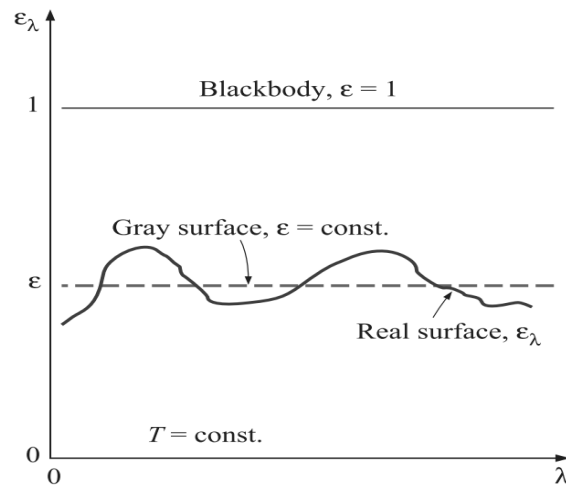


Figure A.3. Comparison of the emissivity of a real surface with those of a gray surface and a blackbody at the same temperature (Çengel, 2012).

A.5. Radiation Exchange Between Surfaces

For the analysis of radiative heat transfer, one should consider not only the surface temperatures and their characteristics but also their geometric orientation with respect to each other. This is can be done in highly complex ways by dividing surfaces into segments and follow numerical procedures for each section or lumping surfaces for simplification and follow case based approach.

A.5.1. The radiation shape factor

One of the key problems in calculating radiation heat transfer between surfaces is to determine the fraction of the total diffuse radiation *leaving* one surface and *goes directly* to another surface and vice versa.

The effects of the geometry on radiant energy exchange can be analyzed conveniently by defining the term shape factor. Radiation shape factor, F_{1-2} , is defined as the fraction of diffusely distributed radiation that leaves a surface A_1 and reaches surface A_2 . The first subscript appended to the radiation shape factor denotes the surface from which the radiation emanates, while the second subscript denotes the surface receiving the radiation. The *shape factor* is also often called the *configuration factor* or the *view factor* or the *geometry factor* (Kalogirou, 2014) (Kreith *et al.*, 2010).

$$F_{1-2} = \frac{\text{Radiation leaving surface 1 that goes directly to surface 2}}{\text{Total radiation leaving surface i in all directions}} \quad (\text{A.9})$$

Shape factors for a large number of geometric arrangements have been evaluated and ready to be used in literature. Methods of view factor algebra uses basic rules of reciprocity and summation that are to be discussed in the next section but is applicable for fairly simplified geometries. Calculation of shape factors for arbitrary surfaces in three dimensions is quite complex and is carried out numerically. Within the scope of well stirred furnace model, numerical evaluation of shape factors will not be handled.

A.5.2. The enclosure rule

For an enclosure consisting of N surfaces, the energy leaving any surface inside must be incident on all the surfaces making up the enclosure. This includes the surface itself if it is concave and can in effect see itself. All fractions of energy leaving the e th surface and reaching the other surfaces must total unity. In general, for a N surface enclosure in which surface e is a part (Janna, 2000) .

$$\sum_{r=1}^N F_{e,r} = 1 \quad (\text{A.10})$$

A.5.2. Reciprocity rule

This theorem can be used to determine geometric factor of one surface from the knowledge of the other. Eventhough this equation is derived in the limit that the temperatures of surfaces are equal, since area and view factors do not depend on temperature, the relationship must be true whether or not the temperatures are equal (Nellis and Klein, 2009).

$$A_1 F_{1-2} = A_2 F_{2-1} \quad (\text{A.11})$$

This product, having the dimensions of area, is called direct exchange area usually designated with $\overline{s_1 s_2}$ and $\overline{g_1 s_2}$ in the literature.

A.5.3. Electrical circuit analogy

An inspection by Oppenheim and Calif (1956) shows that heat flow by radiation in enclosures and the flow of electric current between potentials are analogous. Between two black surface 1 and 2, the net rate of radiation heat transfer ($q_{1 \rightarrow 2}$) is driven by a difference in their blackbody emissive powers, $E_{b,1} - E_{b,2}$, and the resistance to the radiative heat transfer is the inverse of the product of the area and view factor (Kreith *et al.*, 2010).

$$q_{1 \rightarrow 2} = \frac{(E_{b,1} - E_{b,2})}{R_{1,2}} \quad (\text{A.12})$$

The denominator $R_{1,2}$, is sometimes referred to as the surface to surface, geometrical or space resistance:

$$R_{1,2} = \frac{1}{A_1 F_{1,2}} = \frac{1}{A_2 F_{2,1}} \quad (\text{A.13})$$

The space resistances tends to increase as either the area of the surface or the view factor between the surfaces is reduced; this is meaningful as reducing the area or view factor will reduce the ease of radiative interaction of subject surfaces.

Electrical circuit analogy is a useful tool to formulate net exchange for radiation problems which does not include high numbers of radiative interactions among surfaces. For an advanced model that include complex geometries and complicated network, such analogy may be tortuous rather than being practical.

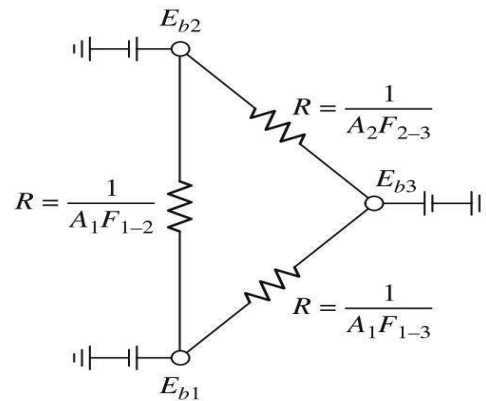


Figure A.4. Equivalent network for radiation in blackbody enclosure consisting of three surfaces.

A.5.4. Special surface case : Radiatively adiabatic surfaces

Special attention must be paid on no-flux or radiatively adiabatic surfaces. Their characteristic is rather important, since they totally and diffusely reflect and emit radiation, i.e intensity is independent of direction, at the same rate of exposure. Under steady-state operation, interior refractory walls of industrial furnaces can be regarded as of such type. Furnace refractory walls receive energy by both convection and radiation while lose energy by conduction. In application, the radiative contribution is so large than the other mechanisms so that they can be essentially regarded as re-radiators or no-flux surfaces.

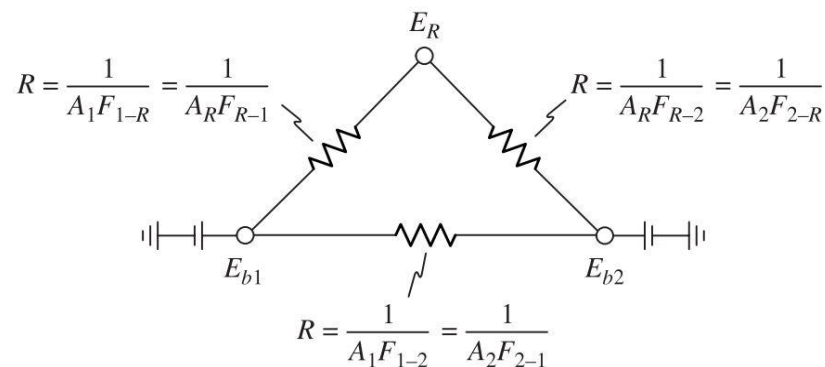


Figure A.5. Equivalent network radiation in an enclosure consisting of two black surfaces and an adiabatic surface.

Some part of radiation emitted from A_1 (showed with E_{b1} node) straightly hits A_2 (showed with E_{b2} node) while the other part goes to A_R where it is totally reflected from. Regarding the reflected part, some returns to A_1 again while rest hits A_2 . By this explanation, one can conclude that resistors work in both directions. Since refractory walls are radiatively adiabatic, they must get rid of all the incident radiation by either reflection or radiation, their emissive power will act in the steady state like a *floating potential*.

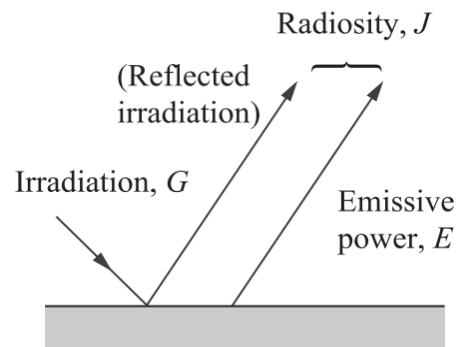


Figure A.6. The three kinds of radiation flux: emissive power, irradiation and radiosity (Çengel, 2012).

A.5.5. Heat transfer between diffuse gray surfaces

The calculation of radiative heat transfer between gray surfaces include the total radiation leaving the surface regardless of its source. In this respect, an energy quantity representing the rate of radiation streaming away from a unit area of the surface in all directions should be defined. Mentioned quantity is referred as *radiosity*, denoted with J . For a blackbody, it is simply equal to the emissive power, E_b , hence reflection was cancelled out since blackbody absorbs all incident radiation (Çengel, 2012) .

$$J = \epsilon E_b + \rho G \quad (\text{A.14})$$

Remember that for a blackbody, J is equal to blackbody emissive power E_b . In addition, the radiosity associated with a surface is a particularly complex function of wavelength since the spectral distribution of the radiation emitted from the surface may differ substantially from the spectral distribution of radiation reflected from the surface; this

complexity can be ignored for gray surface calculations as surface characteristics are considered to be independent of wavelength. The net rate of radiation heat transfer from surface 1 can be calculated using an energy balance on the surface expressed in terms of irradiation and radiosity.

$$q_1 = A_1 J_1 - A_1 G_1 \quad (\text{A.15})$$

First term in subtraction is equal to radiosity and the later is irradiation. By using adiabatic surface assumption and equalizing radiosity to irradiation, one can arrange the equation as below (Nellis and Klein, 2009):

$$q_1 = \left(\frac{\varepsilon_1 A_1}{1 - \varepsilon_1} \right) (E_{b,1} - J_1) \quad (\text{A.16})$$

The driving force for heat transfer is the difference between the surface's blackbody emissive power and its radiosity ($E_{b,1} - J_1$). This equation is highly important because it relates the blackbody emissive power of the surface to the radiosity and can be applied to any gray surface involved in radiation exchange. Such equation is not required for blackbody surfaces since radiosity is basically equal to emissive power.

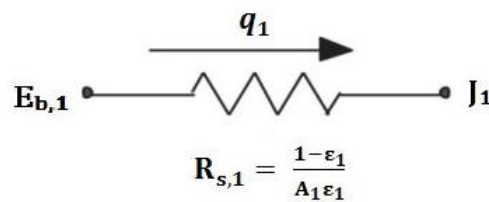


Figure A.7. Surface resistance converting blackbody emissive power to radiosity.

Analogy similar to space resistances can be made for graybody surfaces. The resistance between surface's blackbody emissive power and its radiosity is called the *surface resistance* ($R_{s,i}$).

$$R_{s,1} = \frac{1 - \varepsilon_1}{A_1 \varepsilon_1} \quad (\text{A.17})$$

The surface resistance and the space resistance both have units m^{-2} (in the SI system). Note that if the surface is black (i.e. if $\epsilon_1 = 1$), then the surface resistance limits to 0 and the resistor disappears; this reveals the reason why blackbodies do not have surface resistance. Also, if the surface is a perfect reflector, (i.e. if $\epsilon_1 = 0$), then the surface resistance becomes infinitely large. In this limit, the surface does not communicate radiatively with its environment; all incident radiation is reflected and the surface emits no radiation.

A.6. Evaluation of Combustion Gas Radiative Properties

Combustion gases emit radiation also absorb radiation. Wavelength of emittance and absorptance are dependent on the structure of the gas molecules and are quite complicated. Air is usually regarded as a transparent medium since it consists symmetric diatomic molecules which neither emit nor absorb in the infrared, and inert gases (N_2 , O_2 and Ar), however, humid air absorb some radiation but not significantly. Considering a combustion environment, uncombusted hydrocarbons, e.g. CH_4 , and other molecules CO_2 , H_2O , CO , etc., emit and absorb in the infrared. Although absorption and emission of solid surfaces vary with wavelength smoothly, gases exhibit strong and sharp oscillations with wavelength but only in narrow bands centered around wavelengths specific to gas species (Karan and Baukal, 2013). This is a very important feature to be used in engineering representation of combustion gases.

For engineering heat transfer purposes, the radiative properties of gas mixtures are usually defined in terms of the total emissivity and absorptivity. The total emissivity of a gas depends on the gas temperature T_g , the “partial pressure- (mean) path length” product pL_m , and to a small extent on the total pressure; it is denoted by $\epsilon_g(T_g, pL_m)$. The total absorptivity depends on the same parameters and in addition the source temperature of the radiation being absorbed, T_s ; it is denoted by $\alpha_g(T_g, T_s, pL_m)$ (Truelove, 1983).

Radiative gas property models which yield total emissivities and absorptivities of gas mixtures may be conveniently classified into four general categories associated with narrow-band models, exponential wide-band models (EWBM), weighted sum of gray gases models (WSGG), and charts and correlations (Smith, et al., 1982). Considering the applicability for engineering calculations, weighted sum of gray gases models (WSGGM) found by Hottel

and Sarofim, is the most feasible approach by far. Consequently, techniques other than WSGG models will not be covered in this thesis.

A.6.1. Weighted sum of gray gas models

WSGG concept postulates that the “total emissivity - pL_m ” relationship for any gas mixture can be represented by the sum of the emissivities of several hypothetical gray gases and one clear gas, weighted by temperature dependent factors. The number of gray gas in the model is chosen to satisfy desired degree of accuracy. The total emissivity of the WSGGM is calculated from the following equation:

$$\varepsilon_g = \sum_{l=0}^N a_{g,l} (1 - e^{-k_l P_{part} L_m}) \quad (A.18)$$

- $a_{g,l}(T_g)$: Temperature Dependent Emissivity Weighting Factors for the l th Gray Gas at temperature T_g .
- K_l : Pressure Absorption Coefficient ($\text{atm}^{-1}\text{m}^{-1}$)
- $(1 - e^{-k_l p L})$: Emissivity of the i th Gray Gas
- P_{part} : Sum of Partial Pressures of Participating Gases (atm)
- L : The (Mean) Beam Length (m)

Each of the gray gases has a constant pressure absorption coefficient k_l , where the clear gas has $k_0=0$ ($l=0$ represents clear gas). The weighting factor $a_{g,l}$, may be physically interpreted as the fractional amount of black body energy in the spectral regions where the effective pressure absorption coefficient is about k_l . The purpose to include clear gas component is to represent the non-absorbing regions, or windows, in the gas absorption spectrum. A three term expansion of WSGG model is named as two-gray-plus-one-clear-gas. For many engineering purposes, single gray gas approximation yields plausible simplification (Truelove, 1983).

The weighting factors are calculated from the equation below:

$$a_{g,l}(T_g) = \sum_{p=1}^p b_{g,l,p}(T_g^{p-1}) \quad (\text{A.19})$$

The total emissivity is an increasing function of the partial pressure- (mean) beam length product (pL_m) and approaches unity in the limit. Therefore, the weighting factors $a_{g,i}$ s must be positive and sum to unity. This is the point where clear gas existence affects the total emissivity. Eventhough clear gas has $k_0=0$, it affects the total emissivity/absorptivity by affecting the sum of weighting factors of other gray gas(es).

In this work, weighted sum of gray gas model parameters proposed by in the literature is used to calculate emissivity of combustion gas mixture (Dorigon *et al.*, 2013).

APPENDIX B: PROPERTIES OF SPECIES AND MIXTURES

B.1. Thermodynamic and Transport Properties of Species and Mixtures

Within the scope of this thesis, NASA polynomials are used to calculate heat capacities, viscosities and thermal conductivities of each species involved in reaction phase and flue gas phase. These polynomials are given as two sets, which are valid for temperature interval of 300-1000 K and 1000-5000 K. Specific set is used for corresponding condition. Coefficients provided for in units of micropoise (μP), and thermal conductivity in units of microwatts per centimeter kelvin ($\mu\text{W}/\text{cm}\cdot\text{K}$).

B.1.1. Heat capacities of species and mixtures

Heat capacity of pure components are calculated according to the following formula.

$$\frac{C_p(T)}{R} = a_1 + a_2T + a_3^2T^2 + a_4^3T^3 + a_5^4T^4 \quad (\text{B.1})$$

Where numerical values for coefficients are given in Table B.1 and Table B.2 for corresponding conditions. As the universal gas constant, R , is chosen to be 8.3144621 (kJ/kmol-K), heat capacity's unit becomes (kJ/kmol-K).

Heat capacity of a gas mixture is calculated as below:

$$C_{p,mix} = \sum_i C_{p,i} \cdot y_i \quad (\text{B.2})$$

Table B.1. Heat capacity coefficients for $300 \text{ K} < T < 1000 \text{ K}$.

Species	a1	a2	a3	a4	a5
CH ₄	5.14987613E+08	-1.36709788E+06	4.91800599E+03	-4.84743026E+00	1.66693956E-03
H ₂ O	4.19864056E+08	-2.03643410E+05	6.52040211E+02	-5.48797062E-01	1.77197817E-04
H ₂	2.34433112E+08	7.98052075E+05	-1.94781510E+03	2.01572094E+00	-7.37611761E-04
CO	3.57953347E+08	-6.10353680E+04	1.01681433E+02	9.07005884E-02	-9.04424499E-05
CO ₂	2.35677352E+08	8.98459677E+05	-7.12356269E+02	2.45919022E-01	-1.43699548E-05
O ₂	3.78245636E+08	-2.99673415E+05	9.84730200E+02	-9.68129508E-01	3.24372836E-04
N ₂	3.53100528E+08	-1.23660987E+04	-5.02999437E+01	2.43530612E-01	-1.40881235E-04

Table B.2. Heat capacity coefficients for $1000 \text{ K} < T < 5000 \text{ K}$

Species	a1	a2	a3	a4	a5
CH ₄	1.63552643E+08	1.00842795E+06	-3.36916254E+02	5.34958667E-02	-3.15518833E-06
H ₂ O	2.67703787E+08	2.97318329E+05	-7.73769690E+01	9.44336689E-03	-4.26900959E-07
H ₂	2.93286579E+08	8.26607967E+04	-1.46402335E+01	1.54100359E-03	-6.88804432E-08
CO	3.04848583E+08	1.35172818E+05	-4.85794075E+01	7.88536486E-03	-4.69807489E-07
CO ₂	4.63659493E+08	2.74131991E+05	-9.95828531E+01	1.60373011E-02	-9.16103468E-07
O ₂	3.66096083E+08	6.56365523E+04	-1.41149485E+01	2.05797658E-03	-1.29913248E-07
N ₂	2.95257626E+08	1.39690057E+05	-4.92631691E+01	7.86010367E-03	-4.60755321E-07

B.1.2. Thermal conductivities of species and mixtures

Thermal conductivities, “k”, of pure components are calculated according to the following formula. Coefficients provided for thermal conductivity in units of microwatts per centimeter kelvin ($\mu\text{W}/\text{cm}\cdot\text{K}$).

$$\ln(k) = A \cdot \ln(T) + \frac{B}{T} + \frac{C}{T^2} + D \quad (\text{B.3})$$

Where numerical values for coefficients are given in Table B.3 and Table B.4 for corresponding conditions. Thermal conductivity of a gas mixture is calculated from individual pure component conductivities according to Riblett’s method as below (Graves and Vysocki, 1999):

$$k_{\text{mix}} = \frac{\sum_i k_i \cdot MW_i^{1/3} \cdot p_i}{\sum_i p_i \cdot MW_i^{1/3}} \quad (\text{B.4})$$

Table B.3. Thermal conductivity coefficients for $300 \text{ K} < T < 1000 \text{ K}$.

Species	A	B	C	D
CH ₄	0.11770360E+01	-0.17422121E+03	0.22865563E+05	-0.55146852E+00
H ₂ O	0.15541443E+01	0.66106305E+02	0.55969886E+04	-0.39259598E+01
H ₂	0.93724945E+00	0.19013311E+03	-0.19701961E+05	0.17545108E+01
CO	0.83001480E+00	0.59139032E+02	-0.98639405E+04	0.70962875E+00
CO ₂	0.53726173E+00	-0.49928331E+03	0.37397504E+05	0.32903619E+01
O ₂	0.81595343E+00	-0.34366856E+02	0.22785080E+04	0.10050999E+01
N ₂	0.94306384E+00	0.12279898E+03	-0.11839435E+05	-0.10668773E+00

Table B.4. Thermal conductivity coefficients for $1000 \text{ K} < T < 5000 \text{ K}$.

Species	A	B	C	D
CH ₄	0.49214767E+00	-0.91598343E+03	0.87265127E+05	0.48489412E+01
H ₂ O	0.79349503E+00	-0.13340063E+04	0.37864327E+06	0.23591474E+01
H ₂	0.74368397E+00	-0.54941898E+03	0.25676376E+06	0.35553997E+01
CO	0.65030086E+00	-0.15100725E+03	-0.16723855E+05	0.21699139E+01
CO ₂	0.66068182E+00	-0.12741845E+03	-0.81580328E+05	0.21817907E+01
O ₂	0.80805788E+00	0.11982181E+03	-0.47335931E+05	0.95189193E+00
N ₂	0.65147781E+00	-0.15059801E+03	-0.13746760E+05	0.21801632E+01

B.1.3. Viscosities of species and mixtures

Viscosities, “ μ ”, of pure components are calculated according to the following formula. Coefficients provided for viscosity in units of micropoise (μP).

$$\ln(\mu) = A \cdot \ln(T) + \frac{B}{T} + \frac{C}{T^2} + D \quad (\text{B.5})$$

Where numerical values for coefficients are given in Table B.5 and Table B.6 for corresponding conditions. Viscosity of a gas mixture is again calculated from individual pure component viscosities but interaction parameters should be taken into account. According to Wilke’s method interaction parameters are calculated as below (Poling *et al.*, 2001):

$$\varphi_{ij} = \frac{\left[1 + \left\{ \frac{\mu_i}{\mu_j} \right\}^{1/2} \cdot \left\{ \frac{MW_j}{MW_i} \right\}^{1/4} \right]^2}{8 \left\{ 1 + \left\{ \frac{MW_i}{MW_j} \right\} \right\}^{1/2}} \quad (\text{B.6})$$

As the binary interaction parameters are known, mixture viscosity can be calculated as below:

$$\mu_{\text{mix}} = \sum_i \frac{y_i \mu_i}{\sum_j y_j \varphi_{ij}} \quad (\text{B.7})$$

Table B.5. Viscosity coefficients for $300\text{ K} < T < 1000\text{ K}$.

Species	A	B	C	D
CH ₄	0.57388074E+00	-0.98544160E+02	0.20012204E+04	0.17536015E+01
H ₂ O	0.78387780E+00	-0.38260408E+03	0.49040158E+05	0.85222785E+00
H ₂	0.68887644E+00	0.48727168E+01	-0.59565053E+03	0.55569577E+00
CO	0.60443938E+00	-0.43632704E+02	-0.88441949E+03	0.18972150E+01
CO ₂	0.54330317E+00	-0.18823898E+03	0.88726567E+04	0.24499362E+01
O ₂	0.63839563E+00	-0.12344438E+01	-0.22885810E+05	0.18056937E+01
N ₂	0.60443938E+00	-0.43632704E+02	-0.88441949E+03	0.18972150E+01

Table B.6. Viscosity coefficients for $1000\text{ K} < T < 5000\text{ K}$.

Species	A	B	C	D
CH ₄	0.65074534E+00	-0.98544160E+02	0.20012204E+04	0.17536015E+01
H ₂ O	0.50714993E+00	-0.68966913E+03	0.87454750E+05	0.30285155E+01
H ₂	0.70504381E+00	0.36287686E+02	-0.72255550E+04	0.41921607E+00
CO	0.65060585E+00	0.28517449E+02	-0.16690236E+05	0.15223271E+01
CO ₂	0.65318879E+00	0.51738759E+02	-0.62834882E+05	0.15227045E+01
O ₂	0.63839563E+00	-0.12344438E+01	-0.22885810E+05	0.18056937E+01
N ₂	0.65060585E+00	0.28517449E+02	-0.16690236E+05	0.15223271E+01

APPENDIX C: CODE FLOW CHARTS

C.1. Model Solution Flow Charts of Main Code

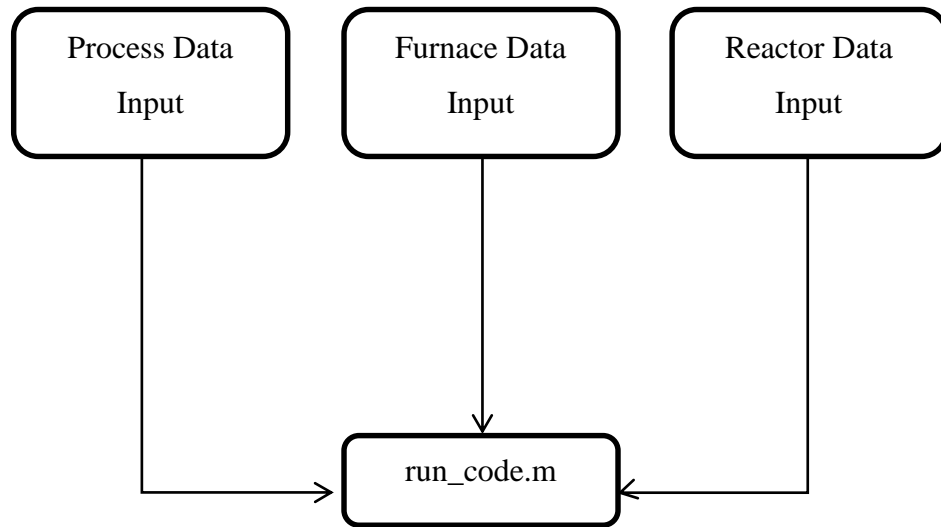


Figure C.1. All required parameters are defined in the main code.

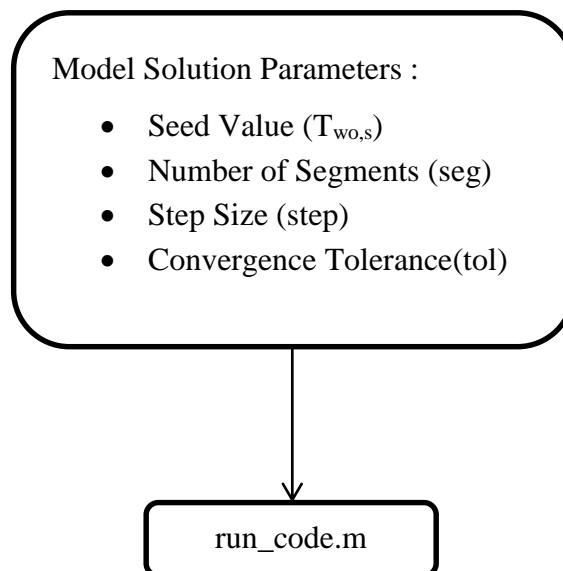


Figure C.2. Solution parameters are defined in main code.

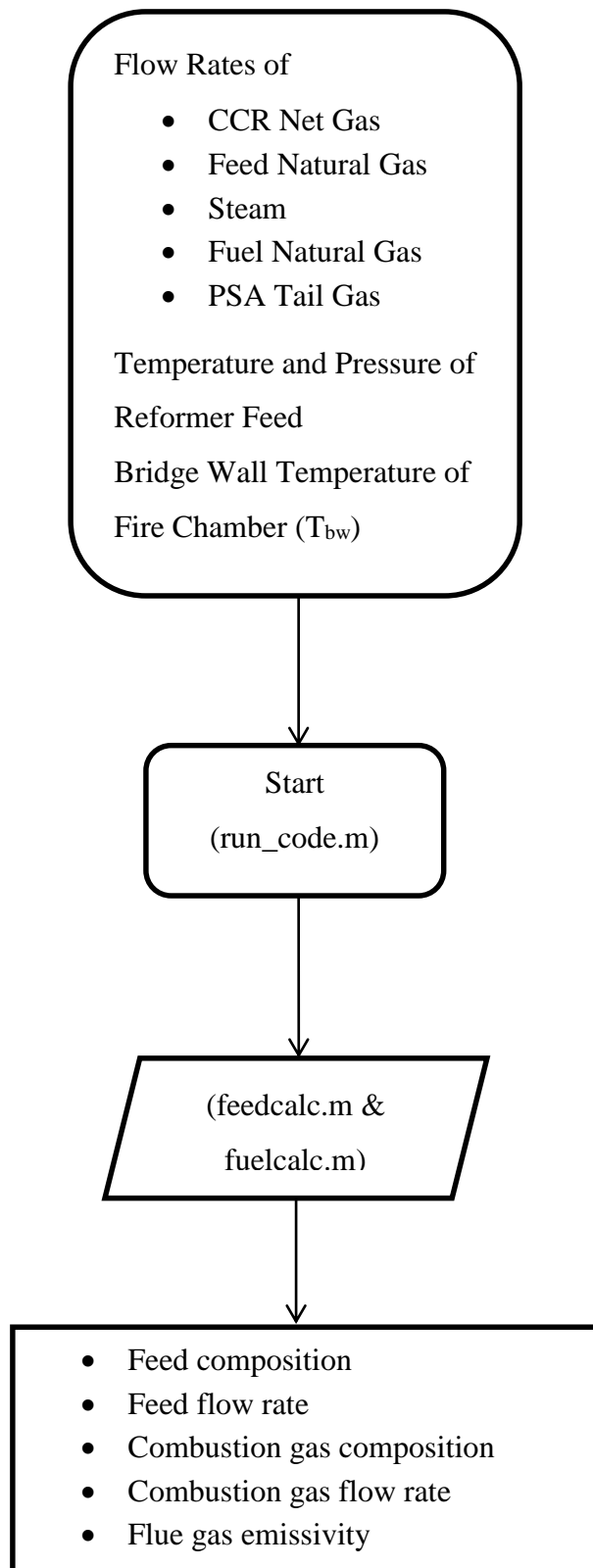


Figure C.3. Calculation of process input variables for reactor and furnace model.

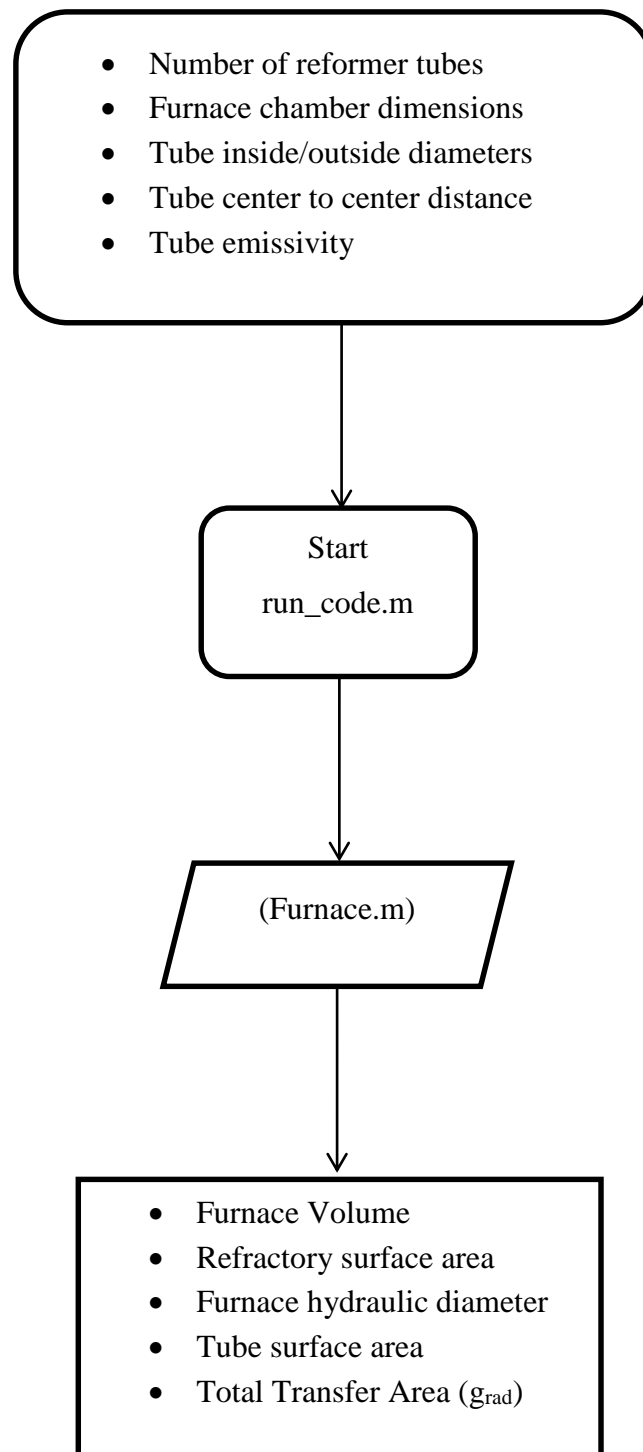


Figure C.4. Calculation of total transfer factor and related furnace parameters.

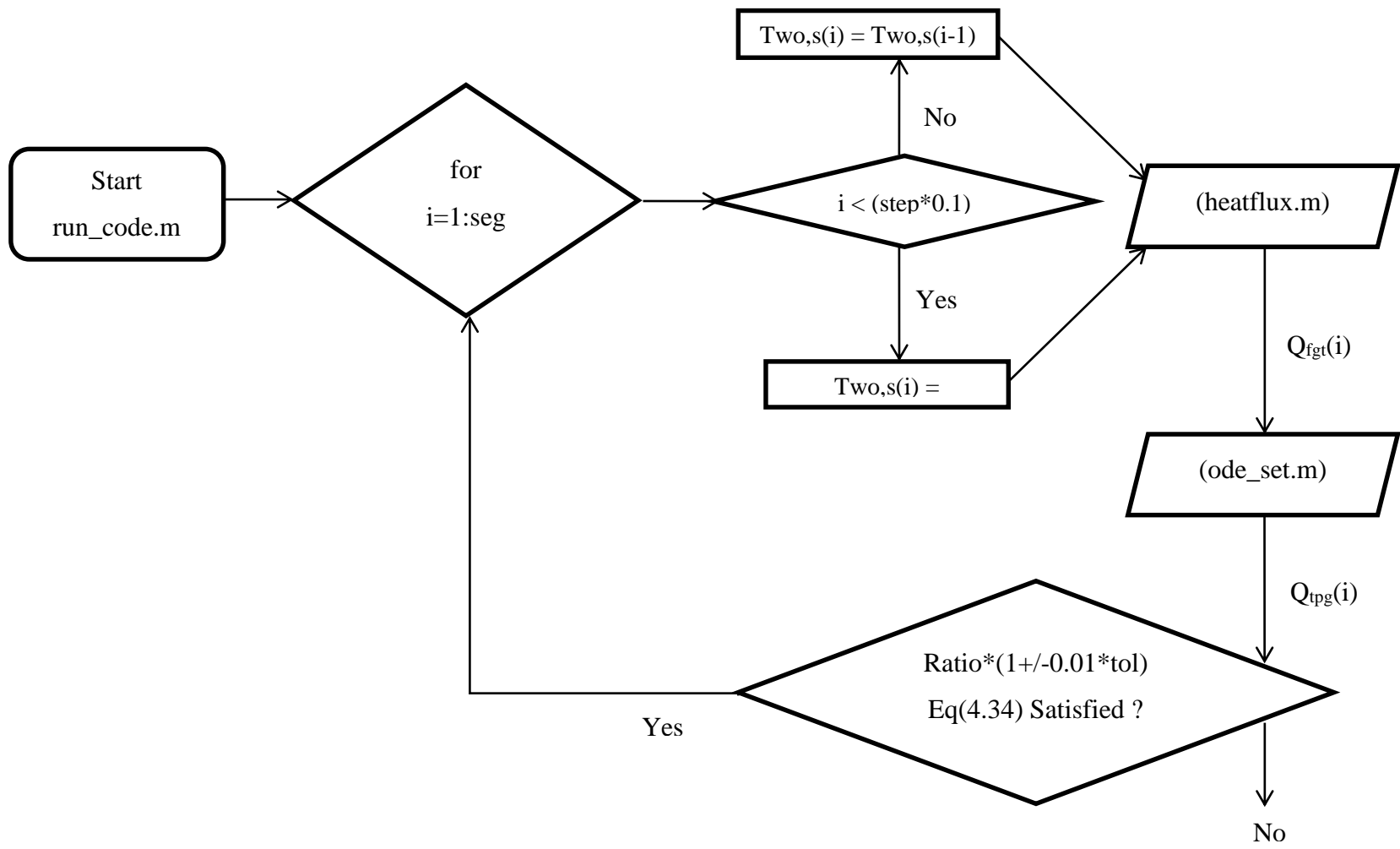


Figure C.5. First part of the main solution algorithm.

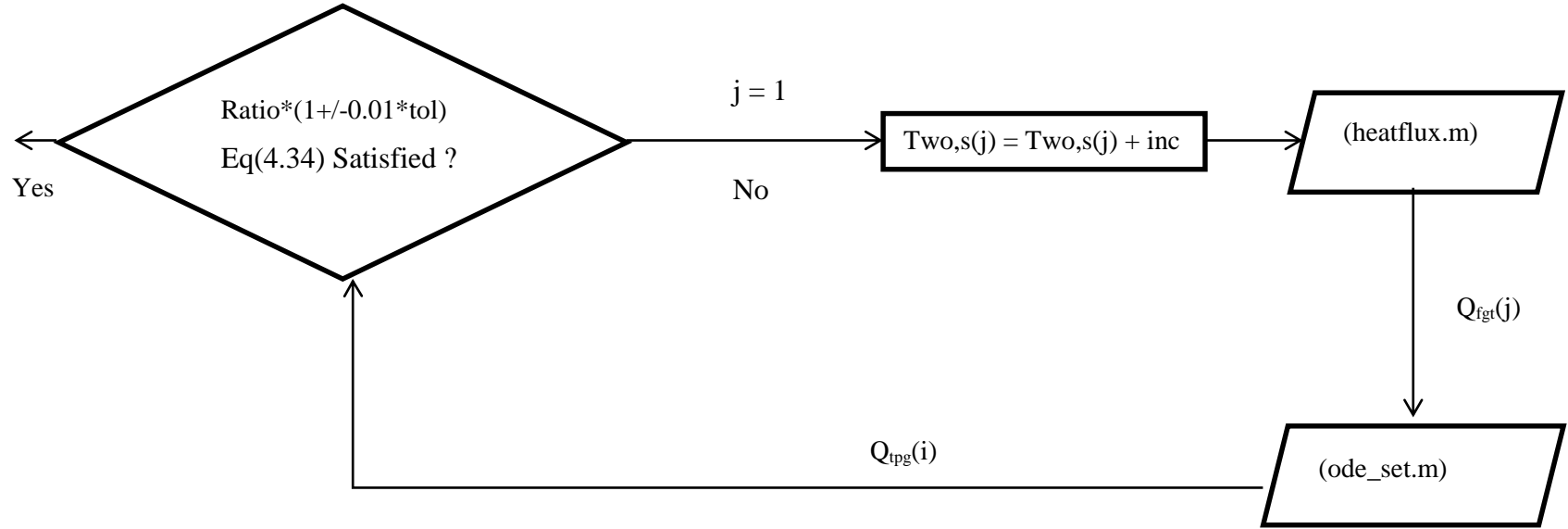


Figure C.6. Second, iterative, part of the main solution algorithm.

REFERENCES

- Baade, W. F., U. N. Parekh, and V. S. Raman, 2001, *Hydrogen In: Kirk Othmer Encyclopedia of Chemical Technology*, John Wiley and Sons Inc., pp. 759-801.
- Basse, R., 2014. Operational and Performance Improvements in Foster Wheeler Terrace Wall Reformers, Foster Wheeler, Paris.
- Batu, A. and N. Selçuk, 2002. "Modeling of Radiative Heat Transfer in the Freeboard of a Fluidized Bed Combustor Using the Zone Method Analysis". *Turkish Journal of Engineering and Environmental Sciences*, pp. 49-58.
- Baukal, C. E. J., 2000, *Heat Transfer in Industrial Combustion*, CRC Press, New York
- Beek, J., 1962, "Design of Packed Catalytic Reactors", *Advances in Chemical Engineering*, Vol. 3, pp. 203-271.
- Bicakova, O. and P. Straka, 2012, "Production of hydrogen from renewable resources and its effectiveness", *International Journal of Hydrogen Energy*, Vol. 37, pp. 11563-11578.
- Bressan, L., C. Davis, 2014, "Driving Costs in Hydrogen Production", *Gasworld*, Issue September 2014, pp. 44-48.
- Caranno, G. and A. Nava, 2005, Hydrogen - Innovative Business Solutions and Steam Reformer Technology for 2005 and Beyond, Foster Wheeler Italiana Equipment Division, Moscow.
- Carberry, J. J. and V. Arvind, 1987, *Chemical Reaction and Reactor Engineering*, Marcel Dekker, New York.
- Çengel, Y., 2012, *Heat Transfer A Practical Approach*, 2nd Edition , McGraw-Hill, New York.
- Dixon, A. G., J. Boudreau, A. Roceleau, A. Troupel, M. E. Taskin, M. Nijemeisland, E. H. Stitt, 2012, "Flow, Transport, and Reaction Interactions in Shaped Cylindrical Particles for Steam Methane Reforming", *Industrial & Engineering Chemistry Research*, pp. 15839-15854.

- Dixon, A. G., M. E. Taskin, M. Nijemeisland and E. H. Stitt, 2008, "Wall-to-Particle Heat Transfer in Steam Reformer Tubes: CFD Comparison of Catalyst Particles", *Chemical Engineering Science*, Vol. 63, pp. 2219-2224.
- Dorigon, L. J., G. Duciak, R. Brittes, F. Cassol, M. Galarca, F. H. R. França, 2013, "WSGG Correlations Based on HITEMP2010 for Computation of Thermal Radiation in Non-Isothermal, Non-Homogeneous H₂O/CO₂ Mixtures". *International Journal of Heat and Mass Transfer*, Vol. 64, pp. 863-873.
- Dybkjaer, I., 1995, "Tubular Reforming and Autothermal Reforming of Natural Gas - An Overview of Available Processes", *Fuel Processing Technology*, pp. 85-107.
- Engemasa Engenharia e Materias LTDA., 2011, Centrifugally Cast Tubes - Coils and Catalyst Tubes for Petrochemical Applications, ENGEMASA, Sao Carlos.
- Farhadi F., M. B. Babaheidari, and M. H. Motamed, 2005, "Radiative Models for the Furnace Side of a Bottom-Fired Reformer", *Applied Thermal Engineering*, Vol. 25, pp. 2398-2411.
- Fleshman, J. D., 2004, FW Hydrogen Production In: *Handbook of Petroleum Refining Processes*, 3rd Edition, pp. 285-316, McGraw-Hill Education LLC, New York.
- Fogler, H. S., 2005, *Elements of Chemical Reaction Engineering*, Pearson Education Inc., New Jersey.
- Foster Wheeler Fired Heater Division, 2006, Building Fired Heaters Around the World, Foster Wheeler, Alberta.
- Foster Wheeler, 2006, "Steam- Hydrocarbon Reformer Furnace Design", <https://www.fwc.com/getmedia/3f65b6f5-ab13-4f8f-91fe-782e097ccdfc/Steam-Hydrocarbon-Reformer-Furnace-Design.pdf.aspx>, [Accessed May 2015].
- Froment, G. F., K. B. Bischoff and J. De Wilde, 2011, *Chemical Reactor Analysis and Design*, John Wiley & Sons, Inc., Danvers.
- Geankoplis, C., 1983, *Transport Processes and Unit Operations*, Prentice Hall International, New Jersey.
- Ghouse, J. H. and T. A. Adams II, 2013, "A Multi-Scale Dynamic Two-Dimensional Heterogeneous Model for Catalytic Steam Methane Reforming Reactors", *International Journal of Hydrogen Energy*, Vol. 38, pp. 9984-9999.

- Graves, R. S. and D. C. Vysocki, 1999, *Insulation Materials: Testing and Application*, American Society for Testing and Materials, Philadelphia.
- Gray, W. and Müller, R., 1974, *Engineering Calculations in Radiative Heat Transfer*, Pergamon Press, Oxford.
- Gupta, R. B., 2009, *Hydrogen Fuel: Production, Transport and Storage*, CRC Press, Taylor & Francis Group, Florida.
- Hagen, J., 2006, *Industrial Catalysis - A Practical Approach*. 2nd Edition, Wiley - VCH Verlag GmbH & Co. KGaA, Weinheim.
- Hottel, H. C., 1974. First Estimates of Industrial Furnace Performance - One-Gas-Zone Model Reexamined. In: *Heat Transfer in Flames*, John Wiley & Sons Inc., pp. 5-28, Massachusetts.
- Hottel, H. and A. Sarofim, 1967, *Radiative Heat Transfer*, McGraw-Hill Inc., New York.
- Hou, K., *Experimental Studies of Intrinsic Kinetics and Diffusion During Methane Steam Reforming*. Ph.D. Thesis, Department of Chemistry and Applied Chemistry Science Research Institute, University of Salford, 1998.
- Hyman, M., 1968, "Simulate Methane Reformer Reactions", *Hydrocarbon Processing*, Vol. 47, pp. 131-137.
- Ibrahim, H. A.-H., 2010. Fired process heaters. In: E. P. Leite, ed. *Matlab - Modeling, Programming and Simulations*, pp. 327-364, Sciyo, Rijeka.
- Iordanidis, A., *Mathematical Modeling of Catalytic Fixed Bed Reactors*, Ph.D. Thesis, University of Twente, 2002.
- Janna, W. S., 2000, *Introduction to Radiation Heat Transfer*. In: *Engineering Heat Transfer*, 2nd Edition, CRC Press., Tennessee.
- Kalogirou, S. A., 2014, *Solar Energy Engineering Process and Systems*, 2nd Edition, Academic Press, Oxford.
- Karan, J. and C. E. J. Baukal, 2013. *Heat Transfer*. In: *The John Zink Hamworthy Combustion Handbook*. 2nd Edition, CRC Press, Florida.

- Kreith, F., R. M. Manglik, and M. S. Bohn, 2010, *Principles of Heat Transfer*, Cengage Learning, Stamford.
- Kulkarni, B. and L. Doraiswamy, 1980, "Estimation of Effective Transport Properties in Packed Bed Reactors", *Catalysis Reviews: Science and Engineering*, pp. 431-483.
- Latham, D. A., *Mathematical Modeling of an Industrial Steam Methane Reformer*, M. Sc. Thesis, Queen's University, Ontario, Canada, 2008.
- Leva, M. and M. Grummer, 1948, "Heat Transfer to Gases Through Packed Tubes: Effect of Particle Characteristics", *Industrial and Engineering Chemistry*, Vol. 40, pp. 415-419.
- Lloyd, L., 2011, *Handbook of Industrial Catalysts*, Springer, New York.
- McCabe, W., J. Smith, and P. Harriot, 2001, *Unit Operations of Chemical Engineering*, Mc Graw-Hill, New York.
- Minea, A. A., 2013, *Introduction to Industrial Heat Transfer. In: Advances in Industrial Heat Transfer*, CRC Press, Boca Raton.
- Modest, M., 2003, *Radiative Heat Transfer*, Academic Press Elsevier Science, San Diego.
- Modest, M. F., 2000. Radiation. In: *The CRC Handbook of Thermal Engineering*. CRC Press, Boca Raton.
- Mullinger, P. and B. Jenkins, 2014, *Industrial and Process Furnaces - Principles, Design and Operation*, Elsevier Ltd., Oxford.
- Murty, C. and M. Murthy, 1988, "Modeling and Simulation of a Top-Fired Reformer", *Industrial Engineering and Chemistry Research*, Vol. 27, pp. 1832-1840.
- Nellis, G. and S. Klein 2009, *Radiation. In: Heat Transfer*, Cambridge University Press, New York.
- Nielsen, J. R. and L. J. Christiansen, 2011, *Concepts in Syngas Manufacture*, Imperial College Press, London.
- Nielsen, J. R. R., 1984, *Catalytic Steam Reforming. In: Catalysis*, Springer Berlin, pp. 1-117, Heidelberg.

- Nielsen, J. R. R., 2008. *Steam Reforming*. In: *Handbook of Heterogeneous Catalysis*, pp. 2882-2903, John Wiley and Sons, Weinheim.
- Oppenheim, A. and B. Calif, 1956, "Radiation Analysis by the Network Method". *Transactions of ASME Journal of Heat Transfer*, pp. 725-735.
- Pantoleonos, G., E. Kikkinides and M. C. Georgiadis, 2012. "A Heterogeneous Dynamic Model for the Simulation and Optimisation of the Steam Methane Reforming Reactor", *International Journal of Hydrogen Energy*, Vol. 37, pp. 16346-16358.
- Pedernera, M. N., J. Pina, D. O. Borio and V. Bucala, 2003, "Use of a Heterogeneous Two-Dimensional Model to Improve the Primary Steam Reformer Performance", *Chemical Engineering Journal*, pp. 29-40.
- Plehiers, P. M. and G. F. Froment, 1989, "Coupled Simulation of Heat Transfer and Reaction in a Steam Reforming Furnace", *Chemical Engineering Technology*, Vol. 12, pp. 20-26.
- Poling, B. E., B. Prausnitz, and J. O'Connell, 2001, *The Properties of Gases and Liquids*, 5th Edition, McGraw-Hill, New York.
- Quon, W. L., *A Compact and Efficient Steam Methane Reformer for Hydrogen Production*, Ph.D. Thesis, The Faculty of the Department of Chemical and Biomolecular Engineering University of Houston, 2012.
- Rhine, J. M. and R. J. Tucker, 1991, *Modeling of Gas-Fired Furnaces and Boilers and Other Industrial Heating Processes*, McGraw-Hill, New York.
- Rostrup-Nielsen, J. R., 1984, "Catalytic Steam Reforming", *Catalysis Science and Technology*, Vol. 5, pp. 1-117.
- Rothenberg, G., 2008. "Catalysis - Concepts and Green Applications". *Applied Organometallic Chemistry*, Vol. 22, Issue 7, pp. 412-691.
- Sanaye, S. and E. Baheri, 2007, "Thermal Modeling of Radiation and Convection Sections of Primary Reformer of Ammonia Plant", *Applied Thermal Engineering*, pp. 627-636.
- Sankararao, B. and J. H. Lee, 2012. "Dynamic Modeling, Simulation and Control (using MPC) of an Industrial Steam Reformer", The International Conference on Control,

- Automation and Systems, Korea Advanced Institute of Science and Technology, Jeju Island, Korea.
- Saunders, P., 2007. "Temperature Measurement of Reformer Tubes", *Materials at High Temperatures*, Vol. 24, pp. 307-313.
- Shayegan, J., M. M. Hashemi and K. Vakhshouri, 2008, "Operation of an Industrial Steam Reformer Under Severe Condition : A Simulation Study", *The Canadian Journal of Chemical Engineering*, pp. 747-755.
- Singh, C. and D. Saraf, 1979, "Simulation of Side Fired Steam-Hydrocarbon Reformers", *Industrial and Engineering Chemistry Process Design and Development*, Vol. 18, pp. 1-7.
- Smith, T. F., Z. F. Shen and J. N. Friedman, 1982. "Evaluation of Coefficients for the Weighted Sum of Gray Gases Model", *Journal of Heat Transfer*, Vol. 104, pp. 602-608.
- Soliman, M., A. Adris, A. Al-Ubaid, and S. El-Nashaie, 1992, "Intrinsic Kinetics of Nickel/Calcium Aluminate Catalyst for Methane Steam Reforming", *Journal of Chemical Technology and Biotechnology*, Vol. 55, pp. 131-138.
- Soliman, M., S. El-Nashaie, A. Al-Ubaid and A. Adris, 1988. "Simulation of Steam Reformers for Methane". *Chemical Engineering Science*, pp. 1801-1806.
- Stitt, E., 2003, Reactor Technology for Syngas and Hydrogen. In: *Sustainable Strategies for the Upgrading of Natural Gas: Fundamentals, Challenges, and Opportunities*, Springer & NATO Public Diplomacy Division, pp. 185-216, Dordrecht.
- Subramani, V., P. Sharma, L. Zhang and K. Liu, 2010, *Catalytic Steam Reforming Technology for the Production of Hydrogen and Syngas*. In: K. Liu, C. Song & V. Subramani, eds. *Hydrogen and Syngas Production and Purification Technologies*, John Wiley & Sons Inc. Publication, pp. 14-126, New Jersey.
- Taşkın, M., *CFD Simulation of Transport and Reaction in Cylindrical Catalyst Particles*, Ph.D. Thesis, Worcester Polytechnic Institute, 2007.
- Toledo, E., E. Morais and D. Melo, 2011, "Suiting Dynamic Models of Fixed Bed Catalytic Reactors for Computer Based Application", *Scientific Research*, pp. 778-785.

- Toolsee, E. W. and R. Patel, 2006, "Maximize ammonia production cost-effectively", *Hydrocarbon Processing*, Issue of April 2006, pp. 67-72.
- Truelove, J. S., 1983. *Furnaces and Combustion Chambers. In: Heat Exchanger Design Handbook*, Hemisphere Publishing Corporation, pp. 1238-1269, Düsseldorf.
- Tucker, R. J., 1986, "Direct Exchange Areas for Calculating Radiation Transfer in Rectangular Furnaces", *Journal of Heat Transfer*, Vol. 108, pp. 707-710.
- Twigg, M. V., 1989, *Catalyst Handbook*, Wolfe Publishing, London.
- Viskanta, R. and M. Mengüç, 1987. "Radiation Heat Transfer in Combustion Systems", *Prog. Energy Combust. Sci.*, Vol. 13, pp. 97-160.
- Wakao, N. and S. Kaguei, 1982, *Heat and Mass Transfer in Packed Beds*, Gordon and Breach Science Publishers Inc., Yokohama.
- Wesenberg, M. H. and H. Svendsen, 2007, "Mass and Heat Transfer Limitations in a Heterogeneous Model of a Gas-Heated Steam Reformer", *Industrial and Engineering Chemistry Research*, Vol. 46, pp. 667-676.
- Wesenberg, M. H., *Gas Heated Steam Reformer Modeling*, Ph.D. Thesis, Norwegian University of Science and Technology, 2006.
- Xu, J. and G. F. Froment, 1989. "Methane Steam Reforming, Methanation and Water-Gas Shift: I", *AIChE Journal*, Vol. 35, pp. 88-96.
- Yang, W. C., 2003, *Handbook of Fluidization and Fluid-Particle Systems*, Marcel Dekker Inc., New York.
- Yu, Z., E. Cao, Y. Wang, Z. Zhou, Z. Dai, 2006. "Simulation of Natural Gas Steam Reforming Furnace", *Fuel Processing Technology*, Vol. 87, pp. 695-704.
- Zamaniyan, A., H. Ebrahimi, and J. S. S. Mohammadzadeh, 2008. A Unified Model for Top Fired Methane Steam Reformers Using Three-Dimensional Zonal Analysis. *Chemical Engineering and Processing*, Vol. 47, pp. 946-956.
- Zamaniyan, A., A. Zoghi and H. Ebrahimi, 2008, "Software Development for Design and Simulation of Terraced Wall and Top Fired Primary Steam Reformers", *Computers and Chemical Engineering*, pp. 1433-1446.

Zhang, Z. and D.P. DeWitt, 2009, *Radiation Heat Transfer. In: Albright's Chemical Engineering Handbook*, CRC Press, Indiana.

Zyskin, A.G., A.K. Avetisov, V.L. Kuchaev, E.N. Shapatina, L.J. Christiansen, 2007. "Simulation of the Kinetics of Complex Heterogeneous Catalytic Reactions Under Diffusion Limitations". *Kinetics and Catalysis*, Vol. 48, Issue 3, pp. 337-344.